# ON THE PROBLEMS RELATED TO THE ORGANIZATION OF SURFACE MODIFIED COLLOIDAL PARTICLES AT THE AIR-WATER INTERFACE

THESIS SUBMITTED TO

**THE UNIVERSITY OF PUNE**

FOR THE DEGREE OF

**DOCTOR OF PHILOSOPHY**

IN

**PHYSICS**

BY

**Mr. K Subramanya Mayya**

**PHYSICAL CHEMISTRY DIVISION**

**NATIONAL CHEMICAL LABORATORY**

**PUNE 411 008**

**I N D I A**

M A R C H  1 9 9 9

*Dedicated*
*to*
*my Parents, Teachers*
*and*
*my Dear Uncle*

राष्ट्रीय रासायनिक प्रयोगशाला (वैज्ञानिक तथा औद्योगिक अनुसंधान परिषद) पुणे - 411 008.

NATIONAL CHEMICAL LABORATORY (COUNCIL OF SCIENTIFIC & INDUSTRIAL RESEARCH) PUNE 411 008.

टेलीफोन 336451-52 तार : केमेस्ट्री टेलेक्स 0145-7266 फैक्स उत्तर बैक कोड : एन. सी. एल. पीएन
TELEPHONE 331453 GRAM : CHEMISTRY TELEX 0145-7653 FAX 0212-330233 ANSEWER BACK CODE : NCL PN
0145-7586 0212-334761

# CERTIFICATE

This is to certify that the work discussed in the thesis entitled "**ON THE PROBLEMS RELATED TO THE ORGANISATION OF SURFACE MODIFIED COLLOIDAL PARTICLES AT THE AIR-WATER INTERFACE**" by **Mr. K Subramanya Mayya**, for the degree of Doctor of Philosophy was carried out under my supervision in the Physical Chemistry Division of National Chemical Laboratory, Pune. Such material as has been obtained by other sources have been duly acknowledged in this thesis. To the best of my knowledge, the present work or any part thereof, has not been submitted to any other University for the award of any other degree or diploma.

Murali Sastry

Date: 24 March, 1999.

Place: Pune

Dr. Murali Sastry

(Research Guide)

# ACKNOWLEDGEMENTS

It is of immense pleasure for me to express my deep sense of gratitude and sincere thanks to my research guide, *Dr. Murali Sastry*, Physical Chemistry Division, National Chemical Laboratory, Pune, for his invaluable guidance, constant encouragement, untiring involvement and sharing his vast and precious scientific knowledge throughout the course of this work. I am most indebted to him for exposing me to this exciting and interesting field of research. The time which we spent together in the field of research will be a memorable one, and I would really thank him for being with us in all situations as a constant source of motivation.

I wish to thank Dr. P Ganguly, Head, Physical Chemistry Division, for his encouragement towards my work, in the form of making available the Langmuir Trough.

I would also like to thank Drs. K Vijayamohanan, Anil Kumar, D V Paranjape, I S Mulla, D Chakaravarthy, K R Patil, S K Choudhary, S D Sathye, Shridhar, P A Joy .for their encouragements.

Working under a single roof, it was a good company of Mr. Natarajan and Mrs. S Adyanthaya who have always helped us in one way or the other.

I wish to thank Dr. S R Sainkar, who always was ready to do our SEM samples, which was a boost to our enthusiasms. I would also like to thank Mrs. A Mitra and Ms. N R Pavaskar for characterizing our XRD samples. I am also thankful to Dr. P Singh, for TEM measurements, Drs. Pradhan and Pathak for DSC measurements, and Mr. Badrinarayan and Mr. A B Mandale for XPS measurements. I am very much thankful to Dr. S K Date, Head, SIL for making available all the Special Instrumentation Laboratory facilities,

I wish to thank, my labemates, Mrs. Vijaya, Anand, Madhu and Neeta for their encouraging suggestions and fruitful discussion. I would also like to thank Milind for so much of his good wishes.

I wish to also thank my colleagues in the Division, Varsha, Sachin, Kollam, Samsun, Sonali, Deepali, Sushama and Mohd. Aslam for their cooperation.

I am very much grateful to my parents and other family members for their constant inspiration and encouragement.

I am thankful to the authorities of NCL, Pune for giving me the opportunity to work in NCL. Finally I am thankful to the CSIR for financial support in the form of both Project Assistant and Senior Research Fellowship.

K Subramanya Mayya

C O N T E N T S

CHAPTER I: INTRODUCTION



CHAPTER II : EXPERIMENTAL TECHNIQUES



CHAPTER Ill : SURFACE MODIFICATION OF COLLOIDAL PARTICLES



CHAPTER IV : ELECTROSTATIC IMMOBILIZATION OF SURFACE MODIFIED COLLOIDAL PARTICLES AT THE AIR-WATER INTERFACE

# CHAPTER I

# *INTRODUCTION*



---

This chapter highlights with examples concepts from biology taken for synthesis of advanced materials. Role of electrostatic interactions in synthesis of nanoscale organizates has been discussed. The chapter highlights the exploitation of air-water interface for organization of colloidal particles, and in light of the developments made in this direction, the work presented in the thesis

---

## 1.1 FUTURE FOR ADVANCED MATERIALS USING CONCEPTS FROM BIOLOGY:

The creation of nanometer-scale devices [1] has fascinated and inspired the scientific community for more than a decade. Today the focus is on the "engineering up" (building structures using atoms and molecules) approach for the construction of nanoscale structures and nanosystems. This is mainly due to the fact that it is very difficult to realize efficient 'Very large scale integrated systems (VLSIs)', using the 'engineering down' approach (moving from bulk to nanostructures) [2]. This is one of the several reasons why wet chemical methods are becoming increasingly popular in the synthesis of advanced materials. There is a growing realization that, significant progress can be made in the development of nanoscience/nanotechnology by transferring concepts found in the biological world into the chemical arena [3]. Molecular self-assembly is one such strategy which derives inspiration from the biological world, in which many processes involve interfacial interactions and shape selectivity that guide the formation of complex, multicomponent three dimensional structures [4]. Self-assembly is the spontaneous organization of molecules or objects into stable, well-defined structures by noncovalent forces [5-7]. Voluminous literature is available which emphasize/apply this development under various headings like Supramolecular Chemistry, Membrane Mimetic Chemistry, Biomimetics, molecular tectonics, soft lithography etc. [8].

There are numerous processes with the help of which nature has been synthesizing materials, or caging toxic materials, immaterial whether the moiety is organic or inorganic. This absence of a demarcation between organic and inorganic materials in its choice, the size range it deals with being in nanoscale (Nature's Nanoscience) and building from the molecular components have been a source of inspiration behind the development of new strategies for synthesis applicable to nanostructures [3, 6]. For example a protein called ferritin, found in the livers of humans and a wide range of other organisms, forms 8-nanometer-wide cages with a strong affinity for iron oxide. When free iron in our bodies picks up oxygen and forms rust, it does so inside the ferritin structures, which keep the toxic compound safely caged. Stephan Mann and his group have found that the protein can cage several other compounds besides iron oxide, including manganese oxide and iron sulfide [9]. This means that in principle one can grow nanoparticles of known size using these concepts. In this spirit Brus et al have grown quantum dots in tiny reaction vessels called "inverse

micelles" [10]. There are many such mimetic (to imitate) systems available, some of which have been mentioned later in this chapter.

## 1.2 INTEREST IN QUANTUM DOTS:

Band gap engineering as it is known today, has been of great interest due to its technological importance. Band-gap engineering by size and dimension quantization is important since it leads to mechanical, chemical, electrical, optical, magnetic, electro-optical, and magneto-optical properties which are very different from those observed for bulk material [11]. Reduction in size to the nanometer scale results in quantum size effects at dimensions comparable to the electron Bohr radius [12]. The electronic one dimensionality leads to a quantum wire, whereas dimension zero results in a quantum dot, and two dimensionality leads to quantum wells. Realization of quantum dots can lead to new generations of computers with extremely high memory storage capacities. Quantum dots can be tuned by changing their diameters to absorb and emit light at any desired wavelength. This property makes it feasible to construct a finely tunable and efficient semiconductor laser [13]. Semiconductor quantum dots can in principle be designed to capture a single electron at a time [14], and exploitation of this concept can lead to the manufacture of ultrahigh density integrated circuits and information storage devices which are based on the presence or absence of individual electrons. Single electron transistor (SET) have already been put in to practice by Alivisatos *et al* with Cadmium selenide semiconductor nanocrystallites approximately 5nm in size [15]. In addition to the above mentioned applications, clusters are now being used as chemical sensors, spectroscopic enhancers and microimaging methods to name a few [16-18]. A structure of great interest for developing nanoscale electronics is a planar array of metal islands separated from each other by tunnel barriers. Electronic conduction in such a structure can be varied from the metallic to the insulating limit by controlling the size of the islands and the strength of the coupling between them. Correlated single-electron tunneling in a patterned superlattice of this type has been proposed as a future basis for nano-electronic digital circuits [19]. These are some of the reasons why there is growing interest in organization of colloidal particles.

Majority of the techniques which are used for organization of colloidal particles or for that matter synthesis of nanostructures use noncovalent interactions. They play a major role in molecular recognition, which determine the structure of biological macromolecules, and in synthesizing artificial molecules to the efficiency that exists in

biology. This has become a technologically challenging task today. Molecular recognition events represent the basis of information processing at the supramolecular level. They give rise to changes in electronic, ionic, optical and conformational properties and thus translate themselves into the generation of a signal. Molecular interactions form the basis of the highly specific recognition, reaction, transport, regulation, etc., processes that occur in biology, such as substrate binding to a receptor-protein, enzymatic reactions, assembling of protein-protein complexes, immunological antigen-antibody association, intermolecular reading, translation and transcription of the genetic code, signal induction and neuro transmitters, and cellular recognition.

Some of the non-covalent interactions which are used for synthesis of nanostructures are Hydrogen bonding, Hydrophobic effect, Electrostatic interactions, Van-der-Waal's forces etc. Recently a new noncovalent interaction has come into being known as cation-$\pi$ interaction [20]. The stronger the interaction, the smaller the area of molecular surface that must be designed to achieve a given strength of interaction, and the easier the synthetic task.

Hydrophobic interactions have been extensively used for organization of colloidal particles. Colloidal particles are derivatized using long chain molecules which expose hydrocarbon chains, and hence are rendered hydrophobic. This particles are then organized at the air-water interface [21, 22]. The use of interdigitated bilayers for derivatizing the clusters, which obviates the use of bifunctional molecules make use of hydrophobic interaction between the long chain fatty lipid molecules on the curved surface of cluster. This aspect has been highlighted in the chapter 3 of this thesis. In the above said strategy, clusters are synthesized in an aqueous environment, where hydrophobic interaction between the long alkane chains are maximized by forming interdigitated bilayers and this strategy has been used to derivatize the colloidal particles, which were then organized at the air-water interface.

Electrostatic interactions play a central role in variety of biological processes the origin of which arise from the coulomb force between the charges. One very important aspect of electrostatic interaction concerns the range of the interaction [23]. The inverse square dependence of the coulomb force makes it very long range. The ions in solution or for that matter in a lattice are surrounded by counterions, and the electrostatic field gets screened and decays more rapidly than from a truly isolated charge. This makes all electrostatic interactions much shorter range, still of much longer

Here, interactions between nano-crystal surfaces and the host matrix is controlled through a choice of functional group in the host polymers. *In-situ* preparation of nanocrystals in Zeolite [48] porous glasses [49] and organo-clay complexes [50] has also been demonstrated.

**1.3-4 Organization at air-water interface:**

Air-water interface has been extensively used to organize colloidal particles. Langmuir-Blodgett technique a well understood area for deposition of lamellar multilayer films has been used to deposit multilayer films [Discussed in detail in chapter 2 section 2.1]. Fendler *et al* were the first to demonstrate the importance of the air-water interface for organization of colloidal particles [51]. Colloidal particulate films of different technologically important materials, like silver, cadmium sulfide, $Fe_2O_3$, lead sulfide etc. were formed/organized at the air-water interface. Some of these have been discussed below.

**1.3-4a.** Chemical Generation of Nanocrystalline Particulate films:

A surfactant monolayer was spread on an aqueous solution of the metal salt and injection of the reactant gas into the closed system induced crystallization. Evolution of a nanocrystalline particulate film, has been discussed in terms of the following steps. Formation of metal-sulfide bonds at a large number of sites at the monolayer-aqueous interface. Downward growth of well-separated nanocrystalline metal sulfide particles followed by coalescence of clusters into interconnected arrays of semiconductor particles. Formation of the "first layer" of a porous sulfide semiconductor particulate film composed of 20-40 Å thick, 30-80 Å diameter particles. Diffusion of fresh metal ions to the monolayer head group area. Formation of a "second layer of the porous sulfide semiconductor particulate film (by using the first three steps). Build-up of "subsequent layers" of the sulfide semiconductor particulate film up to plateau thickness beyond which the film cannot grow.

Cadmium Sulfide [52-57], Zinc Sulfide [52-55, 57], lead sulfide [55, 58-59], cadmium selenide [60] and lead selenide [60-61], silver [62] and gold [63] metallic nanoparticulate films have been chemically grown, insitu, under monolayers

**1.3-4b** . Electrochemical Generation of Nanocrystalline Particulate Films:

A Negatively charged monolayer was taken which provides binding sites for silver ions. These ions were reduced at the cathodic surface. The initially formed silver particles extend the cathode and provide a mechanism for the continued reduction of silver counterions at the monolayer surface. With time, silver particles were found to grow concentrically, forming larger and larger circles at the monolayer-water interface [64]. Their absorption spectrum on quartz is unusual in that it shows an inter-band transition at 321 nm, in addition to an absorption maximum at 387 nm.

**1.3-4c**. Spreading Surfactant-Stabilized Nanoparticles on Aqueous Solution and Transferring them Solid Substrates:

Colloidal particles were hydrophobized using surfactants, which were spread at the air-water interface. Particulate films were formed at the air-water interface by dispersing surfactant-stabilized nanoparticles on a aqueous subphase which was contained in a Langmuir trough [65]. The technique can be regarded as analogous to monolayer formation from simple surfactants. Surfactant coated CdS [66], $TiO_2$ [67], $Fe_3O_4$ [68], lead zirconium titanate [69], palladium [70], silver [21, 71] and Platinum [22] nanoparticles have been prepared. Platinum nanoparticles were hydrophobized using using a polymer called Polyvinylpirolidone, and was spread at the air-water interface, while the organization of silver particles as described by Fendler *et al*, was carried out by spreading the silver particles hydrophobized using oleic acid. Oleic Acid was found to tranfer the clusters from the aqueous phase into the volatile organic phase.

**1.3-4d**. Nanoparticles between Langmuir-Blodgett Films:

Langmuir Blodgett films are routinely and reproducibly formed by moving a clean plate through a monolayer, supported on an aqueous solution [72]. Hydrophobic substrates preferentially attract the tails of surfactants and the monolayer is transferred during immersion. Depending whether the substrate is hydrophobic or hydrophillic one can get Y-type or X-type films [refer chapter 2]. Apposing surfactant headgroups in LB films, obtained by Y- or X-type deposition, provide suitable sites for nanoparticles or nanoparticulate films. Indeed, size-quantized CdS[73-81], CdSe [73], CdTe[73], CdSxSe1-x [73], CdSxTe1-x [73], CoS [85] and PbS [83-85] particles have been insitu generated by the exposure of the appropriate metal carboxylate(s) Y-type LB films to

to $H_2S$, $H_2Se$, $H_2Te$ respectively. In a similar way gold nanoparticles were obtained on shining UV light (Photoreduction) on LB film of Octadecylamine/chloroaurate ion [86]. Alternatively, appropriately charged nanoparticle sol dispersed in the subphase, can be electrostatically attracted to an oppositely charged monolayer surface and thus, be inserted between LB films.[ 75-76, 88-91]. The method is illustrated by insertion of sodium hexametaphosphate (HMP) stabislized CdS nanoparticles between the headgroups of LB films, formed from DOBAB [76]. Stabilized $Fe_3O_4$[91] and $Fe_2O_3$ [89] nanoparticles have been similarly introduced into LB films. However, this method has not been studied in detail.

## 1.4 Method described in this thesis:

Though air-water interface was used to organize colloidal particles, the role of electrostatic interactions, and their effective utilization for fine tuning the cluster density etc., was not demonstrated. Electrostatic forces are the basis of the work described in this thesis. The technique described in the thesis makes use of electrostatic interactions between oppositely charged surface modified colloidal particles and the headgroup of the amphiphilic molecules at the air-water interface for organization. Colloidal particles were synthesized using standard wet chemical methods, and were derivatized with functional groups of choice using a bifunctional molecule and interdigitated bilayers, which are once again, stabilization using electrostatic forces. The work described in this thesis can be represented in the form of following equation.

| Colloid Chemistry + Self Assembly = Nanoscale Architecture |
|---|

Colloid Chemistry is well standardized, and the high level of control that can be exercised over the chemical composition, size and polydispersity of colloidal nanoparticles [93] has resulted in colloids becoming important starting points in the organization of mesoscale structures [51].

The thesis has been divided into seven chapters. Chapter I gives a brief introduction to the thesis, followed by chapter II, which describes different characterization techniques used for characterization of colloidal particles in solution as well as in Langmuir-Blodgett films. Emphasis is on the three dimensional self assembly of bifunctional molecule onto colloidal particles, which render the dual purpose of

charging as well as stabilizing the particles. Clusters can be charged either positively or negatively either by using a bifunctional molecule, or using interdigitated bilayers. Chapter III addresses the modification of colloidal particle surfaces to incorporate functionalities such as carboxylic acid (-COOH) and amine ($-NH_2$) groups. A two-pronged approach for the surface modification of the colloidal particles was used, the first based on chemisorption of a bifunctional molecule on the colloidal particle surface (yielding the so-called "3-D SAMs") while the second method used interdigitated bilayers. The latter approach in addition to yielding useful surface functionality to the colloidal particles, has thrown up interesting questions regarding self-assembly of surfactants on nanoscale-curved surfaces. Depending on the pH of the colloidal solution, the clusters can be charged negatively (clusters with $-COO^-$ groups) or positively (clusters with $-NH_3^+$ groups) and can thereafter be electrostatically attracted to Langmuir monolayers of fatty amines and fatty acids respectively.

Electrostatic immobilization of surface-modified colloidal particles at the air-water interface has been discussed in Chapter IV. Silver, gold and Q-state CdS colloidal particle films were deposited onto different substrates after forming a monolayer of these clusters with suitable amphiphiles at the air-water interface. It is shown that the cluster density at the air-water interface and consequently in built-up LB films can be regulated by simple variation of the hydrosol pH. The variation in the hydrosol pH alters the degree of ionization of the functional groups on the colloidal particle surface as well as in the Langmuir monolayer thereby modulating the electrostatic interaction between the two. Details of the electrostatic complexation at the air-water interface was studied using $\pi$-A isotherm measurements. The formation of lamellar films of the particles deposited by the LB technique was studied using UV-visible Spectroscopy, QCM, Ellipsometry, Optical Interferometry, TEM, XPS measurements etc.

In addition to the pH of the hydrosol, the charge on the Langmuir monolayer can be regulated using neutral, spacer molecules. Chapter V deals with the role of spacer molecules in the electrostatic immobilization process of surface modified colloidal particles. It was observed that the cluster density in the Langmuir monolayers as well as the time rate of cluster incorporation (complexation kinetics) decreased with increase in the molar concentration of the spacer molecule, thereby indicating that the electrostatic model used to explain the complexation is sound.

The investigation into the electrostatically controlled immobilization process of colloidal particles at the air-water interface is carried further through a study of the partitioning of carboxylic acid derivatized clusters based on their size in Chapter VI. Simultaneous immobilization of gold and silver clusters (130 ± 30 and 70 ± 12 Å diameter respectively) from the same colloidal subphase at the air-water interface using octadecylamine Langmuir monolayers has been followed by π-A isotherm measurements as well as optical absorption, quartz crystal microgravimetry (QCM) and X-ray fluorescence (XRF) analysis of the built-up LB films. Even for small concentrations of gold relative to silver clusters in the subphase, the density of the larger gold clusters in the LB films was found to be surprisingly high in relation to the smaller silver clusters. This unusual "reverse fractionation" of clusters observed is discussed in terms of the energetics associated with the distortion of the amine matrix during electrostatic association of the colloidal particles.

## 1.5 References:


1. Feynman, R.P.; *Eng. Sci.*, **1960**, *23*, 22.
2. Philp, D.; Stoddart, J.F., *Angew. Chem. Int. Ed. Engl.*, **1996**, *35*, 1154.
3. Mann, S; *Nature*, **1993**, *365*, 499.
4. Terfort, A.; Bowden, N., Whitesides, G.M., *Nature*, **1997**, *386*, 162.
5. Lehn, M.-M., *Angew. Chem. Int. Ed. Engl.* **1990**, *29*, 1304.
6. Whitesides, G.M.; Mathias, J. P.; Seto, C.T. *Science*, **1991**, *254*, 1312
7. Whitesides, G.M.; *Sci. Am.*, **1995**, *273(9)*, 146.
8. Xia, Y.; Whitesides, G.M., *Angew, Chem. Int. Ed.* **1998**, *37*, 550.
9. Mann, S., *J. Chem. Soc. Dalton Trans.* , **1993**, 1.
10. Steigerwald, M.L.; Alivisitos, A.P.; Gibson, J.M.; Harris, T.d.; Kortan, r.: Muller, A.J.; Thayer, A.M.; Duncan, T.M.; Douglass, D.C.; Brus, L.E., *J. Am. Chem. Soc*, **1988**, *110*, 3046.
11. Fendler, J.H.; "Membrance-Mimetic Approach to Advanced Materials", *Advances in Polymer Science Series*, **1994**, *113*, Springer-Verlag, Berlin.
12. Weller, H., *Angew. Chem. Int. Ed. Engl.*, **1993**, *32*, 41.

13. Colvin, V.L.; Schlamp, M.C.; Alivisatos, A.P., *Nature*, **1994**, *370*, 354.
14. Devoret, M.H.; Esteve, D.; Urbina, C., *Nature*, **1992**, *360*, 547.
15. Klein, D.L.; Roth, R.; Lim, A.K.L.; Alivisatos, A.P.; McEuen, P.L., *Nature*, **1997**, *389*, 699.
16. Hayat, M.A.; *Colloidal Gold: Principles, Methods, and Applications*, **1991**, Academic, SanDiego.
17. Bassell, G.J.; Powers, C.M.; Taneja, K.L.; Singer, R.H., *J. Cell Biol.*, **1994**, *126*, 863.
18. Creighton, J.A.; Blatchford, C.G.; Albrecht, M.G., *J. Chem. Soc. Faraday II*, **1979**, *75*, 790.
19. Chen, R.H.; Likharev, K., *J. Appl. Phys.* **1995**, *78*, 2520.
20. Dougherty, D.A., *Science*, **1996**, *271*, 163.
21. Meldrum, F. C.; Kotov, N. A.; Fendler, J. H., *Langmuir*, **1994**, *10*, 2035.
22. Sastry, M.; Patil, V.; Mayya, K. S. ; Sainkar, S.R.; Singh, P. ; *Thin Solid Films*,**1998**, *324*, 239.
23. Jacob Israevachvili; *'Intermolecular and Surface Forces'*, **1985**, Academic press, London.
24. Honig, B.; Nichollos, A., *Science* **1995**, *268*, 1144.
25. Tukano, K.; Hachisu, S., *J. Colloid Interface Sci.*, **1978**, *66*, 124.
26. Seto, C.T.; Whitesides, G.M., *J. Am. Chem. Soc.*, **1991**, *113*, 712.
27. Alivisatos, A.P., *Science*, **1996**, *271*, 933.
28. Nuzzo, R.G.; Allara, D.L., *J. Am. [1]Chem. Soc.*, **1983**, *105*, 4481.
29. Tillman, N.; Ulman, A.; Elman, J.F., *Langmuir*, **1989**, *5*, 1020.
30. Bain, C.D.; Evall, J.; Whitesides, G.M., *J. Am. Chem. Soc.*, **1989**, *111*, 7155, pale-Gros demage, C.; Simon, E.S.; Prime, K.L.; Whitesides, G.M., *J. Am. Chem. Soc.*, **1991**, *113*, 12.
31. Ulman, A.; Tillman, N., *Langmuir*, **1989**, *5*, 1418.
32. Murray, C.B.; Kagan, C.R.; Bawendi, M.G., *Science*, **1996**, *270*, 1335.
33. Colvin, V.L.; Goldstein, A.N.; Alivisatos, A.P., *J.Am.Chem.Soc.*, **1992**, *114*, 15221.
34. Brust, M.; Bethell, D.; Schiffrin, D, J.; Kiely, C.J., *Adv. Mater.* **1995**, *7*, 795.
35. Musick, M.D.; Keating, C.D.; Keete, M.H.; Natan, M.J., *Chem Mater.* **1997**, *9*, 1499.
36. Brust, M.; Etchonique, Calvo, e.J.; Gordillo, G.J., *Chem. Comm.* **1996**, 1949.

63. Yi, C.; Sanchez Mendieta, V.; Lopez Castanares, R. ; Meldrum, F. C.; Fendler, J. H., *J. Phys. Chem*, **1995,** *99*, 9869.

64. Kotov, N. A.; Zaniquelli, M. E. D.; Meldrum, F. C.; Fendler, J. H., *Langmuir*, **1993**, *9*, 3710.

65. F. C. Meldrum, J. H. Fendler, in *Biomimetic Approaches in Materials Chemistry* **1995.**(Ed: S. Mann), VCH, New York,

66. Kotov, N. A.; Meldrum, F. C.; Wu, C.; Fendler, J. H., *J. Phys. Chem.* **1994**, *98*, 2735.

67. Kotov, N. A.; Meldrum, F. C.; Fendler, J. H., *J. Phys. Chem.* **1994**, *98*, 8827.

68. Meldrum, F.C.; Kotov, N. A.; Fendler, J. H., *J. Phys Chem.* **1994**, *98*, 4506.

69. Kotov, N. A.; Zavala, G.; Fendler, J. H., *J. Phys. Chem.*, **1995**, *99*, 13065.

70. Meldrum, F.C.; Kotov, N. A.; Fendler, J. H., *Chem. Mater.*, **1995**, *7*, 1112.

71. Meldrum, F. C.; Kotov, N. A.; Fendler, J. H., *J. Chem. Soc. Faraday Trans.* **1995**, 90.

72. Ulman, a.; *An Introduction to Ultrathin Organic Films: From Langmuir Blodgett to Self Assembly*, **1991**, Academic Press, Boston.

73. Smotkin, S.; Lee, C.; Bard, A. J.; Campion, A.; Fox, M. A.; Mallouk, T. E.; Webber, S. E.; White, J. M., *Chem. Phys. Lett.* **1988**, *152*, 265.

74. Grieser, F.; Furlong, D. N.; Scoberg, D.; Ichinose, I.; Kimizuka, N.; Kunitake, T., *J. Chem. Soc. Faraday Trans.*, **1992**, *88(15)*, 2207.

75. Furlong, D. N.; Uquhart, R.; Grieser, F.; Tanaka, K.; Okahata, Y.; *J. Chem. Soc. Faraday Trans.*, **1993**, *89(12)*, 2031.

76. Xu, S; Zhao, X. K.; Fendler, J. H.; *Adv. Mater.*, **1990**, *2*, 183.

77. Moriguichi, Hosoi, K.; Nagaoka, H.; Tanaka, I.; Teraokda, Y.; Kagawa, S.; *J. Chem. Soc. Faraday Trans.*, **1994**, *90(2)*, 349.

78. Geddes, J.; Urquhart, R. S; Furlong, D. N.; Lawrence, C. R.; Tanaka, K.; Okahata, Y.; *J. Phys. Chem.* **1993**, *97*, 13767.

79. Peng, G.; Lu, R.; Zhao, Y.Y.; Qu, L. H.; Chen, H.Y.; Li, T.J., *J. Phys. Chem.* **1994**, *98*, 7052.

80. Pike, K.; Byrd, H.; Morrone, A. A.; Talman, D. R.; *Chem. Mater.*, **1994**, *6*, 1757.

81. Luo, Z.; Zhang, Z. Q.; Liang, Y. Q.; *Langmuir*, **1994**, *9*, 3213.

82. Urquhart, S.; Furlong, D. N.; Mansur, H.; Grieser, F.; Tanaka, K.; Okahata, Y.; *Langmuir*, **1994**, *10*, 899.

83. Luo, X.Z.; Zhang, Z.Q.; Liang, Y.Q., *Langmuir*, **1994**, *9*, 3213.

84. Peng, G.; Lu, R.; Zhao, Y. Y.; Qu, L. H.; Chen, H. Y.; Li, T. J., *J. Phys. Chem.* **1994**, *98*, 7052.

85. Peng, X.; Guan, S.; Chai, X.; Jiang, Y.; Li, T, *J. Phys. Chem.* **1992**, *96*, 3170.

86. Zhu, R.; Min, G.; Wei, Y.; Schmitt, H.J., *J. Phys. Chem.* **1992**, *96*, 8210.

87. Ravaine, S.; Fanucci, G.E.; Seip, C.T.; Adair, J.H.; Talham, D.R., *Langmuir,* **1998**, *14*, 708.

88. Du, Z.; Zhang, Z; Zhao, W.; Zhu, Z.; Zhang, J.; Jin, Z.; Li, T., *Thin Solid Films* **1992**, *210/211*, 404.

89. Peng, X. ; Zhang, Y.; Yang, J. ; Zou, B.; Xiao, L. ; Li, T., *J. Phys. Chem.*, **1992**, *96*, 3412.

90. Tain, Y.; Wu, C.; Fendler, J. H., *J. Phys. Chem.* **1994**, *98*, 4913.

91. Zhao, K.; Xu, X.; Fendler, J. H., *J. Phys. Chem.* **1990**, *94*, 2573.

92. Schmid, G.; Ed. *Clusters and Colloids*, **1994**, VCH: Weinheim.

# CHAPTER II



## EXPERIMENTAL TECHNIQUES

The different experimental techniques used during the course of the present work are discussed in this chapter

The main emphasis of this thesis is the organization of surface-modified colloidal nanoparticles using electrostatic interactions at the air-water interface and the subsequent formation of multilayer nanoparticle films. The complexation of charged colloidal silver, gold' and CdS nanoparticles with surfactant monolayers has been studied using a Langmuir surface pressure balance. The built-up multilayer films have been thereafter characterized using a variety of techniques such as UV-vis spectroscopy, quartz crystal microgravimetry( QCM) , ellipsometry , Fourier Transform Infrared spectroscopy (FTIR), Transmission Electron Microscopy (TEM), etc.

## 2.1 LANGMUIR-BLODGETT TECHNIQUE

The study of Langmuir monolayers such as oil on water goes back to the Babylonians who used it to foretell the future [1]. However, the first report on the preparation of a Langmuir film was attributed to Benjamin Franklin [2]. It was in the 19th century following Agnes Pockels work that the area of Langmuir films was firmly established [3]. The first study on the deposition of multilayers films of long chain carboxylic acids onto a solid substrate was carried out by Katherine Blodgett [4]. In the following sections, the conditions necessary for the formation of Langmuir monolayers at the air-water interface and for transferring these films on the solid substrates is discussed.

### 2.1-1 Amphiphilic molecules:

Only molecules which are amphiphilic in nature can form Langmuir films. An amphiphilic molecule has a hydrophobic and a hydrophilic part. The hydrophobic end is normally a long chain of hydrocarbons called the tail and the hydrophilic moiety is called the head and is polar in nature, as shown in Fig. 2.1 Amphiphilic molecules or ions in an aqueous solution respond to the hydrophobic effect by migration to the surface of the aqueous medium to form monolayers in which the polar head group remains in the water while the hydrophobic moieties are expelled from it.

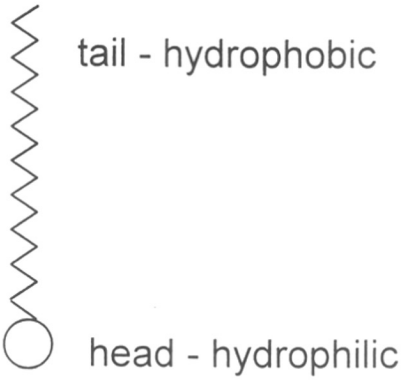


**Figure 2.1:** Schematic representation of an amphiphilic molecule showing the head and tail

### 2.1-2 Pressure-Area Isotherms ($\pi$-A isotherm)

Monolayers of amphiphilic molecules at an interface can exist in a number of different physical states, analogous to the gaseous, liquid and solid states of matter in bulk. Information regarding the transition between these states can be obtained by measuring the surface pressure of a monolayer as a function of the surface concentration [5]. *The surface pressure $\pi$ is the lateral pressure that must be applied to prevent the film from spreading.* In the case under study in this thesis, where complexation of colloidal particles at air-water interface is concerned, the pressure-area isotherm give a very important piece of information regarding the cluster complexation. The lift off area in the pressure-area isotherm was found to increase with time, indicating that cluster complexation was taking place [Figures 4.1, 4.5, 4.10, 4.14, 4.15 in chapter 4 of this thesis]. Expansion of the Langmuir Monolayer with complexation of ions, has been reported in literature [6].

A plot of the surface pressure versus the surface concentration or the area per molecule is the pressure-area ($\pi$-A) isotherm, an example of a pressure-area isotherm is shown in figure 2-2. Pressure-area isotherms are rich in information on stability of

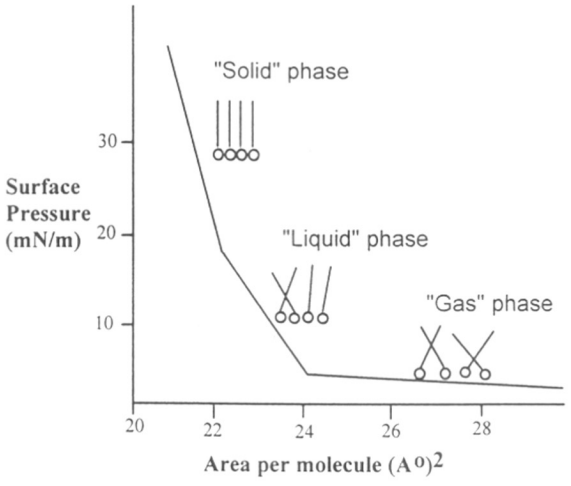


**Figure2.2:** A typical pressure-area (π-A) isotherm showing the various phase transitions of the floating monolayer.

the molecules in the two-dimensional system, phase transitions and conformational transitions.

When the surface is sparsely covered, the surface monolayers are gaseous in nature and they consist of individual absorbed molecules moving independently (Fig.2.3a). As the pressure is increased the cohesive forces between the hydrocarbon chains leads to the condensation of the gas-like film to a liquid-like film. This liquid-like film, unlike the bulk liquid state is highly compressible. This is because the hydrocarbon chains of the amphiphilic molecules can form a coherent film while lying disoriented on the surface, and can change their orientation, when the applied surface pressure is increased, until they are perpendicular to the surface to a molecular area many times smaller than that of the most expanded liquid-like film. The compression process is not necessarily continuous and two or more distinct "liquid" phases and transition between them can be observed.

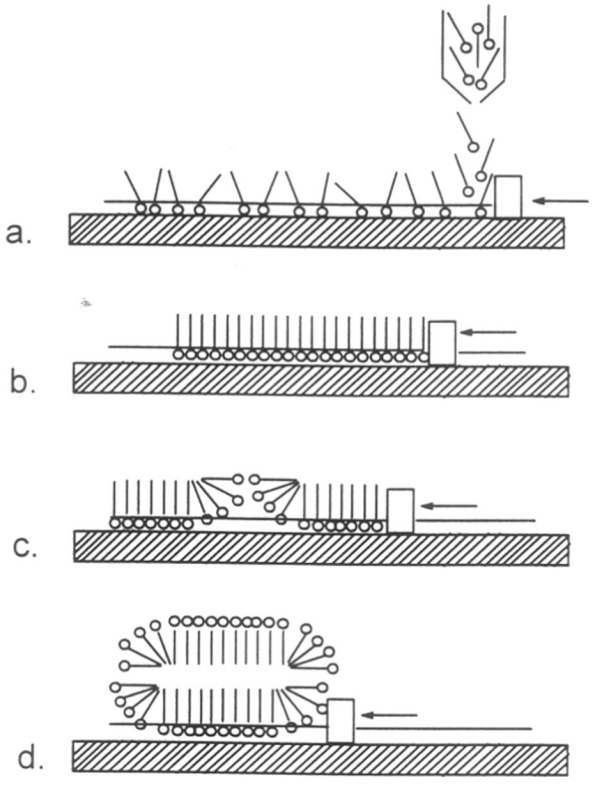


**Figure 2.3:** Various phases of the floating monolayer during compression. a. individual adsorbed molecules (gas-like phase). b. compression to a solid-like phase. c. beginning of collapse d. collapse of the monolayer

At high compression, a further transition to a solid like state may be observed (Fig. 2.3b), in which the adsorbed molecule becomes immobile and there exists a lateral order in the film. This generally requires the existence of an attractive force of cohesion between the head groups in addition to the force of cohesion between hydrocarbon chains. The limiting surface area at high pressure, for all amphiphilic molecules with saturated alkyl chains and sufficiently small head groups is always found to be about 21Å [5] per molecule. If further pressure is applied to the monolayer, it collapses due to mechanical instability (Fig.2.3c and 2.3d), and a sharp decrease in the pressure is observed. This collapse pressure is a function of the temperature, the pH of the subphase, and the speed of compression.

The pressure-area isotherm thus gives some idea of the amount of pressure which has to be applied to the film on the subphase, to enable deposition of the LB film in the solid-like phase. Thus at appropriate pressure, the film can be transferred to the

substrate. There are two methods of deposition. These two methods, and the types of films which can be obtained will be the subject of the next section.

### 2.1-3 The LB film preparation technique

The LB film preparation technique is shown schematically in figure 2.4. In a typical experiment, a drop of dilute solution of the appropriate surfactant is dissolved in a volatile solvent like chloroform ($CHCl_3$), and this is spread on the air-water interface. Due to their amphiphilicity, the molecules orient themselves on the water surface with their heads in the water and their tails in the air. This film is then compressed as shown in figure 2.3 until the molecules are in a solid-like phase with two dimensional order.

There are two different methods of transfer of monolayers from the air-water interface onto a solid substrate. The first and the more conventional is the **vertical** deposition technique developed by Langmuir and Blodgett [4b]. The other method is the **horizontal** deposition method (Schaefer's method) [7]. The latter was originally invented about 1000 years ago by the Japanese, in connection with the Japanese printing art called the "sumi-nagashi". It is the earliest technical application of organic monolayer. Schaefer's method is useful for the deposition of rigid films (e.g., polymer films), which are at the two-dimensional order region in the $\pi$-A diagram. In this method a compressed monolayer is first formed at the air-water interface, then a flat substrate is placed horizontally on the monolayer film.

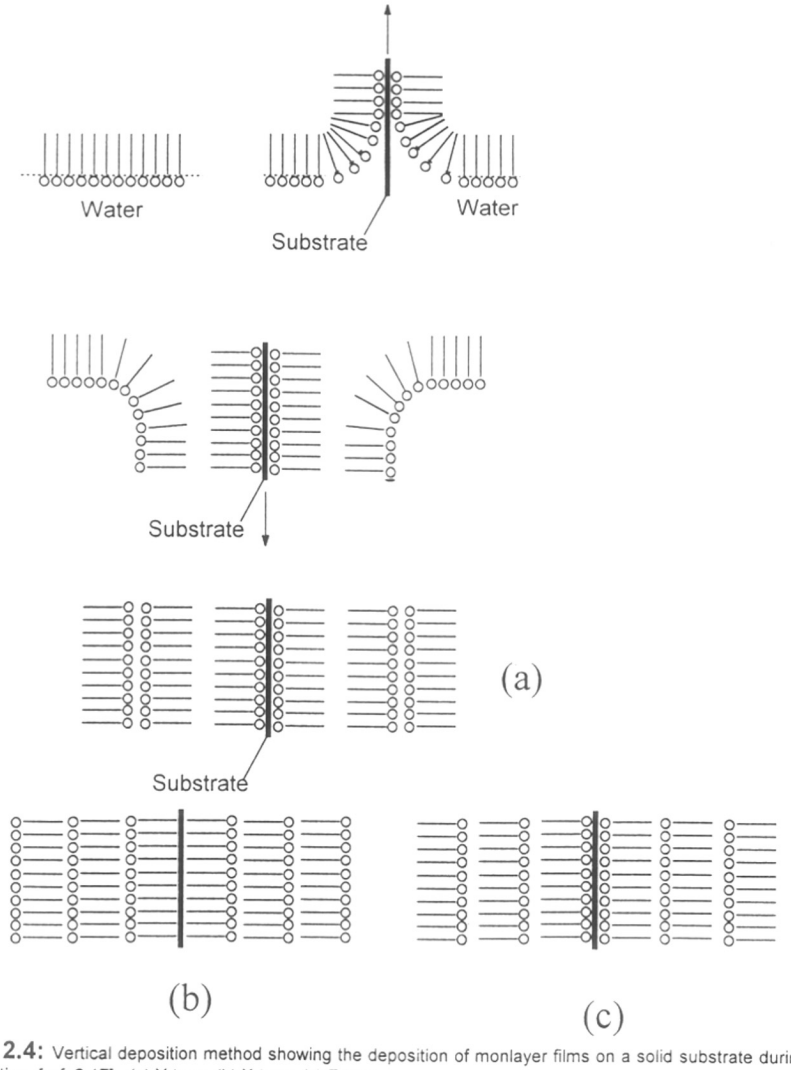


**Figure 2.4:** Vertical deposition method showing the deposition of monlayer films on a solid substrate during dipping and retraction. [ref. 2.17]. (a) Y-type (b) X-type (c) Z-type.

When this substrate is lifted and separated from the water-air interface, the monolayer is transferred to the substrate, theoretically keeping the molecular direction. In the vertical deposition method (figure. 2.4), when a substrate is moved through the water-air interface, a monolayer is transferred either during the dipping or during the retraction step [8, 3c, 3d]. In spite of the long history of this technique, the details of the

deposition methods are not really understood. One of the most detailed studies has been carried out by Peterson et al. [9]

### 2.1-4 Types of LB films

A monolayer is usually transferred during the retraction (upstroke) when the substrate is hydrophilic and hydrophilic head groups interact with the surface. On the other hand, if the substrate is hydrophobic the monolayer will be transferred during immersion (downstroke), and the hydrophilic heads will interact with the surface. If the deposition starts with a hydrophilic substrate, it becomes hydrophobic after the first deposition and thus the second monolayer will be transferred in the immersion. This mode of deposition is called Y-type (Figure 2.4a) is the most stable, because the interaction between adjacent monolayers are either hydrophobic-hydrophobic or hydrophilic-hydrophilic.

Films can also be deposited only in the downstroke (X-type, Fig.2.4b) and deposition speed may then affect the mode [4b, 10]. A third possible deposition is when films are formed only during upstroke (Z-type, Figure 2.4c). The X-type and Z-type films are non-centrosymmetric and may hence be important in non-linear optical (NLO) applications.

The amount of amphiphile actually deposited on the substrate depends on a number of factors [4a] and is measured using the deposition ratio. The deposition/transfer ratio is defined as $A_L/A_s$, where $A_L$ is the decrease in area occupied by the monolayer in the subphase (at constant temperature and pressure), and $A_s$ is the area of the substrate which is covered by the monolayer.

## 2.2 UV-VISIBLE SPECTROSCOPY:

### 2.2-1 Theory

UV-visible spectroscopy is a powerful tool for the characterization of colloidal particles [11]. In particular, noble metal particles are ideal candidates for study with UV-vis spectroscopy, since they exhibit strong surface plasmon resonance absorption in the visible region, and are highly sensitive to surface modification. The light absorption by small metal particles is described by Mie's theory.[12] The absorption spectrum of particles in a given solvent can be calculated from the optical constants of the bulk

metal, although the absorption of the particles is often vastly different from that of the bulk metal itself [13-14]. The simplest case is when the particles are spherical and their size is small compared to the wavelength of light, and the particles are well separated in solution. At particle sizes between about 3 and 20 nm, there is not a strong dependence of the absorption spectra on particle size This is because the particles are below the size at which higher order terms in the Mie formula for the absorption constant become significant. Thus, one has to regard only the dipole term which depends only on the total metal concentration in the solution and not on particle size. The absorption coefficient in $mol^{-1}$. L. $cm^{-1}$ is calculated from the relation

$$\alpha = \frac{18\pi}{\ln 10} \frac{10^5}{\lambda} \frac{M n_0^3}{\rho} \frac{\varepsilon_2}{(\varepsilon_1 + 2n_0^2) + \varepsilon_2^2} \qquad (2.1)$$

where $\lambda$ is the wavelength of light in nanometers, M and $\rho$ are the molecular weight and density of the metal, $n_o$ is the refractive index of the solvent and $\varepsilon_1$ and $\varepsilon_2$ are the real and imaginary parts of the dielectric constant of the metal. When the size of the particles becomes smaller than the mean free path of the electrons, the absorption bands are broadened; this is accounted for using size-corrected values of $\varepsilon_2$ [15]

$$\varepsilon_2 = \varepsilon_{2(bulk)} + (\omega_p^2 / \omega^3)(v_F/R) \qquad (2.2)$$

where $\omega$ is the light frequency, $\omega_p$ the plasmon frequency, $v_F$ the electron velocity at the Fermi level and R the particle radius($R/v_F$, mean time of the free movement of the electrons).

Resonance with the incident light is reached at the wavelength, where the negative value of $\varepsilon_1$ of the metal is equal to twice the dielectric constant of the medium (eq. 2.1 above). Silver particles have the unique property that plasmon absorption and interband transitions occur in separated wavelength regimes, while Gold and copper are metals which also possess plasmon resonances in the visible (Au 520 nm; Cu 570 nm); however, these resonances are superimposed by interband transitions. *This property of silver makes it an ideal candidate to study the effect of surface modification using*

*various surfactants on colloidal particles* [16]. A prerequisite for the formation of an intense plasmon absorption band is that $\varepsilon_2$ of the metal is not too large.

Resonance is produced by a collective excitation of all the free electrons in the particles. As is shown in the figure 2.5, the movement of the electrons under the influence of the electric field vector of the incoming light leads to a dipole excitation across the particle sphere, the positive polarization charge acting as a restoring force, which makes the electrons oscillate.

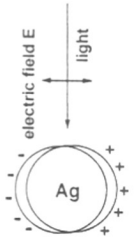


**Figure 2.5:** Polarization of a spherical metal particle by the electrical field vector of the incoming light.

Thus, the electron density within a surface layer, the thickness of which is about equal to the screening length of a few angstroms, oscillate, whereas the density in the interior of the particle remains constant ("surface plasmon"). Therefore, any changes in the electron density of this surface layer, will lead to changes in the plasmon absorption.

### 2.2-2 Effect of Agglomeration of colloidal particles on the optical spectra:

A large change in the absorption spectra is seen when the colloidal particles agglomerate. It arises mainly due to the formation of linear strings of small spherical particles, for which the polarizability is anisotropic on account of coupling between the plasma modes of the individual constituent spheres [17]. It has been shown that there are two plasma modes which are prominent in extinction, and they are in-phase coupled oscillations of the individual sphere dipoles respectively perpendicular and parallel to the string axis. The transverse mode remains at roughly the sphere resonance wavelength while the longitudinal mode moves to longer wavelengths with increase in the length of the string.

These colloidal metal particles when transferred into films [18] the plasmon absorption maxima was found to red shift as is obvious from equation 2.1. In a recent

report, Pileni *et al* have reported that the plasmon absorption further shifts to red because of the coupling of plasmon frequencies of the neighboring clusters when these clusters are arranged in close-packed region [18].

### 2.2-3 UV-visible Spectroscopy of Semiconductor Colloids

UV-visible spectroscopy is also used as finger print technique for measuring the size of the semiconducting particles. It is well known that as the cluster size decreases below the bulk limit, the first excited electronic state shifts to higher energies. Brus [19-20] has derived an analytical approximation for the lowest energy eigenvalue (first excited electronic state) as function of cluster size for semiconductor particles which agrees very well with experimentally determined "band gap" values for different semiconductor nanoparticles [21]. The expression is [19] :

$$E(R) = E_g \cdot \frac{h^2 \cdot \pi^2}{2 \cdot R^2} \cdot \left( \frac{1}{m_e} + \frac{1}{m_h} - \frac{1.8 \cdot e^2}{\varepsilon \cdot R} \right) \quad \text{.....(2.3)}$$

where $E_g$ is the bulk band gap, R is the cluster radius, $m_e$ and $m_h$ are the effective masses of the electron and hole respectively in the cluster and all other parameters have their usual meaning.

## 2.3 QUARTZ CRYSTAL MICROGRAVIMETRY

The advantages of conceptual simplicity, relative ease of modification, chemical inertness of the substrates, low cost, and ready availability of piezoelectric transducers makes quartz crystal microgravimetry(QCM) a very powerful technique to study various adsorption processes. QCM is extensively used to investigate adsorption of self-assembled monolayers of n-alkyl thiols on Au surface [22]. Recently OKahata *et al* have used quartz crystal as a substrate for LB films and studied the swelling and flaking behavior of LB films in a water phase [23]. Roser and co-workers [24] used in-situ QCM measurements to analyze entrainment characteristics of mixed behenic acid/behenate salt LB films deposited vertically on QCM and modeled it by a combined first-order rate equation derived from fick's law. For the work discussed in this thesis. QCM has been extensively used for calculating volume fraction of clusters incorporated in the organic matrix and to follow the kinetics of cluster incorporation.

Quartz crystal microgravimetry comprises a thin quartz crystal sandwiched between two metal electrodes that establishes an alternating electric field across the crystal, causing vibrational motion of crystal at its resonant frequency. In 1850, Jacques & Pierre Curie discovered that a mechanical stress applied to the surface of various crystals like rochelle salt, quartz and tourmaline, afforded a corresponding electrical potential across the crystal whose magnitude was proportional to the applied stress [25]. Shortly after their initial discovery, converse piezoelelctric effect was also verified, in which application of a voltage across these crystals afforded a corresponding mechanical strain. The inverse piezoelectric effect is the basis of the QCM. AT-cut quartz resonator, in which thin quartz wafer is prepared by slicing a quartz rod at an angle 35° with respect to the x axis of crystal resonates in the thickness shear mode. Application of electric field across the crystal causes a vibrational motion of the quartz crystal, with amplitude parallel to the surface of the crystal [26]. The result of the vibrational motion of the quartz crystal is the establishment of a transverse acoustic wave that propagates across the thickness of the crystal, reflecting back into the crystal at the surfaces. When a uniform layer of foreign material is added to the surface of the quartz crystal, the acoustic wave will travel across the interface, and will propagate through the layer. This leads to decrease in the frequency of the crystal. Frequency changes on deposition of the film can be converted to mass loading using the Sauerbrey formula [27].

$$\Delta f = -2 \cdot f_o^2 \cdot \frac{\Delta m}{A \cdot \left(\mu_q \cdot \rho_q\right)^{\frac{1}{2}}} \qquad (2-4)$$

where $\Delta f$ - frequency shift, $f_o$ - frequency of the crystal prior to a mass change, $\Delta m$ - mass change, A - Piezo electrically active area, $\rho_q$ - density of quartz , $\mu_q$ - shear modulus for quartz. ($\mu_q = 2.95 \times 10^{11}$ g cm$^{-1}$ s$^{-2}$, $\rho_q$=2.65g/cm$^3$ ).

### 2.3-1 High Mass Loading

As mass loading is increased, the sensitivity of the QCM decreases, which can be readily understood by inspection of Sauerbrey equation. High mass loading will result in a significant decrease in $f_o$ during the process, resulting in a decrease in the

numerator of the Suerbrey equation with a corresponding decrease in QCM sensitivity. QCM measurements mentioned in this thesis were performed on a FTM5 microbalance using 6MHZ quartz crystal. The stability and resolution of the microbalance was ± 1HZ, yielding a mass sensitivity of 12.1 ng/cm$^2$. Typically, QCM measurements are considered accurate provided the mass of the film does not exceed 2% of the mass of the crystal.

### 2.3-2 Volume fraction calculation of clusters in Langmuir-Blodgett films:

The cluster density is defined in terms of percentage of volume fraction which is volume clusters divided by total volume of film (volume of clusters + volume of organic molecules). Volume fraction of clusters in the film is calculated as follows.

$$\text{Volume\_fraction} = \frac{\text{Volume}_{\text{clusters}}}{\text{Total\_Volume\_film}} \qquad (2 - 5)$$

Since the film consists of clusters embedded in the bilayer of amine,

$$\text{Total\_Volume\_film} = \text{Volume}_{\text{clusters}} + \text{Volume}_{\text{amine}} \qquad (2 - 6)$$

where volume of amine is calculated as

$$\text{Volume}_{\text{amine}} = \text{Mass}_{\text{amine}} \cdot \text{Density}_{\text{amine}} = \frac{2 \cdot A}{a} \cdot \frac{\text{Mol\_Wt}_{\text{amine}}}{\text{Avagadro\_No}} \qquad (2 - 7)$$

where 'a' is the area per molecule at film transfer on quartz crystal and A is the area on the crystal sensitive to mass loading which in the case of the crystal used for the measurement in the thesis is 0.664 cm$^2$. Total weight of the film is calculated from the frequency change obtained for the deposition of one bilayer of the cluster film. Therefore volume of clusters is calculated as

$$\text{Volume}_{\text{cluster}} = \frac{\text{Mass}_{\text{film}} - \text{Mass}_{\text{amine}}}{\text{Density}_{\text{metal}}} \qquad (2 - 8)$$

## 2.4 OPTICAL INTERFEROMETRY:

Optical Interferometry has been used to measure the thickness of the films. Interferometry is based on the fact that light reflected from the front and back interfaces of a film travels different distances, giving rise to interference effects. The thickness 'd' of the film is given by the following relation.

$$d = \Delta N\lambda/2 \qquad (2.9)$$

where, $\Delta N$ is the step height in fringes and $\lambda$ is the monochromatic wavelength of light.

## 2.5 ELLIPSOMETRY:

Ellipsometry has emerged as one of the most versatile techniques for the study of optical properties of thin films on either solid or liquid surfaces. The technique, which is based on the principle that the state of polarization of light changes on reflection from an interface, is extremely sensitive to the changes in the optical constants of the surface. This technique is also known as reflection polarimetry or polarimetric spectroscopy. In its broadest sense, ellipsometry is measurement of the state of polarization of light. *Paul Drude* was the first to develop fundamental equations of ellipsometry, which demonstrated potential monolayer sensitivity for the detection and characterization of thin films on specular surfaces [28].

When a polarized light beam reflects from any specular surface, changes occur in both the amplitude and phase of the oscillating parallel and perpendicular vector components of the electric field associated with the beam. The main objective of an ellipsometry experiment is to measure these amplitude and phase changes, which provide us information about the reflecting surface through the Fresnel reflection coefficients [29]. In this study, null ellipsometry has been used for the study of thin nanoparticle multilayer films.

## 2.5-1 NULL ELLIPSOMETRY

### 2.5-1a Measurement of ellipsometric angles Ψ and Δ - Calculation of thickness of film:

All the measurements which have been discussed in the thesis were performed for different thickness films on Si(111) on a Gaertner L 118 manually operated null ellipsometer in the polarizer-compensator-sample-analyser (PCSA) mode. The basic experimental setup of the null ellipsometer used in the study of the optical properties of thin colloidal metal and organic composite films is shown in figure 2.6.

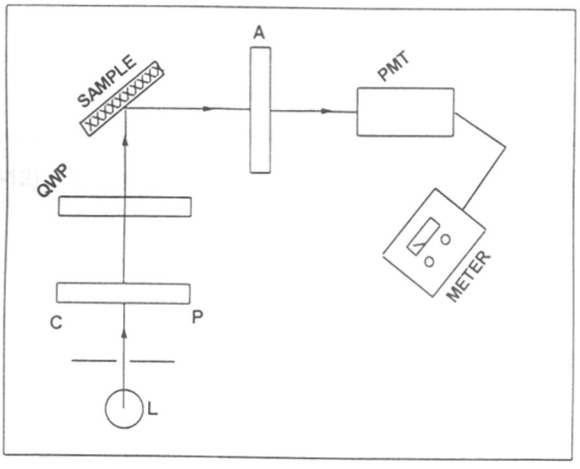


Figure 2.6: Schematic of the various optical elements and their configuration in the null-ellipsometry measurements.

The light source (L) is a monochromatic He-Ne laser (λ = 6328 Å) with a collimator (Fig). The azimuths of the polarizer (P) in conjunction with a compensator (QWP, a quarter wave plate made of mica) determine the state of polarization of the light incident on the sample surfaces (S). The azimuth of the compensator was kept fixed at 45° with respect to the plane of incidence for all measurements reported in this thesis. In null ellipsometry, the state of polarization of the incident light is adjusted by changing the azimuth of the polarizer (P) such that the light reflected from the sample surface is linearly polarized. This can be checked using another polarizer, the analyzer (A) which would give extinction of light under crossed conditions. To obtain improved sensitivity a photo multiplier tube (PMT) is used to detect the null position. Under these null conditions, the ellipsometric angles Ψ and Δ are related to the Fresnel coefficients of

their reflecting surface and the azimuths of the analyzer and polarizer ($A_o$ and $P_o$ respectively) through equation (2-10).

$$\rho = \frac{r_p}{r_s} = \tan\psi \exp(i\Delta) \qquad (2 - 10)$$

where $r_p$ and $r_s$ are Fresnel reflection coefficients [30]

$$\Psi = A_o \text{ and } \Delta = 270 - 2P_o \qquad (2 - 11)$$

In case where a uniform thin film of refractive index $n_1$ and thickness d rests on a infintely thick substrate of refractive index $n_2 - i.k_2$ ( the substrate may be absorbing at the wavelength used for the measurement, hence the imaginary component to the refractive index), the whole system being in an ambient of refractive index $n_o$ (figure 3), the Fresnel reflection coefficients are related to the system material properties through the equation (2-12). For the sample with multiple interfaces, $r_p$ and $r_s$ are given as follows [31]

$$r_{pj} = \frac{n_j \cdot \cos(\phi_j - 1) - n_{j-1} \cdot \cos(\phi_j)}{n_j \cdot \cos(\phi_j - 1) + n_{j-1} \cdot \cos(\phi_j)} \qquad j = 1, 2, \ldots\ldots (2 - 12a)$$

$$r_{sj} = \frac{n_{j-1} \cdot \cos(\phi_j - 1) - n_j \cdot \cos(\phi_j)}{n_{j-1} \cdot \cos(\phi_j - 1) + n_j \cdot \cos(\phi_j)} \qquad j = 1, 2, \ldots\ldots (2 - 12b)$$

In the case of the study under consideration in the thesis, there are only two interfaces and hence the range variable runs only up to 2. Reflection from the two interfaces (ambient-film and film-substrate) introduces a phase shift

$$\delta = 2\pi / \lambda \; n_1 \; d \cos(\phi_1) \qquad (2 - 13)$$

With incorporation of Equation 2-12 in 2-10, the exact equation of ellipsometry now becomes

$$\tan(\psi)\cdot\exp(i\cdot\Delta)=\frac{\left(r_{p1}+r_{p2}\cdot e^{-2\cdot i\cdot\delta}\right)\cdot\left(1+r_{s1}\cdot r_{s2}\cdot e^{-2\cdot i\cdot\delta}\right)}{\left(1+r_{p1}\cdot r_{p2}\cdot e^{-2\cdot i\cdot\delta}\right)\cdot\left(r_{s1}+r_{s2}\cdot e^{-2\cdot i\cdot\delta}\right)} \qquad (2-14)$$

Equation (2-14) involves complex quantities and yields two equations on separating the real and imaginary parts: thus one set of measurements of $\Psi$ and $\Delta$ under certain experimental conditions can be used to determine two unknowns such as the thickness and refractive index of the film. Equation (2-14) cannot be inverted analytically and must therefore be solved numerically. A small application written in Mathcad, written by Murali Sastry [32] was used to numerically solve these equations and calculate the thickness of the films.

In order to find out the thickness of the film containing the colloidal particles, it is important to know the refractive index of the film colloidal particle composite. The effective refractive index of the composite film was determined using Maxwell - Garnett Formalism.

### 2.5-2 Maxwell-Garnett formalism:

Like the Mie theory, the Maxwell-Garnett formalism is also effective medium approximation theory. The particles of interest are orders of magnitude smaller than the wavelength of the incident light, and furthermore the volume fraction of metal in the medium ("the filling factor", f ) is very small. Assuming the size distribution to be monodispersed, the theory predicts an effective dielectric permeability $\varepsilon_{eff}$ according to [33]

$$\varepsilon_{eff}=\varepsilon_m\cdot\frac{1+\frac{2}{3}\cdot f\cdot\alpha}{1-\frac{1}{3}\cdot f\cdot\alpha} \qquad (2-15)$$

for particles dispersed in a medium characterized by a dielectric permeability $\varepsilon_m$. $\alpha$ is the polarizability of the particles in the medium of dielectric permeability $\varepsilon_m$ given by

$$\alpha=3\cdot\frac{\varepsilon_c-\varepsilon_m}{\varepsilon_c-2\cdot\varepsilon_m} \qquad (2-16)$$

The filling factor, f could be got from Quartz crystal Microbalance measurements as explained in the this chapter [page 13, section 2.3-2] and $\varepsilon_c$. $\varepsilon_c$ for various materials are available in literature. [ for example, silver - 1.278 - i.1.364 , gold - 1.315 + i 1.524 [34] and Cds - 2.48 + i 0.03 [35].

## 2.6 FOURIER TRANSFORM INFRA-RED SPECTROSCOPY OF FATTY LIPID METAL COMPOSITES

### 2.6-1 Principle:

The atoms in a molecule do not remain in a fixed relative position and vibrate about some mean position. Due to this vibrational motion if there is a periodic alteration in the dipole moment then such mode of vibration is infrared (IR) active. The IR region of the electromagnetic spectrum is 100 μm - 1μm wavelength. The vibrating molecule absorbs energy only from radiation with which it can coherently interact, i.e., the radiation of its own oscillation frequency. The appearance or non-appearance of certain vibrational frequencies gives valuable information about the structure of a particular molecule.

Most published work in this area has been for films deposited on silicon substrates, although other substrates can be used for variety of reasons. It is chemically very stable and generally not very reactive even at high temperatures. It is excellent for optical studies of deposited films in the visible region using reflection techniques. It has no very strong lattice absorption bands in the useful regions of the infrared and thus can be used for transmission studies in this region. To correct for the lattice absorption bands in silicon, a silicon sample is used as a reference. All FTIR data presented in the thesis have been presented as obtained except for baseline correction.

Infra-red Spectroscopy affords an excellent insight into the organization of hydrophobic chain, transport and ion exchange properties of the LB film [36, 37]. Ion exchange/ effect of metal ion for the FTIR measurements discussed in this thesis, a thick LB film of 40 monolayers of colloidal particles in octadecylamine was deposited onto a Si (111) wafer. The IR characterization of the film was carried out on a Nicolet 60 SXB FTIR spectrometer operated in the transmission mode at a resolution of 2 $cm^{-1}$. A total of 500 scans yielded a good signal to noise ratio of the IR spectra.

IR studies on vacuum deposited long chain fatty amine film have been used to obtain information of the organization of the hydrocarbon chains as clusters diffuse into the film. FTIR measurements of 1000Å thick octadecylamine film on Si(111) substrates, as a function of cluster incorporation time were carried out ex-situ. Thorough washing and drying of the films was done prior to FTIR measurements. The measurements were made in transmittance mode on a Unicam Genesis FTIR spectrometer operated at a resolution of 2 $cm^{-1}$. A total of 500 scans yielded a good signal to noise ratio for the IR spectra. In transmission mode, the electric field component, E is in the plane of the substrate. The nature of the orientation of molecules on the substrate surface can then be determined from the IR spectrum using the dipole selection rule. According to this rule, only those vibrational modes with dipole moment components parallel to the electric field component are excited. The IR spectrum, therefore have vibrational features with components parallel to the substrate.

### 2.6-2 Peak assignments for Fatty lipids:

The fatty lipids used in this thesis are Octadecylamine, Arachidic Acid and Lauric acid, and the peak assignments have been discussed in general.

#### 2.6-2a *$CH_2$ scissoring band:*

It has been established that the splitting of the $CH_2$ scissoring vibration is caused by crystal field and is characteristic of ortho-rhombic subshell packing. It appears as a doublet at 1473 and 1465 $cm^{-1}$ [38]. Increase in splitting of scissoring band is a measure of the crystallinity in the film [39]. On the other hand, the frequency (1468 $cm^{-1}$) of the singlet due to the $CH_2$ scissoring mode is observed for the hexagonal subshell packing where each hydrocarbon chain is freely rotated around its axis oriented perpendicular to the membrane surface.

#### 2.6-1b *$CH_2$ wagging vibration:*

It is known that band progression arising from the $CH_2$ wagging vibrations of the trans-zigzag hydrocarbon chains appears in the region between 1400 and 1180 $cm^{-1}$ [40]. The band progression due to $CH_2$ wagging vibrations of long-chain fatty acids has been studied in detail by Hayashi and Umemura [41] where they have pointed out that there is a distinct difference in the frequencies between bands due to cis and trans configurations of a molecule. The presence of these progression bands as a series of well resolved peaks is a strong indicator of crystallinity. For example, in the liquid phase

IR spectra of linear alkanes, these bands are weak, broad features, whereas sharp features are seen for the crystalline phase [42-44]. This region of the spectrum is also rich in defect-related bands [45]. Shyder has pointed out that there are four wagging bands between 1300 and 1400 $cm^{-1}$ which can be assigned to defect structures [44].

**2.6-1c *C-H Stretching region:***

The two bands at 2920 and 2850 $cm^{-1}$ have been assigned to the antisymmetric and symmetric $CH_2$ stretching vibrations respectively and two weak bands at about 2960 and 2875 $cm^{-1}$ to the asymmetric/degenerate and symmetric $CH_3$ stretching vibrations respectively. C-H stretching region (2800 - 3000 $cm^{-1}$) has been used to study 2-D self assembled monolayers to determine the orientation of the methylene chains [46-48]. Our experiments, based on transmission IR spectroscopy and of monolayers that are randomly oriented with respect to the beam are not sensitive to this type of information. Nevertheless, the C-H stretching region still holds valuable information. For example, the position of the peaks and the increase in intensity of the methylene stretching vibrations relative to methyl stretching vibration with chain length indicates structural integrity of the molecule. More interestingly, actual peak values of the symmetric and antisymmetric $CH_2$ stretching vibrations, can be used as a sensitive indicator of the ordering of the alkyl chains[46-49]. For example, Nuzzo *et al* reported that the $d^-$ and $d^+$ values for hexadecanethiolate monolayer on gold surface appear at 2920 and 2850 $cm^{-1}$ respectively and concluded that the number of gauche defects in the methylene chains was small [46, 47]. Similarly Porter *et al* reported that monolayers with chains longer than 6 carbon atoms in the alkyl chain, were highly ordered, whereas the smaller molecules resembled the liquid state, i.e., high density of gauche defects ($d^+$ and $d^-$ - 2855 and 2924 respectively).

**2.6-1d *N-H vibrations:***

Typical peaks for the free amine are seen at 3331 $cm^{-1}$. This band shifts to 3198 $cm^{-1}$ on salt formation of primary amine [50, 51]. $NH_3$ symmetric deformation band is observed at 1487 $cm^{-1}$ in case of pure amine and is absent in case of amine salts of chloroplatinic acid. The $NH_3$ antisymmetric deformation appears in the region of 1587 $cm^{-1}$ [52].

## 2.7 TRANSMISSION ELECTRON MICROSCOPY:

The most comprehensive and accurate structure studies are possible with Transmission Electron Microscopy. Film is deposited onto a standard electron microscopy grid of 1/8 inch diameter coated with a carbon film transparent to electrons. Diffraction camera consists of an electron gun, an aperture to define a small beam cross section, a specimen holder and a fluorescent screen and plate camera. Measurements are usually carried out in diffraction mode and in the microscopy mode. The advantage of this arrangement is the possibility of directly viewing the area of which the diffraction pattern arises. The specimen is illuminated by a double-condenser system which allows one to choose the divergence of the incident beam and the size of irradiated specimen area. After passing through the specimen, the beam traverses the objective lens. The specimen image generated by the objective lens is subsequently magnified in one or two more magnification stages by the intermediate and projector lens and projected onto a fluorescent screen or photographic plate. For the TEM measurements discussed in this thesis the beam voltage of 80KV was used.

## 2.8 X-RAY PHOTOELECTRON SPECTROSCOPY

Photoelectron spectroscopy is a surface science technique used in understanding atoms, molecules & solids on the surface. It is based on the well-known photoelectric effect first explained by Einstein in 1905. If photons of energy $h\nu$ shined on a solid having the work function $\phi$ , then the max. kinetic energy $E_k$ of photoemitted electron is given by (figure 1)

$$E_k = h\nu - E_b - \phi \qquad (2.17)$$

where $E_b$ is the binding energy of electron in solid. Employing photons with fixed energy $h\nu$, it is obvious that if kinetic energy $E_k$ and work function $\phi$ of the sample are measured, it is possible to measure binding energy of electron in solid. Binding energies being characteristic of atoms, different elements present in the sample under investigation are identified. Electrons traveling through a material have a relatively high probability of experiencing inelastic collisions with locally bound electrons as a result of which they suffer energy loss. Due to inelastic scattering process, the flux of photoelectrons emerging from the sample is much attenuated. While the exciting photons penetrate deep into the solid sample, the photoelectrons can escape from only

a very short distance beneath the surface (< 100 Å). Therefore photoelectron spectroscopy is a *surface sensitive technique.*

## 2.9 References

1. Tabor, D.J.; *J. Colloid Interface Sci.*, **1980**, *75*, 240.
2. Franklin, B.; *Phil. Trans.R.Soc.*, **1774**, *64*, 445.
3. a)Pockels, A.; *Nature*, **1891**, *43*, 437. b) Pockels, A.; *Nature*, **1892**, *46*, 418, c)Pockels, A.; *Nature*, **1893**, *48*, 152. d) Pockels, A.; *Nature*, **1894**, *50*, 223.
4. a) Blodgett, K.A.; *J. Am. Chem. Soc.*, **1935**, *57*, 1007, b) Blodgett, K.A.; *Phys. Rev.*, **1937**, *51*, 964.
5. Langmuir, I.; *J. Am. Chem. Soc.*, **1917**, *39*, 1848.
6. Ganguly, P.; Paranjape, D.V.; Sastry, M., *Langmuir*, **1993**, *9*, 577.
7. Langmuir, I.; Shaefer, V.J.; *J. Am. Chem. Soc.*, **1938**, *57*, 1007.
8. Tabor, D.J.; *J. Colloid Interface Sci.*, **1980**, *75*, 240.
9. Peterson, I.R.; Russell, G.J.; Roberts, G.G.; *Thin solid films*, **1983**, *109*, 371.
10. Blodgett, K.A.; *J. Phys. Chem.*, **1937**, *41*, 975.
11. Creighton, J.A.; Eadon, D.G.; *J. Chem. Soc., Faraday Tras.* , **1991**, *87*, 3881.
12. Mie. G.; *Ann. Phys.* **1908**, *25*, 377.
13. Aden, A.L.; Kerker, M. *J. Appl. Phys.* **1951**, *22*, 1242.
14. Kerker, M. *The Scattering of light and Other Electromagnetic Radiation,* New York, **1969.**
15. Kreibig, U.; von Fragstein, C. *Z. Phys.* **1969**, *224*, 307. Kreibig, U. *J. Phys. F* **1974**, *4*, 999.
16. Henglein, A.; *J. Phys. Chem.* **1993**, *97*, 5764.
17. Blatchford, C.G.; Campbell, J.R.; Creighton, J.A.; *Surface Science*, **1982**, *120*, 435.
18. Taleb, A.; Petit, C.; Pileni, M.P.; *J. Phys. Chem. B*, **1998**, *102*, 2214.
19. Brus, L.E.; *J.Chem.Phys.*, **1984**, *80*, 4403.
20. Brus, L.E.*J.Phys.Chem.*, **1986**, *90*, 2555.
21. Henglein, A.; *Chem.Rev.*, **1989**, *89*, 1861.
22. Brust, M.; Etchonique, R.; Calvo, E.J.; Gordillo, G.J.; *J.C.S. Chem. Comm.*, **1996**, 1949.

23. Okahata, Y.; Ebato, H.; *Anal. Chem.* **1989**, *61*, 2185.
24. Lovell, M.R.; Roser, S.J.; *Langmuir*, **1996**, *12*, 2765.
25. Curie, P., Curie, J. *C. R. Acad. Sci.*, **1880**, *91*, 294.
26. Buttry, D.A.; Ward, M.D.; *Chem. Rev.*, **1992**, *92*, 1355.
27. Sauerbrey, G.; *Z. Phys.*(Munich), **1959**, *155*, 206.
28. Hall, A. C.; *Surf. Sci*, **1969**, *16*, 1.
29. Azzam, R.M.A.; Bashara, N.M.; *Ellipsometry and Polarized Light.*; **1977**, North-Holland: Amsterdam.
30. Fresnel reflection coefficients are complex quantities describing the ratio of the reflected electric field component to the incident field component for the *p* and *s* directions, respectively. Thus, they are a measure of the amplitude ratio and phase difference upon reflection for the subscripted component. The Fresnel reflection coefficients, $r_p$ and $r_s$ are defined as ratios of the reflected and incident electric fields (including both the amplitude and complex phase factors) for the *p* and *s* components.
31. Easwarakanthan, T; Mas, P; Renard, M; Ravelet, S; *Surf. Sci.*, **1989**, *216*, 198.
32. The ellipsomety calculations for determination of the film thickness were done using an application written by M.S. in Mathcad (a commercial mathematical package of Mathsoft Inc.). The application, ELLIP1.MCD, is available from the Mathsoft public domain on the internet.
33. Granqvist, C.G.; Hunderi, O.; *Phys. Rev. B*, **1977**, *16*, 3513.
34. P.B. Johnson and R.W. Christy, *Phys.Rev.B.*, 1972, **6**, 4370.
35. J. Gottesman and W.F.C. Ferguson, *J.Opt.Soc.Amer.*, 44 (1954) 368.
36. Marshbanks, T.L.; Ahn, D.J.; Franses, E.I. , *Langmuir,* **1994**, *10*, 276.
37. Marshbanks, T.L.; Ranses, E.I.; *J. Phys. Chem*, **1994**, *98*, 2166.
38. Shyder, R.G.; *J. Mol. Spectrosc.***1961**, *7*, 116.
39. Rabolt, J.F.; Burns, F.C.; schlotter, N.E.; Swalen, J.D.; *J. Chem. Phys.* **1983**, *78*, 946.
40. Shyder, R.G.; *J. Mol. Spectrosc.* , **1960**, *4*, 411.
41. Hayashi, S.; Umemura, J.; *J. Chem. Phys.*, **1975**, *63*, 1732.
42. Maroncelli, M.; Qi, S.P.; Strauss, H.L.;
43. Snyder, R.G.; *J. Am. Chem. Soc.*, **1982**, *104*, 6273.
44. Snyder, R.G.; *J. Chem. Phys.*, **1967**, *47*, 1316.

45. Hostetler, M.J.; Stokes, J.J.; Murray, R.W.; *Langmuir*, **1996**, *12*, 3609.

46. Nuzzo, R.G.; Fusco, F.A.; Allara, D.L.; *J. Am. Chem. Soc.*, **1987**, *109*, 2358.

47. Nuzzo, R.G.; Dubois, L.H.; Allara, D.L. *J. Am. Chem. Soc.*, **1990**, *112*, 558.

48. Porter, M.D.; Bright, T.B.; Allara, D.L.; Chidsey, C.E.D. *J. Am. Chem. Soc.*, **1987**, *109*, 3559.

49. Ulman, A.; *Introduction to Ultrathin Organic Films;* **1991**, Academic; New York.

50. Bardosova, M.; Tregold, R.H.; Ali-Adib, Z. *Langmuir* **1995**, *11*, 1273.

51. Pal, S; *Ph.D. Thesis*, **1996**, University of Pune.

52. Ning, G.; Guangfu, Z.; Shiquan, X.; *J. Mol. Struc.*., **1992**, *275*, 85.

# CHAPTER III

## Surface Modification of Colloidal Particles

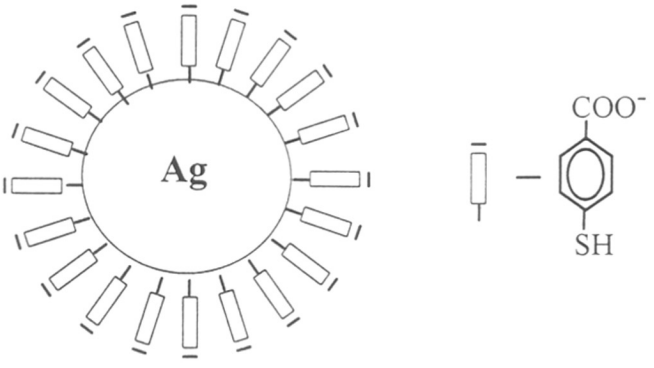


Derivatization of colloidal particles of silver, gold and cadmium sulfide with ionizable functional group by a self-assembly process has been described in this chapter

Part of the work discussed in this chapter has been published: 1) Sastry, M.; Mayya, K.S.; Bandyopadhyay, K. *Coll.Surf.A.* **1997**, *127*, 221; 2) Mayya, K.S.; Patil, V.; Sastry, M. *Langmuir* **1997**, *13*, 3944. 3) Mayya, S.K.; Patil, V.; Sastry, M. *Langmuir*, **1997**, *13*, 3944 4) Patil, V.; Mayya, K.S.; Pradhan, S.D.; Sastry, M. *J. Am. Chem. Soc.* **1997**, *119*, 9281. 5) Sastry, M.; Mayya, K.S.; Patil, V. *Langmuir*, **1998**, *14*, 5921

## 3.1 Introduction

Long chain alkane thiols in solution were found to spontaneously form a close-packed monolayer on metal surfaces [1]. The thiol forms a covalent linkage with the metal surface. It was later found that molecules with many other functional groups also self-assemble to form close-packed monolayers [1]. This strategy of self-assembly was used for surface modification of metals, and then for a variety of applications such as Chemical sensors [2] high density memory devices [3] etc. Self-assembled monolayers (SAMs) [4] provide a versatile route for surface modification important in a multitude of applications ranging from non-linear optical materials [5], as substrates for cell growth [6], high density memory devices [7] and in the formation of nanoparticle monolayer films via covalent attachment [8 c, e]. The above list is by no means exhaustive and newer applications continue to emerge as our understanding of the electronic and chemical properties of SAMs progresses.

Surface modification of colloidal particles has been studied with great interest following the work of Brust *et al* [9] wherein it was demonstrated that alkanethiol molecules could be self-assembled onto colloidal gold particles. This has led to the exciting possibility of modification of the chemical and physical properties of colloidal particles through the use of terminally functionalized capping molecules [10]. The terminal functionality provides an additional degree of freedom that may be used for various applications.

The process of capping colloidal metal particles such as gold and silver with surfactant molecules containing thiol groups (like alkane thiols) may be viewed as "*three dimensional self-assembly*" (3D SAMs) [11], which is expected to be different from self-assembly on planar surfaces(2D SAMs), a well investigated area [12]. There are two major differences between 2D and 3D SAMs [10b, 11]. First is that due to the higher concentration of surface defect-like sites on the clusters leads to higher density of alkanethiolates as compared to 2D Au(111) surfaces. Secondly due to the high radius of curvature of cluster's surface, the methylene units of the alkane chains become progressively less densely packed as one moves further away from the Au core. This means that the outermost functional groups will exhibit greater liberty of movement than those near the core. Murray *et al* carried out a detailed work on 3D self assembly of n-alkane thiols and different aspects of functionalization [10d-e, 11, 12b] of monolayer protected clusters(MPC's). $C^{13}$ NMR spectra showed the absence of resonances of

methylene units proximate to the cluster in the cluster compounds [12], which by Murray *et al* [12b] attributed to the discontinuity in the diamagnetic susceptibility at the gold-hydrocarbon interface and residual dipolar interactions in the alkanethiol monolayer. Badia *et al* [12a] using NMR and Electron Microscopy measurements observed that in the MPC's stabilized using long chain alkane thiols (n=16,18) the chains (for carbon atoms which are not proximate to the cluster core) were in crystalline all trans conformation, and was due to the interdigitation of the chains with the neighboring gold particles. The Differential Scanning Calorimetry measurements by Murray *et al* [12b] showed the interdigitation of 2, 3-4, $CH_2$ groups per chain of $C_{12}$ and $C_{16}$ alkanethiols respectively. I.e., the ordered chain interdigitation begins 10-12 units from the Au core. In all the above discussions, the cluster systems used were prepared in the organic phase, and the importance to these systems are obviously because they behave like simple chemical compounds; they can be precipitated, redissolved and chromatographed without any apparent change in properties.

There are also reports of work on MPC's prepared in aqueous solutions, wherein it has been observed that 3D self-assembly is in most respects similar to 2D self-assembly. For example, it has been observed that the flocculation behavior of carboxylic acid derivatized colloidal particles as a function of pH tracks the wetting behavior of carboxylic acid terminated 2D SAMs [10b, 13].

Very recently it has been demonstrated that interdigitated bilayer assemblies of fatty acid molecules form spontaneously on colloidal silver particle surface [14] while such bilayer structures are not observed on planar silver surfaces. This is because of repulsive coulombic interaction between the ionized carboxylic acid groups in the lauric acid molecules which prevent the formation of bilayer assemblies on planar surfaces. However, nanoscale surface curvature of colloidal particles permit interdigitation of the hydrocarbon chains in the bilayers, thereby maximizing the hydrophobic interaction as well as considerably reducing the electrostatic repulsive interactions of the headgroups, leading to stable bilayer assemblies. The strategy based on interdigitated bilayers enables facile derivatization of colloidal particle surfaces without the use of bifunctional molecules, thereby considerably enhancing the scope of using surface-modified colloidal particles as the starting point in the generation of nanoscale architectures [14]. Interdigitated bilayers have been used to stabilize $Fe_3O_4$ nanoparticles, and very

detailed work has been performed in order to understand the amount of interdigitation [15].

### 3.1-1 Applications of surface modified colloidal particles

Literature on Surface modified colloidal particles has been voluminous, and it is beyond the scope of this thesis to discuss all of them. However, some of the important findings in the recent years have been listed below. Surface modified colloidal particles or MPCs, or now mostly known as cluster compounds, have been used extensively, keeping in mind, various applications, including the one reported by Murray *et al* recently where they study the reactivity of heterofunctionalized MPCs and the role of steric effects on reactivity [16]. This is an important step towards the use of cluster compounds as massively polyfunctional chemical reagents. In an important development, Letsinger *et al* have used gold particles for sequence-specific DNA detection because of its application in the diagnosis of pathogenic and genetic diseases [17, 18]. Their system provides a simple means for calorimetric one-pot detection of a target oligonucleotide in the presence of a mixture of oligonucleotides with sequences differing by one nucleotide, regardless of position, in the target region. Sastry *et al* recently have reported a sol-based assay, wherein silver and gold particles were biotinylated by self-assembly of a biotin disulfide molecule, and the reaction of the surface-modified colloidal particles with avidin molecules was studied using optical absorption spectroscopy [19]. The specific interaction of avidin, a tetrameric protein, with biotin leads to cross-linking of the colloidal particles and a consequent growth of a long wavelength absorption peak.

Organization of colloidal particles has been a subject of great interest, and is also the objective of this thesis. People have used various methods to organize colloidal particles. Depending on the method, people have used the colloidal particles in different forms.

a. Cross-linking the cluster to suitably modified substrates [8a,8b] by self-assembly or self-assembling the surface modified clusters [8c-8e]. Some of the features of the former technique as reported by Natan *et al* that common limitations in substrate size and shape are circumvented by this method, since both surface modification of substrates and colloid binding are solution phase processes. This method is flexible

with regard to the underlying solid support in terms of both shape and surface composition.

b. Hydrophobizing these particles and then spreading them at the air-water interface[20]. Fendler *et al* [20a] have synthesized silver particles in aqueous phase, and hydrophobized them with oleic acid. The oleic acid capped clusters were transferred from the aqueous phase to the organic phase by simple mixing of the aqueous sol with organic solvent.

### 3.2 Synthesis and Characterization of colloidal particles

The colloidal route for synthesis of nanoscale particles, which can be traced back to Faraday [21], is one of the most versatile methods for obtaining these particles, affording a great degree of control over mean particle size and particle size distribution. Among the various standardized synthetic routes available in literature [22-26] we have used few of them.

#### 3.2-1 Borohydride Reduction:

Silver, gold and platinum clusters were synthesized using this route. The silver hydrosol was prepared by borohydride reduction of $Ag_2SO_4$ salt solution as detailed by Vukovic and Nedeljkovic [26]. 100ml of Silver sulfate solution of concentration $10^{-4}$M was added into the dry flask containing 0.01g of sodium borohydride and rigourosly stirred.

$$Ag_2SO4 + NaBH_4 \leftrightarrow Ag + BH_4^- + NaOH$$

The colloidal solution had a pH of ~ 10 and was clear and light yellow in color. Optical absorption studies were performed on the as-prepared sol using a UV/vis Hewlett-Packard 8452 diode array spectrometer (2 nm spectral resolution) and yielded a surface plasmon resonance at 386 nm. The sol was also characterised using Transmission electron microscopy (TEM) measurements which was performed using a Philips TEM 301 T instrument operated at 80 KV. The TEM was performed on carbon coated copper grids.

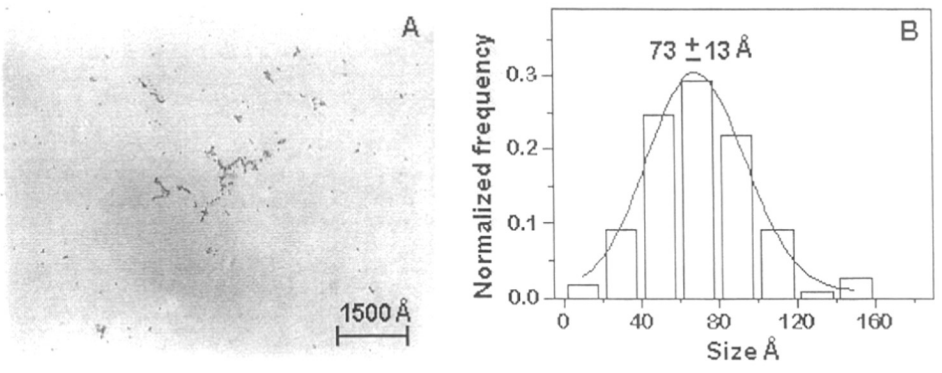


**Fig.3.1** A) TEM Micrograph of silver sol prepared using sodium borohydride reduction B) Particle size distribution of the above micrograph. The histogram was plotted by measuring the size of 200 particles and fitted to a gaussian. The particle mean particle size is 73 Å with standard deviation 12 Å.

20μL of the sol was dried on the grid and observed under the TEM. Fig.3.1A shows a representative micrograph of the silver clusters while the particle size distribution is plotted in Fig.3.1B. A mean cluster size of 73 Å and a standard deviation of 12.3 Å is obtained from the analysis. The resulting 100ml sol was mixed with $10^{-3}$ M 4-CTP in absolute ethanol to give the final concentration of $10^{-5}$ M of 4-CTP, which was rigorously mixed.

Gold particles were similarly synthesized by reducing 100 ml of $1.25 \times 10^{-4}$ M $HAuCl_4$ solution in water using sodium borohydride (0.01 g). A clear red solution was obtained with pH ~ 9. The optical absorption spectra of the sol showed surface plasmon absorption maxima at 510 nm. The TEM measurements were also carried out and the representative micrograph is as shown in Fig 3.2 A. Fig 3.2 A shows the particle size distribution with mean particle size 34Å, with a standard deviation of 7Å. In an attempt to obtain small sized gold clusters, the $HAuCl_4$ ($1.25 \times 10^{-4}$ M) was reduced in the presence of a capping agent, like 4-carboxythiophenol. 100ml of Chloroauric acid solution was mixed with 1 ml of $10^{-3}$ M 4-CTP in absolute ethanol. The concentration of 4-CTP was taken such that the net concentration of molecule in solution after mixing with salt solution was $10^{-5}$ M. The mixture was added to a dry flask containing 0.01g of sodium borohydride. Optical absorption measurements were used to follow the reduction

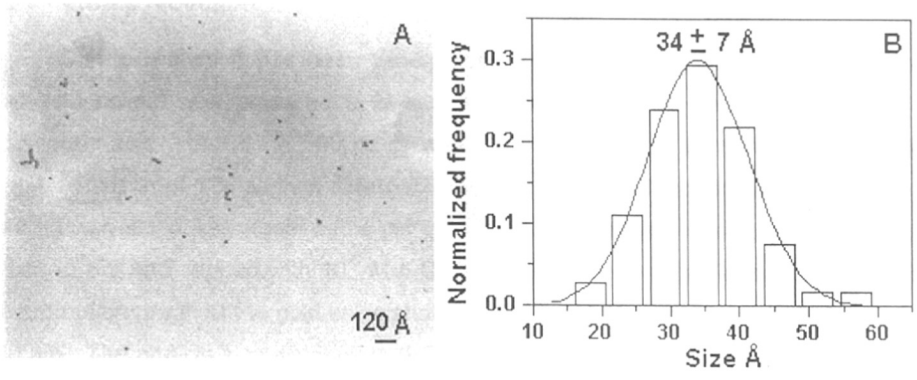


**Figure 3.2** A) Representative TEM micrograph of sodium borohydride reduced gold particles B) Particle size distribution for the above micrograph with mean particle size=34Å, and standard deviation = 7 Å.

process and a plasmon absorption maxima at 502 nm was found to stabilize after 12 hours. pH of the resulting sol was found to be 8.5. TEM measurements were carried out, and a representative micrograph is as shown in figure 3.3A. Figure 3.3B shows the particles size distribution for the same and the particle size was found to be 20 ± 5 Å

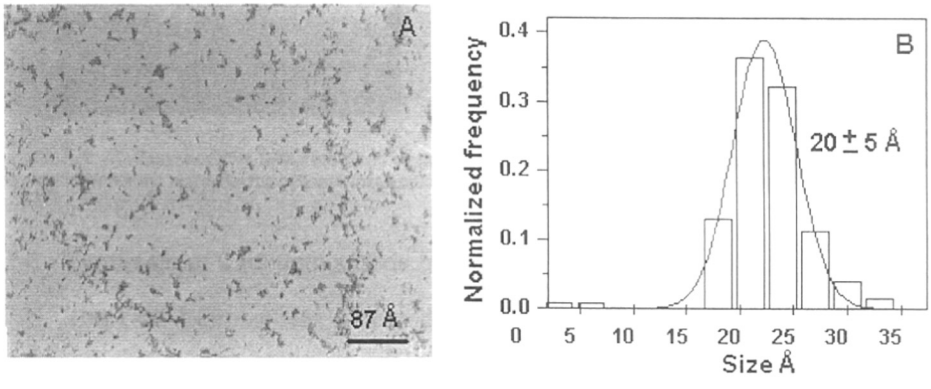


**Figure 3.3** A) Representative TEM micrograph of gold particles obtained by insitu reduction of $HAuCl_4$ in the presence of $10^{-5}$ M 4-CTP. B) Particle size distribution for the above micrograph with mean particle size=20Å, and standard deviation = 5Å.

### 3.2-2 Citrate reduction:

Citrate reduction has been widely used for synthesizing gold, silver particles. The gold colloid was prepared *a la* Lee and Meisel [23] by dissolving 240 mg of chloroauric acid ($HAuCl_4$) in 500 ml of water and the solution brought to a boil after which a solution of 1 % sodium citrate (50 ml) was added with continued boiling for ~ 1 hour. This yielded a hydrosol with a pH of 3. The resultant sol was cooled and the pH raised to 8.5 and capped with $10^{-5}$ M 4-CTP. A typical low magnification transmission electron micrograph of the gold sol is shown in Fig.3.4A, the scale bar corresponding to 120 nm. The particle size distribution (PSD) obtained from the micrographs is shown in Fig.3.4B. A Gaussian fit to the PSD data yielded a mean cluster diameter of 126 Å and a standard deviation of 29 Å.

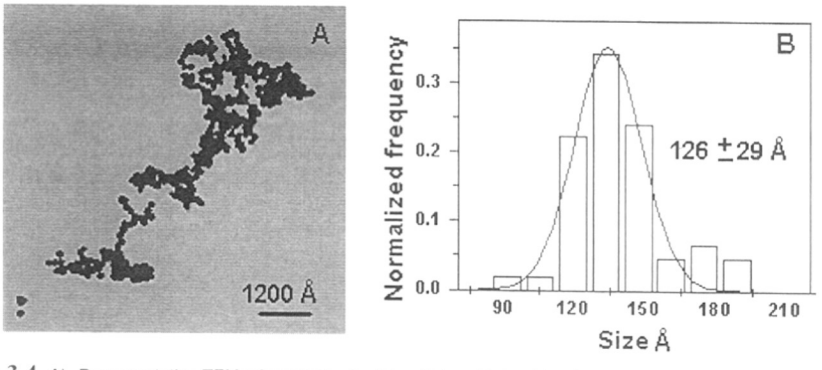


**Figure 3.4** A) Representative TEM micrograph of gold particles obtained by citrate reduction of $HAuCl_4$. B) Particle size distribution for the above micrograph with mean particle size=126Å, and standard deviation = 29Å.

### 3.2-3 Synthesis of Cadmium sulfide particles

The CdS hydrosol was prepared by reacting a $10^{-4}$ M concentrated aqueous solution of $CdSO_4$ with stoichiometric amounts of $Na_2S$ (Cd : S ratio of 1:1) in the presence of the capping molecule, 4-CTP. The concentration of 4-CTP in the aqueous solution was adjusted to $10^{-5}$ M by adding 1ml of 4-CTP dissolved in absolute ethanol to 9 ml of the electrolyte. The reaction was carried out under continuous stirring for 30 minutes after which argon was bubbled in the hydrosol for ca. 40 minutes to remove excess $H_2S$. The formation and stability of CdS colloidal particles stabilized by the bifunctional molecule, 4-CTP, was followed using optical absorption spectroscopy. Figure 3.5 shows the UV-vis spectra for the CdS sol. The absorption edge was found to occur at ~ 450 nm (2.76 eV), which from the particle size-band edge data of Henglein

[27] indicates a cluster size of ~ 3.5 nm and therefore, CdS particles are in the Q-state regime.

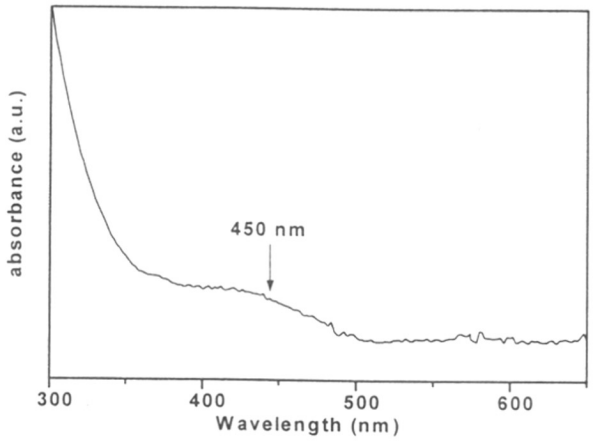


**Figure 3.5** :Optical absorption spectrum from 4-CTP capped CdS hydrosol, showing $\lambda_{max}$ at 450 nm.

### 3.3 Surface Modification

In a freshly prepared colloidal solution, the particles are highly reactive due to very high surface to volume ratio, and tend to flocculate. In order to achieve long term stability of these particles, their surface is modified using suitable surfactants. Many surfactant molecules like alkane thiols, fatty acids, fatty amines and polymers are used for this purpose. However, for a given application as in the case, described in this thesis, clusters have been derivatized with suitable functional groups so that they can be used for organization. It is known that certain molecules spontaneously self-assemble to form close packed monolayers [28]. It is expected therefore that if a surfactant like 4-carboxythiophenol if employed will form a covalent thiolate linkage with the silver colloid surface leaving the carboxylic acid terminal functionality free for organizational purposes. Therefore 4-CTP plays a dual role of capping the clusters as well as charging the clusters (Schematic in the covering page of the chapter). It is known that carboxylic acid group dissociates as

$$COOH \leftrightarrow COO^- + H^+$$

The $pK_a$ for -COOH in 4-CTP was found to be 4.6 [29]. Hence at the pH at which the clusters are synthesized, carboxylic acid groups are completely charged making them highly stable. Figure 3.6 (A) shows the UV-visible spectra of uncapped (a) silver and sol capped by different concentrations of 4-CTP. Spectra b - d represents the sols capped by $10^{-6}$, $10^{-5}$, $10^{-4}$ M concentration of 4-CTP.

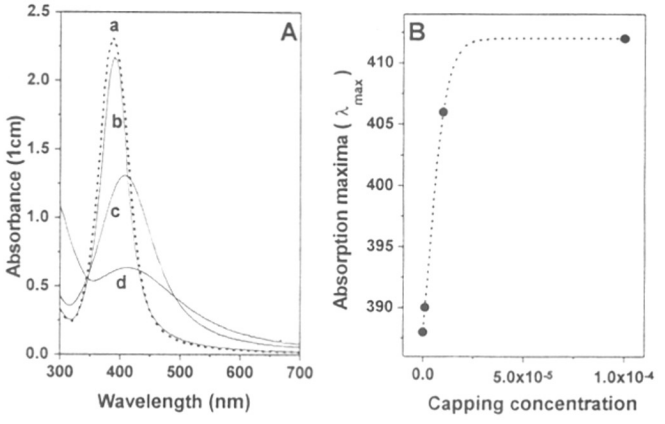


**Fig. 3.6 :** A) shows the UV-visible spectras of uncapped silver and sol capped by different concentrations of 4-CTP. Spectras b - d represents the sols capped by $10^{-6}$, $10^{-5}$, $10^{-4}$, $10^{-3}$ M concentration of 4-CTP respectively. B) shows absorption maxima($\lambda_{max}$) in the optical absorption spectra as a function of capping concentration of the bifunctional molecule.

A systematic red shift followed by damping of the plasmon absorption occurs with increasing capping concentration. Mie theory successfully accounts for the nature of the surface plasmon shifts observed. The plasmon frequency shifts for nucleophilic molecules on silver clusters, have been interpreted qualitatively based on a reduction in the volume available for the free electron gas due to charge localization at the interface [16] which leads to an increase in the effective electron density. The damping may arise due to an increase in the value of $\varepsilon_2$ of silver due to capping molecule adsorption which is related to the lifetime of the plasma oscillations [16]. Figure 3.6 (B) shows absorption maxima($\lambda_{max}$) in the optical absorption spectra as a function of capping concentration of the bifunctional molecule.

### 3.4 Bilayer surfactant assemblies on nanoscale curved surfaces : a new strategy for surface modification of colloidal particles:

As mentioned above due to the high radius of curvature of cluster's surface, the methylene units of the alkane chains become progressively less densely packed as one moves further away from the cluster core. This means that the outermost functional groups will exhibit greater liberty of movement than those near the core. And hence in an aqueous environment, hydrophobic interaction will be maximized by forming interdigitated bilayers. This strategy has been used to derivatize colloidal silver particles as described below.

Scheme 3.1A shows the bilayer formation of fatty acid molecules due to interdigitation of excess fatty acid in the close packed SAM. Optical absorption measurements showed a shift in the surface plasmon resonance from 386 nm for bare silver particles to ~408 nm indicating fatty acid adsorption. The sol capped with lauric acid was found to be exceptionally stable over a long period for concentrations above $10^{-5}$M of lauric acid. Formation of an "interdigitated " bilayer by lauric acid molecule would lead to carboxylic acid derivatization of the particles and explain the observed long term stability. From an application perspective, formation of interdigitated bilayers afford a flexible strategy for derivatization of colloidal particle surfaces *without using terminally functionalized (bifunctional) capping molecules.*

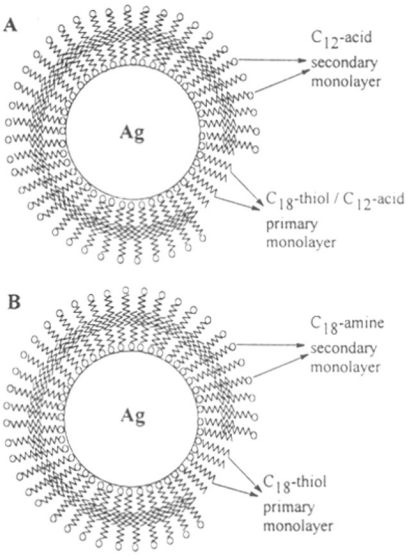


**Scheme 3.1** : A) Cartoon showing the primary and secondary monolayers formed on colloidal silver particles primary monolayer of octadecanethiol followed by lauric acid/octadecylamine secondary monolayer B) the primary and secondary monolayer of lauric acid molecules formed on colloidal silver particles

Therefore if a primary monolayer of say alkane thiol is formed on the metal surface, then it gives us choice of selection of the derivatization using secondary monolayer, i.e., one can either form a secondary monolayer of fatty acid or fatty amine depending on whether the situation needs positively charged or negatively charged cluster for applications. The formation of the primary and secondary monolayers (Scheme 3.1A, B) on the silver colloidal particle surface in sols 1 and 2 [Sol 1 corresponds to alkane thiol as primary monolayer and lauric acid as the secondary monolayer. Sol 2 corresponds to alkane thiol as primary monolayer and octadecylamine as secondary monolayer] was followed stepwise using optical absorption spectroscopy and is shown in Figure 3.7. The colloidal particles were capped with octadecanethiol molecules by mixing 100mL of the hydrosol with 10 mL of an ethanolic solution octadecanethiol whose concentration was adjusted to yield a surfactant concentration of $10^{-5}$ M. At this concentration complete coverage of the silver colloid surface is expected to be achieved with the formation of a primary monolayer (Scheme 3.1). After formation of the alkanethiol primary monolayer, the secondary monolayer incorporation with lauric acid (Sol1, Scheme 3.1 A) and octadecylamine (sol2,Scheme 3.1 B) was achieved in a similar manner using ethanolic solutions of the respective fatty lipids.

Silver exhibits a strong and sharp surface plasmon resonance which is extremely sensitive to surface modification[20] and is therefore a good system for following the adsorption of surfactants using optical absorption spectroscopy. Fig.3.7a shows the optical absorption spectra of the *as-prepared* uncapped silver hydrosol (curve 1), the silver sol 15 min after capping with $10^{-5}$ M octadecanethiol (curve2) , the hydrosol capped with the alkanethiol (curve 2) after further capping with $10^{-5}$ M lauric acid measured 15 min after lauric acid capping (curve 3) and 24 hrs after capping with lauric acid (curve 4, dotted line). It can be seen that the plasmon resonance intensity is reduced at each stage of the primary and secondary monolayer formation which is accompanied by a red shift of the absorption maximum. This clearly shows the sequential formation of a primary alkanethiol and secondary fatty acid monolayer on the silver particle surface. The plasmon resonance wavelength is indicated next to the curves in the figure. We note here that the bilayer capped hydrosol is extremely stable as seen by the almost exact superposition of the spectra recorded after 15 min and 24 hrs of capping with lauric acid (Fig.3.7a, curves 3 and 4).

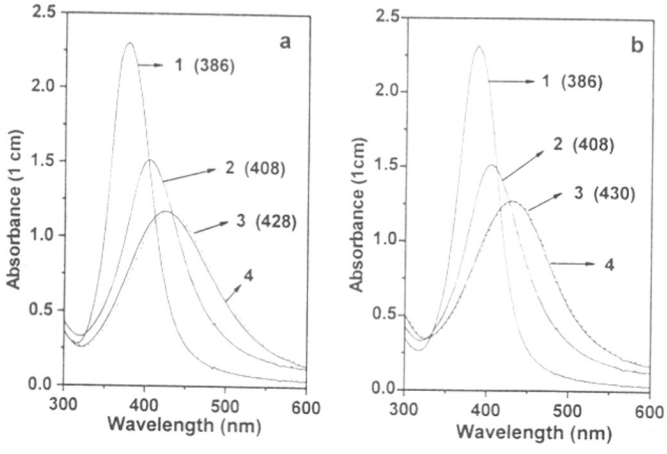


Fig 3.7 : a) Optical absorption spectra of the as-prepared silver sol (curve 1); silver sol capped with $10^{-5}$ M octadecanethiol (curve 2); octadecanethiol capped silver sol on further adsorption of $10^{-5}$ M lauric acid measured 15 min after adsorption (curve 3) and the bilayer capped sol (curve 3) after 24 h of capping with lauric acid (curve 4, dotted line). The surface plasmon resonance wavelengths are given next to the espective spectra.b) Optical absorption spectra of the as-prepared silver sol (curve 1); silver sol capped with $10^{-5}$ M octadecanethiol (curve 2); octadecanethiol capped silver sol on further adsorption of $10^{-5}$ M octadecylamine measured 15 min after adsorption (curve 3) and the bilayer capped sol (curve 3) after 24 h of capping with octadecylamine (curve 4, dotted line). The surface plasmon resonance wavelengths are given next to the respective spectra.

Fig.3.7b shows similar optical absorption spectra for the *as-prepared* silver hydrosol (curve 1), sol shown as curve 1, 15 min after capping with octadecanethiol

(curve 2), sol shown as curve 2 ,15 min after capping with octadecylamine (curve 3) and finally, sol shown as curve 3 recorded 24 hrs after capping with the long chain amine secondary monolayer (curve 4, dotted line). In this case as well, large shifts in the surface plasmon resonance are observed at each stage of monolayer and bilayer formation (values indicated in the figure). The Colloidal particles synthesized and surface modified as described above have been used for organization at air-water interface, which will be described in the next chapter.

### 3.5 References:

1. Nuzzo, R.G.; Allara, D.L.; *J. Am. Chem. Soc.*, **1983**, *105*, 4481, Nuzzo, r.G.; Fusco, F.A.; Allara, D.L.; *J. Am. Chem. Soc.*, **1987**, *109*, 2358, Whitesides, G.M.; Laibinis, P.E.; *Langmuir*, **1990**, *6*, 87.

2. Mirkin, C.A.; Ratner, M.A.; *Annu. Rev. Phys. Chem.* **1992**, *43*, 719.], Non-leniar Optical Materials Li, D.; Ratner, M.A.; Marks, t.J.; Znang, C.H.; Yang, J.; Wong, G.K.; *J. Am. Chem. Soc.,* **1990**, *112*, 7389.

3. Kawanishi, Y.; Tamaki, t.; Sakuragi, M.; Seki, t.; Swuzki, Y.; Ichimura, K.; *Langmuir*, **1992**, *8*, 2601

4. Ulman, A. *An Introduction to Ultrathin Organic Films : From Langmuir Blodgett to Self Assembly.*

5. Li, D.; Ratner, M.A.; Marks, T.J.; Zhang, C.H.; Yang, J.; Wong, G.K. *J. Am. Chem. Soc.* **1990**, *112*, 7389.

6. Tidwell, C.D.; Ertel, S.I.; Ratner, B.D.; Tarasevich, B.J.; Atre, S.; Allara, D.L. *Langmuir* **1997**, *13*, 3404.

7. Kawanishi, Y.; Tamaki, T.; Sakuragi, M.; Segi, T.; Swuzki, Y.; Ichimura, K. *Langmuir* **1992**, *8*, 2601.

8. a)Chumanov, G.; Sokolov, K.; Gregory, B.W.; Cotton, M.T.; *J. Phys. Chem.*, **1995,** *99*, 9466

b)Grabar, K.C.; Allison, K.J.; Baker, B.e.; Bright, R.M.; Brown, K.R.; Freeman, R.G.; Fox, A.P.; Keating, C.D.; Musick, M.D.; Natan, M.J.; *Langmuir,* **1996**, *12*, 2353.

c)Colvin, V.L.; Goldstein, A.N.; Alivisatos, A.P. *J.Am.Chem.Soc.* **1992**, *114*, 5221.

d)Grabar, K.C.; Freeman, R.G.; Hommer, M.B.; Natan, M.J. *Anal.Chem.* **1995**, *67*, 735.

e)Bandyopadhyay, K.; Patil, V.; Vijayamohanan, K; Sastry, M. *Langmuir*, **1997**, *13*, 5244.

9. Brust, M.; Walker, M.; Bethell, D.; Schiffrin, D.J.; Kiely, C. *J. Chem. Soc., Chem. Commun.* **1994**, 801.

10. a) Brust, M.; Fink, J.; Bethell, D.; Schiffrin, D.J.; Kiely, C. *J. Chem. Soc., Chem. Commun.* **1995**, 1655.

b) Weisbecker, C.S.; Merritt, M.V.; Whitesides, G.M. *Langmuir* **1996**, *12*, 3763.

c) Hostetler, M.J.; Green, S.J.; Stokes, J.J.; Murray, R.W. *J.Am.Chem.Soc.* **1996**, *118*, 4212.

d) Green, S.J.; Stokes, J.J.; Hostetler, M.J.; Pietron, J.J.; Murray, R.W. *J.Phys.Chem.B.* **1997**, *101*, 2663.

e) Ingram, R.S.; Hostetler, M.J.; Murray, R.W. *J.Am.Chem.Soc.* **1997**, *119*, 9175.

11. Hostetler, M.J.; Stokes, J.J.; Murray, R.W. *Langmuir* **1996**, *12*, 3604.

12. a) Badia, A.; Gao, W.; Singh, S.; Demers, L.; Cuccia, L.; Reven, L. *Langmuir*, **1996**, *12*, 1262.

b) Terrill, R.H., Postlethwaite, T.A.; Chen, C; Poon, C; Terzis, A.; Chen, A.; Hutchison, J.E.; Clark, M.R.; Wignall, G.; Londono, J.D.; Superfine, R.; Falvo, M.; Johnson Jr., C.S.; Samulski, E.T.; Murray, R.W. *J. Am. Chem. Soc.*, **1995**, *117*, 12537.

13. A semiempirical spectrosopic parameter defined by Whitesides *et al* [3b] and later modified by Sastry *et al* known as "Flocculation parameter" which enables quantitative comparisons to be made for colloidal particles under different conditions.

14. Discussed in detail in section 3.4.

15. Shen, L.; Laibinis, P.E.; Hatton, T.A. *Langmuir*, **1999**, *15*, 447.

16. Templeton, A.C.; Hostetler, M.J.; Kraft, C.T.; Murray, R.W., *J. Am. Chem. Soc.* **1998**, *120*, 1906.

17. Storhoff, J.J.; Elghanian, R.; Mucic, C.R.; Mirkin, C.A.; Letsinger, R.L. *J. Am. Chem. Soc.* **1998**, *120*, 1959.

18. Elghanian, R.; Storhoff, J.J.; Mucic, R.C.; Letsinger, R.L.; Mirkin, C.A.; *Science*, **1997**, *277*, 1078

19. Sastry, M.; Lala, N.; Patil, V.; Chavan, S.P.; Chittiboyina, A.G. *Langmuir*, **1998**, *14*, 4138.

20. a) Meldrum, F.C.; Kotov, N. A.; Fendler, J. H.; *Langmuir*, **1994**, *10*, 2035.

b) Sastry, M.; Patil, V.; Mayya, K. S.; Paranjape, D. V.; Singh, P.; Sainkar, S. R.; *Thin Solid Films*, **1998**, *324*, 239.

21. Faraday, M., *Philos.Trans.R.Soc.London,* **1857**, *147*, 145.

22. van Rheenan, P.R.; McKelvey, M.J.; Glausinger, W.S. *J.Solid State Chem.*, **1967**, *67*, 151.

23. Lee, P.C.; Maisel, D. *J.Phys.Chem.* **1982**, *86*, 3391.

24. Henglein, A. *J.Phys.Chem.*, **1993**, *97*, 5457.

25. a) Matijevic, E.; *Annu. Rev. Mater. Sci.*; **1985**, *15*, 483.

b) Matijevic. E. *Acc. Chem. Res.* **1981**, *14*, 22.

26. Vukovic, V.V.; Nedeljkovic, J.M. *Langmuir* **1993**, *9*, 980.

27. Henglein, *Chem.Rev.*, 89 (1989) 1861.

28. Kawanishi, Y.; Tamaki, T.; Sakuragi, M.; Segi, T.; Swuzki, Y.; Ichimura, K. *Langmuir* **1992**, *8*, 2601.

29. Sastry, M.; Patil, V.; Mayya, K.S.; *J. Phys. Chem.B.*, **1997**, *101*, 1167.

# CHAPTER IV

# Electrostatic Immobilization of surface modified colloidal particles at the air-water interface

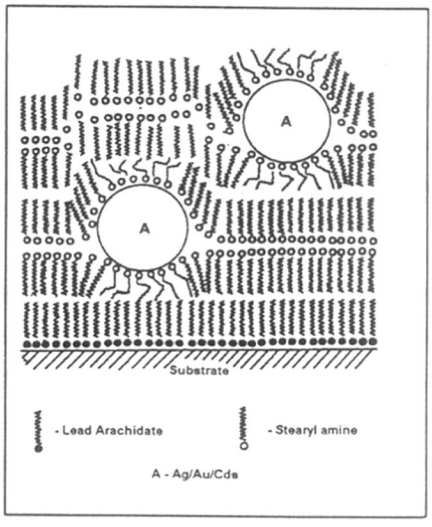


Surface modified colloidal particles of silver, gold and cadmium sulfide have been immobilized at the air-water interface using electrostatic interactions. The monolayer at the air-water interface was characterized using π-A isotherms, and the films after transfer to suitable substrates were characterized using UV-visible Spectroscopy, Quartz Crystal Microgravimetry, Ellipsometry in addition to other characterization techniques.

---

Work in this chapter has been published: **1.** *Mayya, K.S.; Patil, V.; Sastry, M.;* ***Langmuir*****, 1997**, *13*, 2375. **2.** *Sastry, M; Mayya, K.S.; Patil, V.; Paranjape, D.V.; Hegde, S.G.;* ***J Phys Chem B*** **1997**, *101*, 4954. **3.** *Mayya, K.S.; Patil, V.; Sastry, M;* ***J. C. S. Faraday Trans.*** **1997**, *93*, 3377. **4.** *Mayya, K.S.; Patil, V.; Madhu Kumar.; Sastry, M.;* ***Thin Solid Films*****, 1998**, *312*, 300.

## 4.1 Introduction

The area of nanoparticle research has witnessed tremendous growth due to the unusual chemical and physical properties demonstrated by this intermediate state of matter [1]. More correctly, the research activities could be termed "*nanoscale architecture*" since the *generation and organization* of nanoscale structures are of equal importance in the realization of viable device applications. More sophisticated methods have used the Scanning Tunneling Microscope (STM) [2-3] and Atomic Force Microscope (AFM) [4] for the organization of nanoscale structures. Simpler and perhaps experimentally more exciting routes are also being actively pursued, one of which is based on a marriage of colloid chemistry and principles of self-assembly for the growth of monolayer colloidal films [5-7]. The synthesis of nanoparticles under the ordering influence of organic templates such as Langmuir monolayers has also received considerable attention [8-11] motivated partly by attempts to mimic the process of biomineralization. In a slightly different approach, nanoparticles have also been grown in organic matrices such as Langmuir Blodgett films by the chemical insertion procedure [12-17].

Fendler and others have recognized that the air-water interface can be used for the organization of surfactant stabilized nanoparticles and have shown that multilayer films of the nanoparticles can be deposited using the versatile Langmuir Blodgett technique (LB) [18-20], as discussed in the introduction to this thesis [ Chapter I, Page 7-9]. The growth of multilayer nanoparticle films by the LB technique was also shown to be possible through interaction of suitably derivatized colloidal particles from the subphase with the polar group of Langmuir monolayers [21-24]. This latter approach for the deposition of lamellar particulate films has not received much attention.

Biological systems, are full of examples which use electrostatic interactions. Electrostatic forces are used in the preparation of vesicle membranes with asymmetrically or symmetrically bound polyelectrolytes from lipids with polymerizable counterions [25]. Network of spectrin molecules are bound to lipids in the inner-membrane of an animal cell which is responsible for maintaining its shape and stabilizing the plasma membrane - use electrostatic interactions [25]. Electrostatic interactions between $-NH_2$ and -COOH groups play an important role in protein conformation [26]. For a given pH these interactions depend on the number and on the

distribution of the charges, and therefore differ in folded and unfolded states of protein. Though electrostatic interactions were used to form lamellar particulate films of colloidal particles [21-24], there was no control over the number density of particles and the interaction between the colloidal particles and the Langmuir monolayer made use off, was system specific. In this thesis however it is shown that the technique is very general and surface modification of the colloidal particles were rendered using a bifunctional molecule (4-carboxythiophenol) and using interdigitated bilayers of fatty lipids. The bifunctional molecule renders the colloidal particles with carboxylic acid functionality which is negatively charged. A Langmuir monolayer of Octadecylamine was spread on these colloidal particles which were taken as subphase. At a suitable pH both the headgroup ($-NH_2$) of Langmuir monolayer and carboxylic acid functionality of the colloidal particles are fully ionized, and this drives the colloidal particles to the air-water interface. However surface modification using interdigitated bilayers, provided flexibility of choosing the functionality, and accordingly, the molecule for the Langmuir monolayer was chosen. The formation of metal cluster films by this method has not been demonstrated.

Monolayers of octadecylamine ($C_{18}$-amine) molecules were used to immobilize the surface modified (as described in chapter III) colloidal particles on the surface of the hydrosol after which facile transfer of the monolayer to solid substrates was carried out. The charge on the amine monolayer was controlled by varying the colloidal subphase pH. This leads to variation in the degree of cluster incorporation into the Langmuir monolayer and consequently, in the built-up LB films as well. The results of investigation for different colloidal particles used are presented below.

## 4.2 Experimental Section:

In order to follow the kinetics of immobilization of the clusters at the air-water interface, surface pressure- area isotherm measurements ($\pi$-A isotherms, subphase temperature = 25° C) were performed on a Nima model 611 Langmuir trough by dispersing a known quantity of octadecylamine in chloroform on the surface of the cluster hydrosol used as the subphase. Care was taken to spread the amine monolayer only after the bifunctional molecule dispersing agent, absolute ethanol, had fully evaporated, which required typically 15 minutes. After a further 15-20 minutes equilibration of the Langmuir monolayer, $\pi$-A measurements were carried out as a

function of time for two different values of the colloidal subphase pH of 9 and 12. The pH of the subphase was adjusted using dilute $H_2SO_4$ and NaOH. This range was motivated by the fact that the $pK_A$ values of the amine and bifunctional molecules are 10.6 [27] and 4.5 [28] respectively. Thus for the pH values mentioned above, one can systematically vary the charge on the amine molecules (protonated to yield $-NH_3^+$) while the carboxylic acid groups on the clusters remain fully ionized ($-COO^-$), thereby altering the strength of electrostatic interaction between the amine molecules and clusters. At pH = 9, the surface charge density on the Langmuir monolayer is expected to be maximum while at pH = 12, the Langmuir monolayer is completely unprotonated and the charge would be negligible.

The cluster complexed amine monolayer shows a region of fairly large incompressibility which is important for the transfer process. From the isotherms, a surface pressure of 25 mN/m was chosen for this purpose. Therefore, after stabilization of the $\pi$-A isotherms was achieved, the monolayer was compressed to 25 mN/m surface pressure and the monolayer allowed to equilibrate for one hour. A small isobaric reduction in the area/molecule was observed. After one hour, the monolayers were transferred onto quartz and Si (111) wafer substrates by sequential dipping of the substrate in the monolayer covered subphase in the classical Langmuir-Blodgett deposition scheme [29] at a deposition rate of 25 mm/minute. A drying period of 15 minutes between immersions was found to be important for obtaining uniform films. It was observed that good transfer ratios (close to 100 % on both the upward and downward movements) were obtained only if a monolayer of lead arachidate was predeposited on the substrates rendering them hydrophobic as previously observed by Fendler *et al* [22]. Multilayer films of different thicknesses were deposited onto quartz substrates for optical measurements and onto a gold coated AT-cut quartz crystal for Quartz Crystal Microgravimetry (QCM) measurements. QCM measurements were done using an Edwards FTM5 microbalance with a frequency resolution of $\pm$ 1 Hz which for the 6 MHz crystal used, yields a mass resolution of $\pm$ 12 ng/cm$^2$. The quartz crystal frequency change was converted to mass loading using the standard Sauerbrey [30] formula. A thick LB film (40 monolayers) of the silver colloidal particles complexed with octadecylamine was deposited at a colloidal subphase of pH 9 onto a Si (111) wafer for Fourier transform infrared spectroscopy (FTIR) measurements. The infrared characterization of the film was carried out on a Nicolet 60 SXB FTIR spectrometer

operated in the transmission mode at a resolution of 2 $cm^{-1}$. A total of 500 scans yielded a good signal to noise ratio for the infrared spectra. Ellipsometry studies on nanoparticle films of different thickness on Si(111) were performed on a Gaertner L 118 manually operated null ellipsometer in the polarizer-compensator-sample-analyser (PCSA) mode. The light source was a 5 mW He-Ne laser (6328 Å) and measurements were made at an angle of incidence of 70 $^0$. Film thickness values were determined from the ellipsometric angles $\psi$ and $\Delta$ taking the bulk complex refractive index for clusters [31-32] and calculating an effective refractive index for the cluster-octadecylamine film based on the Maxwell-Garnett formalism[33]. The nanoparticle filling fraction used in the calculation of the effective dielectric function of the composite was obtained from QCM measurements. The ellipsometry calculations were made using an application written in Mathcad [34].

## 4.3 SILVER

As mentioned in chapter III [page 49, section 3.3] capping of the silver sol with 4-CTP resulted in a red shift in the surface plasmon resonance from 386 to 405 nm as well as a damping of the plasmon resonance indicative of surface capping [31] . The stability of the carboxylic acid derivatized silver clusters at pH values 8 and above was determined from optical absorption measurements to be excellent and hence any influence of this aspect on the nature of the $\pi$-A isotherms with time may be ruled out.

### 4.3-1 $\pi$-A isotherms

The $\pi$-A isotherms of the $C_{18}$ amine monolayer on the surfactant stabilized silver hydrosol at pH = 9 and pH = 12 are shown in Figs.4.1A and 4.1B respectively. The solid line in Fig.4.1A refers to the isotherm recorded 30 minutes after spreading of octadecylamine while the dotted line is the isotherm recorded after 90 minutes.

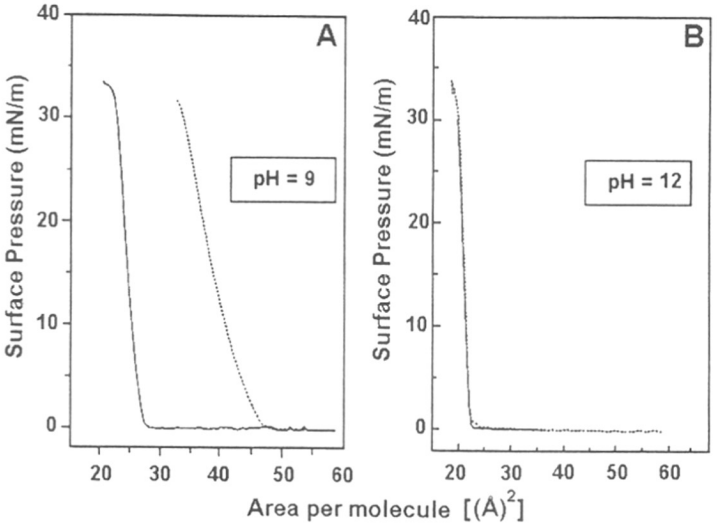


**Figure 4.1** A) π-A isotherms of octadecylamine on surfactant stabilized silver hydrosol (pH =9) after 30 minutes of equilibration (solid curve) and 90 minutes of equilibration (dotted curve).B) π-A isotherms of octadecylamine on surfactant stabilized silver hydrosol (pH =12) after 30 minutes of equilibration (solid curve) and 90 minutes of equilibration (dotted curve).

A large expansion in the monolayer is observed which indicates complexation of the silver clusters to the protonated amine groups of the Langmuir monolayer. The liftoff area [It is the Area per molecule at which the van-der-Waal's interactions between hydrocarbon chain becomes dominant] after equilibration was determined to be 45 Å$^2$/molecule which is considerably larger than the liftoff area for the uncomplexed amine of ~ 20 Å$^2$/molecule. As mentioned above, at pH = 9, both the amine (-$NH_3^+$) and carboxylic acid ($COO^-$) groups are expected to be fully charged. At pH = 12, there is a negligible expansion of the monolayer with time (Fig.4.1b, solid curve- 30 minutes and dotted curve-90 minutes after equilibration) indicating little adsorption of the silver clusters. The liftoff area is close to 20 Å $^2$/molecule which is close to that obtained for uncomplexed amine molecules. The fact that there is a pH dependent complexation of clusters, means that it is necessary to establish the importance of electrostatic interactions in the immobilization of the clusters since it is conceivable that hydrogen bonding between the carboxylic acid groups and the protonated amine groups could also lead to immobilization. Thus, lack of complexation as observed from the π-A isotherms at pH = 12 underscores the importance of electrostatic interactions vis-a-vis hydrogen bonding interactions which are known to be operative in the bonding of glutamine to phospholipids at the air-water interface [35]. Thus, through judicious choice

of the ionizable cluster capping molecule and the amphiphilic molecule in the Langmuir monolayer, regulation of the colloidal particle density in the Langmuir monolayer can be achieved through simple subphase pH variation. In earlier studies, attractive electrostatic interaction between the polar groups of the Langmuir monolayer and charged surfactant molecules on the nanoparticles was used for immobilization of the clusters as demonstrated in the deposition of DODAB-HMP-stabilized CdS clusters-DODAB sandwich multilayers [22]. However, modification of cluster density at the monolayer-colloidal subphase interface as described above has not been recognized till now and may have important applications.

Some other observations pertinent to transfer of the monolayers to form LB films can be made from Fig.4.1. The silver cluster complexed amine monolayer shows a region of fairly large incompressibility which is important for the transfer process. From the isotherms, a surface pressure of 25 mN/m was chosen for the transfer.

### 4.3-2 Quartz Crystal Microgravimetry

The growth of the silver cluster-amine LB films by sequential transfer was followed using QCM, optical absorption and optical interferometry measurements. Fig.4.2 shows a plot of the mass uptake with number of monolayers transferred onto a gold coated quartz crystal with the hydrosol subphase at pH = 9 and 12.

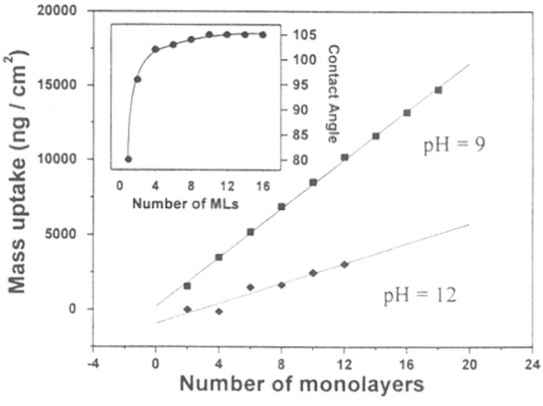


**Figure 4.2 :** QCM mass uptake with time as a function of number of monolayers transferred with the hydrosol at pH = 9 (filled circles) and pH = 12 (filled squares). The solid lines are linear least squares fits to the data. The inset shows the contact angle variation with number of monolayers transferred onto lead arachidate coated quartz substrates.

The gold film was hydrophobic and hence a lead arachidate monolayer was not deposited for these measurements. It is seen from the figure that there is an increase in mass uptake per dip as the pH is reduced from 12 to 9. The mass transfer per dip was determined from a least squares fit to the data which is clearly linear (solid lines are the regression curves). At pH = 12, the mass uptake is consistent with transfer of *only the amine monolayer*. This agrees with π-A isotherms which show no complexation of the clusters at pH = 12. Calculations based on the mass uptake per dip at pH = 9 yield ~ 30 % coverage by 73 Å diameter clusters at unity transfer ratios during the downward and upward strokes. This value of surface coverage is larger than the 15 % obtained for self-assembled gold colloidal films by Natan *et al* [7]. While the low surface coverage for self-assembled colloidal films has been explained in terms of repulsive electrostatic interactions between the clusters, the larger value obtained for the films of this study may be due to shielding of the negative charges on the silver clusters by the positively charged amine molecules. Another factor that needs to be considered is the attractive Van der Waals interactions between the hydrocarbon tails of the amine molecules which can lead to stability of the silver cluster assembly at higher surface coverages. The important point to note from Fig.4.2 is the linearity in the plot at pH = 9 which indicates monolayer by monolayer transfer of the 73 Å diameter silver cluster - $C_{18}$ amine complex.

The inset of Fig.4.2 shows the variation in contact angle [36] with number of monolayers of the silver clusters transferred onto hydrophobized quartz substrates. The lead arachidate monolayer had a contact angle of ~ 80 °. The constancy of the contact angle at 105 ° beyond 4 ML of the silver cluster film clearly indicates transfer of the clusters with the amine monolayer on top as expected for *Y*-type growth of the film. Therefore, any reorganization due to size constraints can be ruled out and lamellar film growth is indicated.

### 4.3-3 UV-visible spectroscopy

Optical absorption spectroscopy is an ideal tool for following the film growth process of silver cluster films due to the strong surface plasmon resonance exhibited by this metal [31]. Fig.4.3a shows the absorption spectra recorded as a function of the number of monolayers in the built-up LB films on hydrophobized quartz substrates at

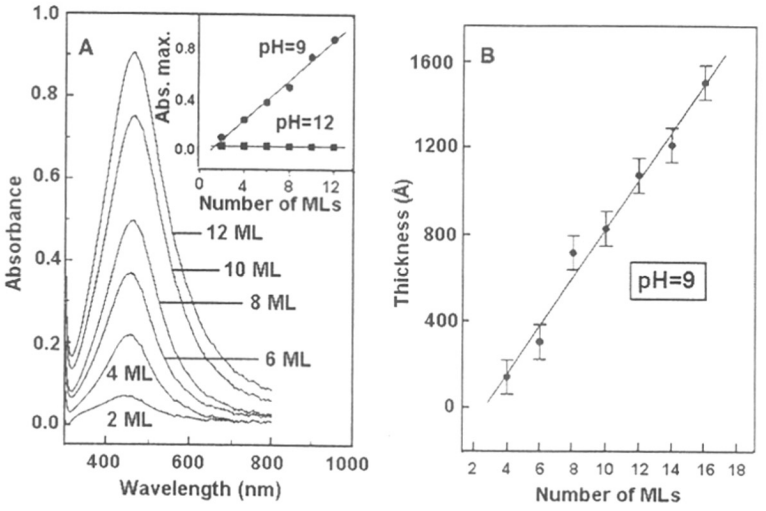


**Figure 4.3:** A) Optical absorption spectra of several multilayer amine-silver cluster LB films deposited on hydrophobized quartz substrates at a pH = 9. The inset shows the variation of the surface plasmon resonance intensity at 460 nm with silver cluster film thickness at pH = 9 (filled circles) and at pH = 12 (filled squares).
B) Silver cluster film thickness as a function of number of monolayers transferred as determined from optical interferometry. The solid line is a linear least squares fit to the data.

subphase pH = 9. The plasmon resonance occurs at 460 nm for all the films and a monotonic growth in resonance intensity is observed as the film thickness increases. As mentioned above, no transfer of the silver clusters was observed by QCM at pH = 12 and this was corroborated by optical absorption measurements of different thickness films on quartz which showed no indication of the expected surface plasmon resonance. The inset of Fig.4.3a shows the variation in the intensity maximum at the surface plasmon resonance with film thickness. As indicated in Fig.4.3a, a systematic increase in the absorbance with film thickness is seen at pH = 9 with a linear regression curve fitting the data very well. The linearity in the absorbance data clearly indicates good monolayer by monolayer transfer [22]. At pH = 12, there was no transfer of the clusters (inset of Fig.4.3a, filled squares). This is in agreement with QCM results which indicated transfer of only the amine film which does not contribute to absorption in this spectral region. The QCM and optical absorption data indicate that lamellar multilayer films of colloidal particles can be deposited by the LB technique without significant variation in the cluster density within the various layers.

### 4.3-4 Optical Interferometry

The thickness of multilayer silver cluster films grown on quartz substrates at a pH = 9 was measured using optical interferometry. Fig.4.3b shows a plot of the measured thickness versus the number of monolayers in the silver cluster film. The film thickness clearly grows linearly with the number of monolayers in the film and the solid line is a linear least squares fit to the data. The slope of the curve yields a thickness increment of ~ 106 Å/monolayer. The amine bilayer thickness is ~ 50 Å [37-38] from which we calculate a cluster diameter of 56 Å. This is in reasonable agreement with the cluster size of 73 ± 12 Å determined from TEM studies of the hydrosol.

### 4.3-5 Fourier Transform Infrared Spectroscopy

While the QCM, optical absorption and interferometry characterization of the silver cluster-amine complex LB films indicate layer-by-layer growth in the classical Y-type transfer sequence, the presence of clusters of the dimensions used in this study is expected to introduce some distortions in the packing and orientation of the $C_{18}$ amine molecules in the layers. This aspect can be studied using infrared spectroscopy as demonstrated by Yang *et al* [39] for $\alpha$-$Fe_2O_3$ - stearate LB films.

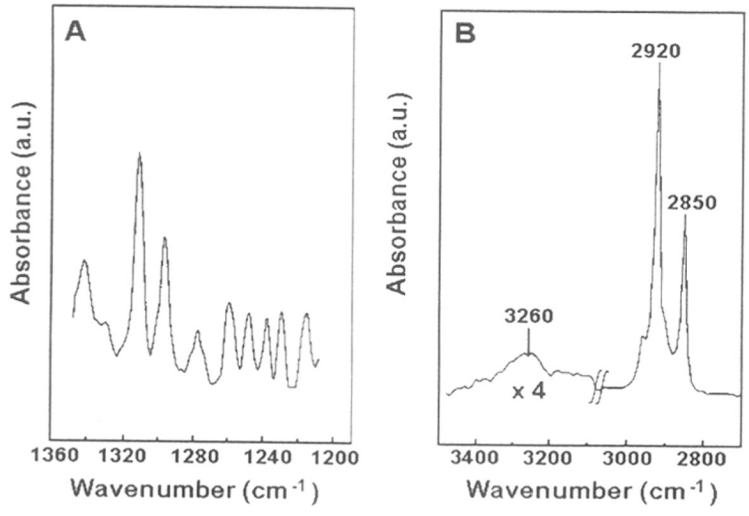


**Figure 4.4** : A) FTIR spectrum of a 40 ML silver cluster-$C_{18}$ amine complex film in the region of the methylene twisting and wagging progression frequencies.
B) FTIR spectrum of a 40 ML silver cluster-$C_{18}$ amine complex film in the region of the C-H and $NH_2$ stretching frequencies.

Fig.4.4a shows the FTIR spectrum of a 40 ML silver cluster-$C_{18}$ amine film in the region 1200-1350 $cm^{-1}$. The band progressions from the methylene wagging and twisting vibrational modes can clearly be seen. The presence of the progression bands as well resolved peaks is a clear indicator of close packing of the alkyl chains of the amine molecules in the monolayers [39-41]. It is known that the methylene wagging and twisting vibrational modes have their transition dipole moments parallel to the alkyl chain axis [42]. The presence of the progression bands shown in Fig.4.4a for the spectra measured in the transmission mode as adopted in this study indicates a tilt of the amine hydrocarbon chains in addition to close packing. Additional evidence for close packing is obtained from the C-H stretching region (Fig.4.4b). The peak positions of the antisymmetric and symmetric methylene stretching vibrations are determined to be 2920 and 2850 $cm^{-1}$ respectively which is characteristic of alkyl chains in a close-packed, crystalline microenvironment. The C-H stretching frequencies are known to shift to higher values (2928 and 2856 $cm^{-1}$ for the antisymmetric and symmetric vibrations respectively) if disorder exists in the chains [41]. Another interesting observation from Fig.4.4b is the position of the $NH_2$ antisymmetric stretching vibration at 3260 $cm^{-1}$. This frequency for pure amine films has been found to be 3331 $cm^{-1}$ while the band shifts to 3200 $cm^{-1}$ for primary amine salts [27]. The intermediate value of 3260 $cm^{-1}$ obtained for carboxylic acid terminated silver cluster-alkyl amine complexes is novel and has not been reported so far.

The attachment of the negatively charged silver clusters to amine molecules at the air-water interface is similar to anion incorporation in fatty amine Langmuir monolayers previously demonstrated [37, 38, 42]. The silver clusters in this case acting as "giant" counterions. From the QCM, optical absorption, optical interferometry and FTIR measurements, it can be concluded that lamellar growth of the silver cluster-amine films has been achieved with some distortion of the amine hydrocarbon chains around the silver colloidal particles.

## 4.4 GOLD:

Colloidal particles of gold have also been used for immobilization. Presented below are the data of the detailed investigation. As mentioned earlier in chapter III [Page 47, Section 3.3-2], capping of the gold sol resulted in a red shift in the surface plasmon resonance from 525 to 530 nm as well as a damping of the plasmon resonance indicative of surface capping [43] . The stability of the carboxylic acid derivatized gold clusters at pH values 8 and above was determined from optical absorption measurements to be excellent and hence any influence of this aspect on the nature of the π-A isotherms with time may be ruled out.

### 4.4-1 π-A isotherms

The π-A isotherms of the $C_{18}$ amine monolayer on the surfactant stabilized gold hydrosol at pH = 8 and pH = 11.5 are shown in Figs.4.5A and 4.5B respectively.

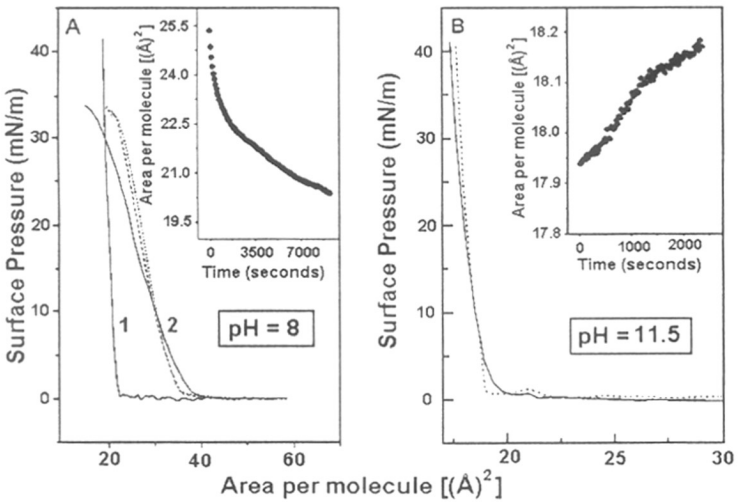


**Figure 4.5** :A] π-A isotherms at pH = 8. Curve 1 - solid line, octadecylamine on water; family of curves 2, amine on gold hydrosol - solid line, time t = 30 minutes; dashed line, time t = 60 minutes; dotted line, time t = 90 minutes after spreading the amine monolayer. Inset shows variation in molecular area with time after compression to surface pressure = 25 nN/m.
B] π-A isotherms of octadecylamine on the gold hydrosol at a pH = 11.5. Solid line, after time t = 60 minutes; dashed line, after time t = 90 minutes of spreading the amine monolayer. Inset shows variation in molecular area with time after compression to a surface pressure of 25 mN/m.

In Fig.4.5A, the π-A isotherm of octadecylamine on pure water at pH=8 is shown for comparison (curve 1). The family of curves indicated as **2** are the isotherms of octadecylamine on the gold hydrosol as a function of time. The solid line refers to the isotherm measured after 30 minutes of spreading the amine monolayer while the dashed and dotted lines correspond to isotherms recorded after 60 and 90 minutes of spreading octadecylamine. It is clear that there is a fairly rapid expansion of the monolayer (compared to curve 1) which indicates complexation of the gold clusters to the protonated amine groups of the Langmuir monolayer. The π-A isotherms stabilize within 60 minutes of spreading the monolayer and an equilibrium liftoff area of 37 $Å^2$/molecule obtained which is considerably larger than that for the amine on water (~ 20 $Å^2$/molecule, curve 1). As mentioned earlier, at pH = 8, both the amine ($-NH_3^+$) and carboxylic acid ($COO^-$) groups are expected to be fully charged. The π-A isotherms of the amine monolayer at pH = 9 showed slower expansion with a smaller liftoff area of 32 $Å^2$/molecule indicating weaker electrostatic interaction. This may be due to reduced protonation of the amine group which would indicate a $pK_A$ value for the surface amine group slightly less than that reported. Such shifts in the $pK_A$ values as well as a broader pH range over which the groups are ionized are known for surface groups [44].

At pH = 11.5, there is no significant expansion of the monolayer with time (Fig.4.5B, solid curve- 60 minutes and dotted curve-180 minutes). The takeoff area is close to 18 $Å^2$/molecule which agrees well with the close packing area expected for unprotonated amine groups [45]. The above results clearly show that controlling the charge on the amine monolayer through the hydrosol pH leads to a variation in the electrostatic interaction between the fully charged clusters and the Langmuir monolayer and consequently, differing levels of complexation of the clusters with the surface monolayer. Thus, through judicious choice of the ionizable cluster capping molecule and the amphiphilic molecule in the Langmuir monolayer, regulation of the colloidal particle density in the Langmuir monolayer can be achieved through simple subphase pH variation.

Another important observation to be noted from Fig.4.5 is that the gold cluster complexed amine monolayer shows a region of fairly large incompressibility which is important for the transfer process. From the isotherms, a surface pressure of 25 mN/m was chosen for the transfer. The monolayers were compressed to this pressure and the

variation in monolayer area with time recorded. This is plotted in the inset of Fig.4.5A (pH=8) and Fig.4.5B (pH=11.5). Little change in the area/molecule is seen for the monolayer at pH = 11.5 while a large reduction from 25.5 to 19.5 Å $^2$/molecule over a period of 150 minutes was recorded for the monolayer at pH = 8. This indicates that the kinetics associated with cluster immobilization is extremely slow and sensitive to the surface charge density. The monolayer area stabilized at 19.5 Å $^2$/molecule after nearly 270 minutes of compression. The nature of the monolayer area-time dependence at pH = 9 was similar to the lower pH data. From the above, optimum conditions for transfer of the gold cluster-amine monolayer were determined to be a surface pressure of 25 mN/m and an equilibration period of ~ 300 minutes.

### 4.4-2. TEM studies

Fig.4.6A shows a typical transmission electron micrograph of the 4 ML gold cluster-octadecylamine film. The scale bar corresponds to 1200 Å. It is observed that there are regions within the film where the gold clusters are in close packing with large gaps between such "domains". The particle size histogram was determined from the micrograph of Fig.4.6A and other micrographs taken at different points on the surface and is shown in Fig..4.6B. A Gaussian fit to the data is shown as a solid line and yields a mean cluster size of 125 Å and a standard deviation of 30 Å. This data is used in the interpretation of the QCM and ellipsometry results presented below.

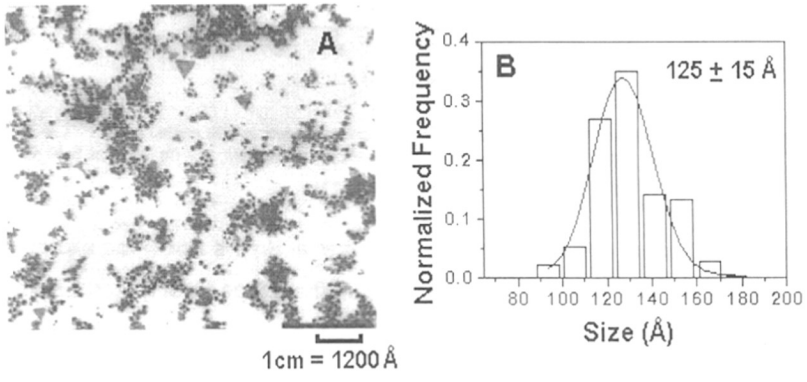


**Figure 4.6 :** A] A typical TEM micrograph of a 4 ML gold cluster-octadecylamine LB film. The scale bar corresponds to 1200 Å.. B] The particle size histogram obtained from TEM measurements of the 4 ML gold cluster-octadecylamine film. The solid line is a Gaussian fit to the data; the parameters of the fit are listed in the figure.

### 4.4-3 QCM and optical absorption studies

The growth of the gold cluster-amine LB films by sequential transfer was followed using QCM and optical absorption measurements. Fig.4.7 shows a plot of the mass uptake with number of immersion cycles of a gold coated quartz crystal into hydrosol subphase at pH = 8, 9 and 11.5. It is to be noted that one immersion cycle of a substrate (one dip) corresponds to transfer of two monolayers (one bilayer) in the Y-type LB film deposition scheme. The gold film was hydrophobic and hence a lead arachidate monolayer was not deposited for these measurements. Good transfers were obtained for a film immersion rate of 25 mm/min and 15 minutes drying between immersion. It is seen from the figure that there is a systematic increase in

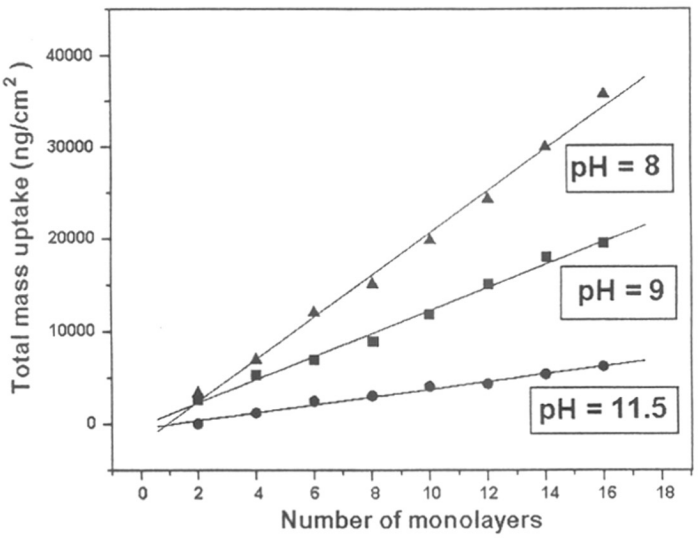


**Figure 4.7** : Mass uptake with number of monolayers transferred from QCM measurements. Filled circles, hydrosol pH = 11.5; filled squares, pH = 9; filled triangles, pH = 8. Solid lines are linear fits to the data.

mass uptake per dip as the pH is reduced from 11.5 to 8. The mass transfer per dip was determined from a least squares fit to the data which is clearly linear (solid lines are the regression curves). At pH = 11.5, the mass uptake is consistent with transfer of *only the amine monolayer*. This agrees with $\pi$-A isotherms which show no complexation of the clusters at pH = 11.5. The cluster density in the film at pH = 8 (maximum mass transfer per dip observed) was determined from the QCM mass uptake assuming an average

cluster size of 125 Å determined from TEM measurements (Fig.4.6) and a surface coverage of 30 % was calculated. This value is larger than the surface coverage of 15 % obtained by Natan *et al* for self-assembled gold clusters [7]. The larger surface coverage observed for clusters immobilized in an LB matrix may be due to screening of the charge on the clusters by the amine molecules and/or additional stabilization arising due to the Van der Waals interactions between the alkyl chains of the amine molecules coordinated to the clusters. An intermediate mass uptake/dip for pH = 9 indicates a smaller gold cluster density in the bilayer and as will be shown below, is consistent with optical absorption measurements of the LB films. The important point to note from Fig.4.7 is the linearity in the plot at all pH values which indicates fairly uniform monolayer by monolayer transfer of 125 Å diameter gold clusters complexed to amine monolayers.

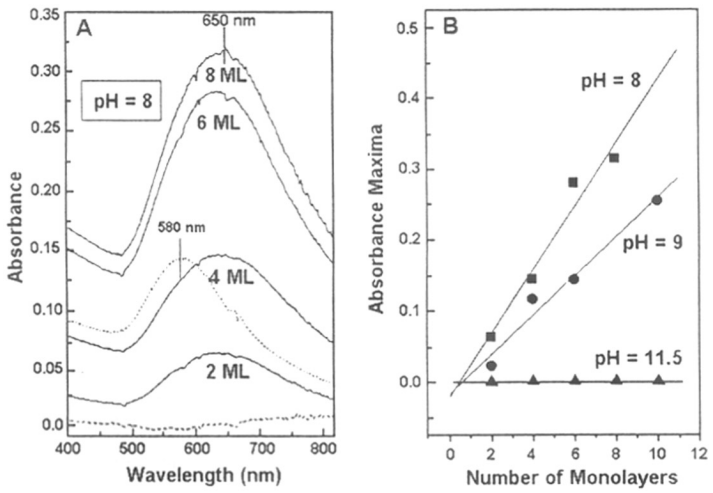


**Figure 4.8** : A] Optical absorption spectra of the gold cluster LB films transferred to hydrophobized quartz substrates of varying thicknesses at colloidal subphase pH = 8. The dashed line refers to the absorption spectrum of an 8 ML film deposited at pH = 11.5 while the dotted line is the spectrum of a 6 ML film deposited at a pH = 9.
B] Variation of the absorption maximum with film thickness for LB films transferred onto hydrophobized quartz at colloidal pH values : 11.5, filled triangles; 9, filled circles; 8, filled squares. The solid lines are linear fits to the data.

Optical absorption spectroscopy is an ideal tool for following the film growth process of gold cluster films due to the strong surface plasmon resonance exhibited by this metal. Fig.4.8A shows the absorption spectra recorded as a function of the number of monolayers in the built-up LB films on hydrophobized quartz substrates at subphase pH = 8. The plasmon resonance occurs at 650 nm for all the films and a monotonic

growth in resonance intensity is observed as the film thickness increases. As mentioned above, no transfer of the gold clusters was observed by QCM at pH = 11.5 and this is corroborated by optical absorption measurements of an 8 ML film on quartz (dashed line) which shows no indication of the expected surface plasmon resonance. For comparison, the absorption spectrum recorded for a 6 ML LB film transferred at a subphase pH = 9 is shown (dotted line). The plasmon resonance for this film (and for other thickness films at this pH) occurs at 580 nm. This large shift in the surface plasmon resonance with subphase pH may be attributed to flocculation of the colloidal particles [46] . Fig.4.8b shows the variation in the intensity at the surface plasmon resonance with film thickness. Here again it is seen that a systematic increase in the absorbance with film thickness for pH = 8 and 9 with a linear regression curve fitting the data very well. The linearity in the absorbance data again clearly indicates transfer of the monolayers with nearly the same cluster density per monolayer [22]. The slope of the curve at pH = 9 is less than that obtained for pH = 8 indicating less gold cluster density per monolayer at pH = 9 in total agreement with QCM data. The QCM and optical absorption data clearly show that multilayer films of colloidal particles can be deposited by the LB technique. Furthermore, the gold cluster density in the hyrdophilic regions of the film can be controlled by variation of the colloidal subphase pH .

### 4.4-4. Ellipsometry measurements

The thickness of the multilayer gold cluster-octadecylamine LB films transferred onto Si (111) substrates at a colloidal subphase pH = 8 was determined ellipsometrically as outlined below. The complex refractive index of the gold cluster-octadecylamine multilayer films was determined using the Maxwell-Garnett effective medium formalism discussed in detail in chapter II [ Page 32, Section 2.5-2] of this thesis [33]. For simplicity, a uniform distribution of gold particles of size 125 Å has been assumed. The filling factor was determined from QCM measurements to be 27 % and the real and imaginary parts of the refractive index for gold at a wavelength of 6328 Å were taken to be from the data of Johnson and Christy [28]

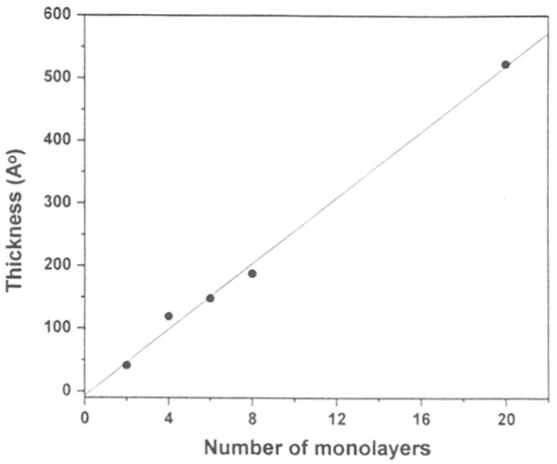


**Figure 4.9** : Ellipsometric thickness as a function of film thickness for LB films of the gold cluster-octadecylamine complex transferred onto Si (111) substrates. The solid line is a linear fit to the data.

to be 1.315 and 1.524 respectively [$\varepsilon_f$ = (1.315 + i 1.524 )$^2$] while $\varepsilon_m$ was taken to be $(1.5)^2$. The film thickness for different LB films was then determined by solving the exact equation of ellipsometry[34]. Fig.4.9 shows a plot of the thickness determined ellipsometrically for the multilayer films transferred onto Si (111) substrates. It is seen that there is a linear increase in the thickness indicating uniform transfer of the gold clusters in the monolayers during each immersion cycle. This result is in agreement with the QCM and optical absorption results presented earlier. A least squares fit to the data shown in Fig. 4.9 yielded a thickness per bilayer of 55 Å. Assuming a thickness per bilayer of 50 Å for the amine molecules [37]and a cluster size of 125 Å, the expected thickness per bilayer is well in excess of that measured ellipsometrically. This result clearly indicates considerable disorder within the gold cluster-octadecylamine monolayers in terms of packing of the clusters. Clusters transferred during successive immersions can then fill gaps in the base multilayer films leading to a much smaller thickness per bilayer as observed. This highlights an important aspect of the study, i.e., while QCM and optical absorption measurements show that the number of clusters transferred per immersion cycle is the same, they do not provide information on the disorder in the films, which has been shown indirectly through ellipsometry measurements. The disorder in the films is not surprising given the dimensions of the gold clusters (125 Å) in comparison with the octadecylamine bilayer dimensions of 50 Å. It may be pointed out here that the ellipsometry results are in agreement with the TEM studies of a 4 ML gold cluster LB film (Fig.4.6) which shows aggregates of clusters

separated by large gaps.

### 4.4-5 XPS and contact angle studies

While good sequential transfer of the monolayers by the LB technique could be done, the consequences of a disordered film structure observed in ellipsometry and TEM studies of the gold cluster LB films needs further investigation. Angle dependent XPS was used to understand the organization of the gold clusters in the amine organic matrix as previously shown for lamellar systems such as LB films [47]. It was found that the ratio of the C 1s to Au $4f_{7/2}$ signals at 60° and 30° electron takeoff angles was 24 and 20 respectively. This indicates that at least a fraction of the gold clusters are on the film surface which is contrary to the expected structure of the clusters embedded below a 25 Å thick amine hydrocarbon chain. Contact angle measurements of the films yielded a mean value of 55 ° which is considerably less than that recorded for the lead arachidate covered surface of 105 ° indicating a more hydrophilic surface. This is only possible if some of the carboxylic acid derivatized clusters are present on the surface as indicated by the XPS measurements. This result also suggests strongly the presence of gaps between clusters in the films. Clusters transferred during successive immersions may then turn over in the gaps to maximize the Van der Waals interactions between the alkyl chains of the amine molecules coordinated to the cluster surface and the molecules in the base film thus exposing the more hydrophilic carboxylic acid groups to the surface. It may be emphasized that this is a tentative explanation for the results obtained. There was no evidence for an additional component in the Au 4f signal arising from the Au-S thiolate bond (expected BE = 84.6 eV) in full agreement with the findings of Schiffrin *et al* [48].

## 4.5 CADMIUM SULFIDE

Semiconductor nanoparticles are being studied in great depth due to their interesting applications in non-linear optics [49], in light emitting diodes [50] and quantum dot lasers [51] to name just a few. In the quantum or the so-called Q-state regime (particle sizes typically less than 5 nm) the ability to change the electronic and optical properties of a material of a single composition solely through change of size of the particle[49] affords great flexibility to band-gap engineering in materials.

While research effort oriented towards understanding the fundamental properties of Q-state semiconductor nanoparticles is important, another aspect which also needs to be pursued is the organization and packaging of the nanoparticles, particularly as thin films, for eventual device construction. As far as CdS is concerned, Q-state nanoparticles of this material have been grown/organized in a Langmuir Blodgett (LB) film matrix by chemical treatment [12, 14, 53-54], under the surface of arachidic acid Langmuir monolayers (MLs) by chemical treatment[8] and by self-assembly to obtain monolayers of the nanoparticles [5]. In a different approach, Fendler and co-workers demonstrated that growth of ordered multilayer CdS nanoparticle films by the LB technique was also possible through interaction of suitably derivatized colloidal particles from the subphase with the polar group of the Langmuir monolayer [22]. However this approach has not recieved much attention, and this thesis makes a sincere attempt to understand the role of electrostatic interactions in the immobilization of Carboxylate derivatized cadmium sulfide particles.

The CdS hydrosol was prepared by reacting a $10^{-4}$ M concentrated aqueous solution of $CdSO_4$ with stoichiometric amounts of $Na_2S$ (Cd : S ratio of 1:1) in the presence of the capping molecule, 4-CTP, which has been discussed in detail in the Chapter III of this thesis [page 47, Section 3.2-3]. It is well known that as the cluster size decreases below the bulk limit, the first excited electronic state shifts to higher energies. Brus [55-56] has derived an analytical approximation for the lowest energy eigenvalue (first excited electronic state) as function of cluster size for semiconductor particles which agrees very well with experimentally determined "band gap" values for different semiconductor nanoparticles[57]. The expression is [55] :

$$E(R) = E_g \cdot \frac{h^2 \cdot \pi^2}{2 \cdot R^2} \cdot \left( \frac{1}{m_e} + \frac{1}{m_h} - \frac{1.8 \cdot e^2}{\varepsilon \cdot R} \right) \quad \text{.....(4.1)}$$

where $E_g$ is the bulk band gap, R is the cluster radius, $m_e$ and $m_h$ are the effective masses of the electron and hole respectively in the cluster and all other parameters have their usual meaning. Taking reported values of $E_g$ (2.4 eV), $m_e$ and $m_h$ (0.19 and 0.8 respectively) and $\varepsilon$ (5.7) for CdS [55, 57] , the cluster diameter, 2R, is calculated from Eq.4.1 to be 5.2 nm. This is larger than the value of 3.5 nm determined from the experimental cluster size-band gap energy correlation curve [57]. It is known that many factors like, the electron and hole effective masses may be different for clusters than the bulk values assumed for the calculation. Therefore the "confined exciton" model for calculation of the excited electronic state is not necessarily accurate and in the rest of the paper, experimentally determined cluster size of 3.5 nm for calculations and discussions are used. This *Thesis* seeks to concentrate on the organization of the clusters at the air-water interface and no attempt has been made to control either the CdS particle size or the width of the colloidal particle size distribution.

### 4.5-1 π-A isotherms

The π-A isotherms of the $C_{18}$ amine monolayer on the 4-CTP stabilized CdS hydrosol at pH = 9 is shown in Fig.4.10. Curve 1 indicates the isotherm after 15 minutes of spreading the octadecylamine monolayer while curve 2 is the isotherm corresponding to 120 minutes of waiting. For comparison, the isotherm of octadecylamine on water at pH = 9 as the subphase is also shown (Fig.4.10, dotted line). It is clear that there is an expansion of the monolayer with time as indicated by increasing liftoff areas from 0.41 $nm^2$ /molecule at time t = 15 minutes to 0.55 $nm^2$ /molecule at t = 120 minutes. These values are to be compared to the liftoff area for uncomplexed amine molecules of ~ 0.20 $nm^2$/molecule (Fig.4.10, dotted curve). The isotherms stabilized after this time period of spreading of the monolayer. The isotherms recorded on the CdS colloidal subphase at pH = 12 showed no expansion with time indicating negligible adsorption of the carboxylic

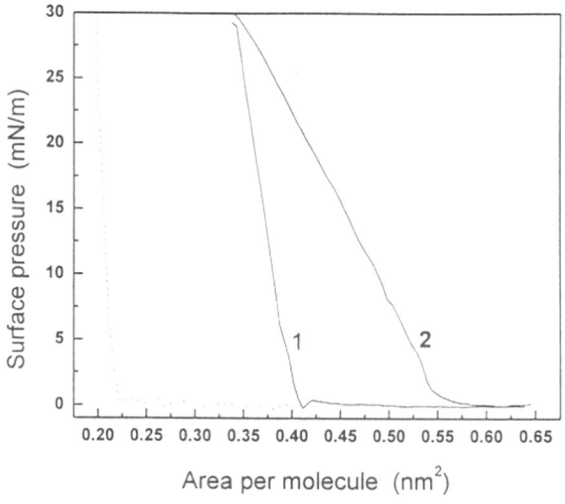


**Figure 4.10:** π-A isotherms of octadecylamine on 4-CTP stabilized CdS hydrosol (pH =9) after 15 minutes of equilibration (curve 1) and 120 minutes of equilibration (curve 2). The dotted line is the isotherm of octadecylamine on water at pH =9.

acid derivatized CdS particles at the amine surface. This is consistent with the fact that the surface charge due to the amine molecules is expected to be zero at this pH, as mentioned earlier. At this point, it is necessary to establish the importance of electrostatic interactions in the immobilization of the clusters since it is conceivable that hydrogen bonding between the carboxylic acid groups and the protonated amine groups could also lead to immobilization. Thus, lack of complexation as observed from the π-A isotherms at pH = 12 underscores the importance of electrostatic interactions vis-a-vis hydrogen bonding interactions which are known to be operative in the bonding of glutamine to phospholipids at the air-water interface [35]. Thus, through judicious choice of the ionizable cluster capping molecule and the amphiphilic molecule in the Langmuir monolayer, regulation of the colloidal particle density in the Langmuir monolayer can be achieved through simple subphase pH variation. In earlier studies, attractive electrostatic interaction between the polar groups of the Langmuir monolayer and charged surfactant molecules on the nanoparticles was used for immobilization of the clusters as demonstrated in the deposition of DODAB-HMP-stabilized CdS clusters-DODAB sandwich multilayers [22]. However, modification of cluster density at the monolayer-colloidal subphase interface as described above has not been recognized till now and may have important applications.

Some other important observations regarding the transfer of monolayers to form LB films can be made from Fig.4.10. The CdS nanoparticle complexed amine monolayer shows a region of fairly large incompressibility which is important for the transfer process. From the isotherms, a surface pressure of 25 mN/m was chosen for the transfer.

### 4.5-2 Quartz Crystal Microgravimetry:

The growth of the CdS nanoparticle-amine LB films by sequential transfer was followed using QCM, optical absorption and ellipsometry measurements. Fig.4.11 shows a plot of the mass uptake with number of monolayers transferred onto a gold coated quartz crystal with the hydrosol subphase at pH = 9.

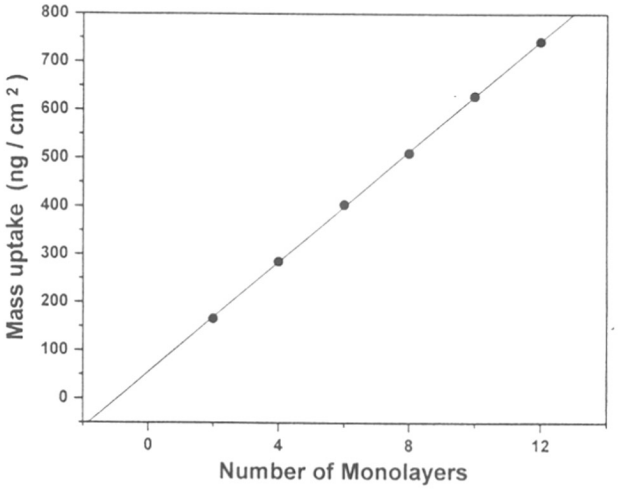


**Figure 4.11:** QCM mass uptake as a function of number of monolayers of CdS-octadecylamine complex transferred from the CdS hydrosol at pH = 9. The solid line is the least square fit to the data.

The mass transfer per dip was determined from a least squares fit to the data which is clearly linear (Fig.4.11, solid line is the regression curve). Calculations based on the mass uptake per dip at pH = 9 yield ~ 30 % surface coverage by 3.5 nm diameter CdS clusters at unity transfer ratios during the downward and upward strokes. This value of surface coverage is larger than the 15 % obtained for self-assembled gold colloidal films by Natan *et al* [7]. While the low surface coverage for self-assembled colloidal films has been explained in terms of repulsive electrostatic interactions between the clusters, the larger value obtained for the films of this study may be due to shielding of the negative charges on the CdS nanoparticles by the positively charged

amine molecules. Another factor that needs to be considered is the attractive Van der Waals interactions between the hydrocarbon tails of the amine molecules which can lead to stability of the CdS nanoparticle assembly at higher surface coverages. The monolayer transfer at pH = 9 was close to unity for up to 30 MLs on the different substrates used in this study beyond which a progressive deterioration in the transfer ratios was observed.

### 4.5-3 UV- visible Spectroscopy

Optical absorption spectroscopy can be used to determine the "band gap" which in the case of Q-state particles, is correctly called the first excitonic transition. Fig.4.12 shows the absorption spectra recorded as a function of the number of CdS-octadecylamine monolayers in the built-up LB films on hydrophobized quartz substrates at subphase pH = 9.

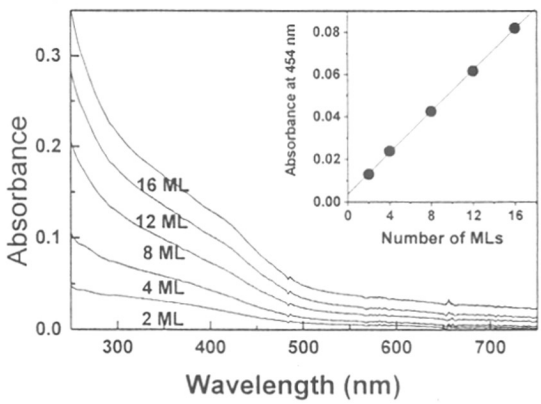


**Figure 4.12:** Optical absorption spectra of several multilayer amine-CdS nanoparticle LB films deposited on hydrophobized quartz substrates at CdS subphase pH = 9. The inset shows the variation of the absorption intensity at 450 nm with film thickness while the solid line is a least squares fit to the data.

The absorption threshold for the CdS LB films occurs at ~ 450 nm and as mentioned earlier, this corresponds to CdS nanoparticles of ~ 3.5 nm diameter [57]. An increase in the absorption intensity at 450 nm can clearly be seen from Fig.4.12. The inset of Fig.4.12 shows the absorbance at 450 nm plotted as a function of number of monolayers in the CdS-octadecylamine LB film. A linear relationship is clearly observed, indicating uniform layer-by-layer transfer of the CdS nanoparticles along with the amine monolayer. As mentioned above, even in the optical absorption spectras no transfer of the CdS nanoparticles at pH = 12 was observed. The QCM and optical absorption data

indicate that lamellar multilayer films of colloidal CdS nanoparticles can be deposited by the LB technique through electrostatic interactions.

### 4.5-4 Ellipsometry

The thickness of multilayer CdS nanoparticle-octadecylamine films grown on Si (111) substrates at pH = 9 was measured using ellipsometry in the manner described in Chapter II [Page 29-33, Section 2.5] of this thesis. The filling factor was determined from QCM measurements to be 5.6 % and the real and imaginary parts of the refractive index for CdS were taken to be 2.48 and 0.03 respectively [58] [$\varepsilon_f = (2.48 + i\ 0.03)^2$] while $\varepsilon_m$ was taken to be $1.5^2$. The film thickness for LB films of different numbers of monolayers transferred was then determined by solving the exact equation of ellipsometry [34] [As described in Chapter II, Section 2.5, Page 29-33]. Fig.4.13 shows a plot of the thickness determined ellipsometrically for the multilayer films transferred onto

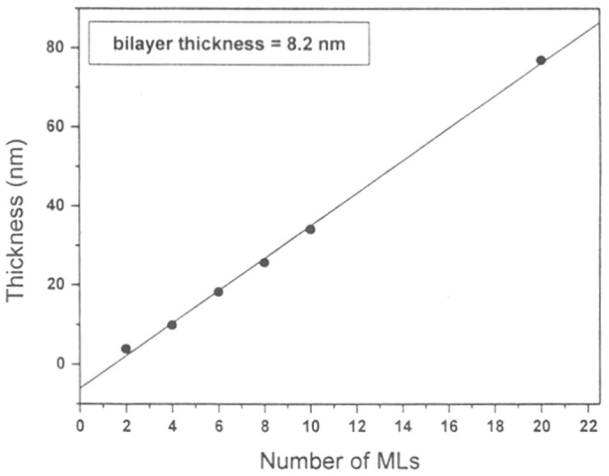


**Figure 4.13:** Thickness of multilayer LB films of CdS nanoparticle-octadecylamine complex as determined from ellipsometry. Details of the calculation are given in the text. The solid line is a least squares fit to the data.

Si (111) substrates. It is seen that there is a linear increase in the thickness indicating good transfer of the monolayers without loss of integrity. This result is in agreement with the QCM and optical absorption results presented earlier. A least squares fit to the data shown in Fig. 4.13 yielded a thickness per bilayer of 8.2 nm. Assuming a thickness per

bilayer of 5.0 nm for the amine molecules[37] leads to a CdS nanoparticle size of 3.2 nm in excellent agreement with optical absorption measurement value of 3.5 nm.

QCM, optical absorption and ellipsometry measurements described above indicate that lamellar growth of the CdS nanoparticle-amine films has been achieved over a fairly large film thickness range. Some distortion in the packing of the amine molecules in the monolayer is to be expected in the vicinity of the nanoparticles due to curvature of the CdS nanoparticle surface, and therefore taking a cue from Yang *et al* [24], a tentative structure for the CdS-octadecylamine LB films is proposed as shown in the opening page of this chapter.

## 4.6 Bilayer formation as a new strategy for surface modification of colloids

Bilayer formation in the manner described in chapter III [page 50, section 3.4] has important implications from the advanced materials point of view. In sections 4.3 to 4.5, using bifunctional molecules, the acid-base electrostatic interaction has been used to immobilize carboxylic acid derivatized metal particles using fatty amine monolayers at the air-water interface. The colloidal particle concentration was controlled through variation of the colloidal subphase pH. Surface modification of colloidal particles with useful functionality using interdigitated bilayers as shown in chapter III [page 50, section 3.4] is a versatile method and obviates the need for bifunctional molecules. Presented below are the data to prove that carboxylic acid and amine derivatized colloidal particles can be electrostatically immobilized at the air-hydrosol interface using the conjugate Langmuir monolayer and good quality multilayer colloidal particle films grown by the Langmuir Blodgett technique.

### 4.6-1 $\pi$-A isotherms

Fig.4.14a shows the $\pi$-A isotherms recorded as a function of time for an octadecylamine Langmuir monolayer on the lauric acid secondary monolayer capped silver colloidal subphase. Curve 1 corresponds to $\pi$-A isotherms recorded 15 min; curve 2 to 30 min and curve 3 to 120 min after spreading the octadecylamine Langmuir monolayer

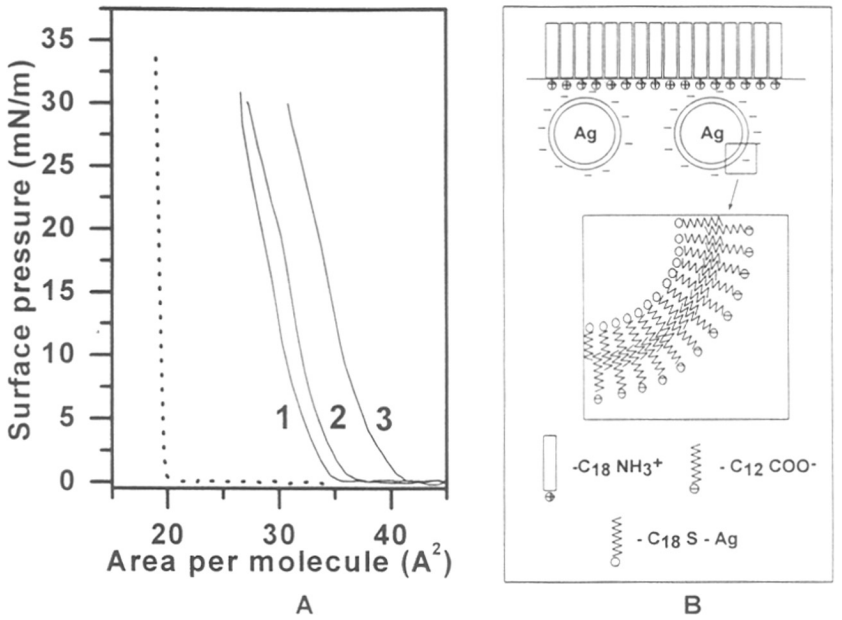


**Figure 4.14** : A) π-A isotherms recorded at different times after spreading the octadecylamine Langmuir monolayer on the lauric acid secondary bilayer capped silver sol (pH = 9) as the subphase - 15 min after spreading (curve 1); 60 min after spreading (curve 2) and 120 min after spreading octadecylamine (curve 3). The dashed line is the π-A isotherm of the fatty amine Langmuir monolayer on pure water at pH = 9.

B) Cartoon showing the electrostatic immobilization of the carboxylic acid derivatized sol with the octadecylamine Langmuir monolayer for which the π-A isotherms are shown in A. The cutaway shows a magnified view of the expected structure of the interdigitated bilayers which leads to carboxylic acid derivatization of the silver sol.

on the subphase. The π-A isotherm recorded for octadecylamine on pure water at pH = 9 is shown for comparison (Fig.4.14a, dotted line). An expansion of the monolayer is clearly seen with time indicating attachment of the silver colloidal particles to the charged amine groups. At the colloidal solution pH of 9, both the carboxylic acid and amine groups are fully ionized (to $-COO^-$ and $-NH_3^+$ respectively) as discussed above in the sections 4.3-4.5. The cartoon in Fig.4.14b shows schematically the electrostatic attachment of the carboxylic acid derivatized silver particles to the octadecylamine Langmuir monolayer as well as a cutaway showing the interdigitated octadecanethiol and lauric acid primary and secondary monolayers. The cartoon is not to scale. Controlled π-A isotherms were recorded for arachidic acid as well as octadecanol Langmuir monolayers on the carboxylic acid derivatized sol and no expansion was observed even after 5 hrs of spreading of the monolayer.

To show the generality of the approach, amine derivatization of the silver colloidal particles was accomplished using octadecylamine as the interdigitated secondary monolayer. The π-A isotherms recorded as a function of time for an arachidic acid Langmuir monolayer on the amine derivatized sol are shown in Fig.4.15a, the dotted curve being the π-A isotherm of arachidic acid on pure water at pH = 9 for comparison. Curve 1 corresponds to π-A isotherms recorded 15 min; curve 2 to 30 min and curve 3 to 120 min after spreading the arachidic acid Langmuir monolayer on the colloidal subphase.

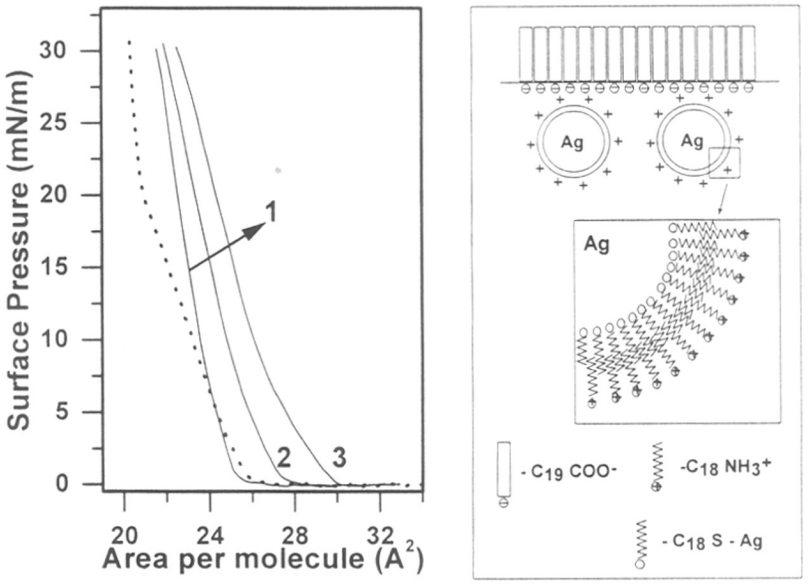


**Figure 4.15** : A) π-A isotherms recorded at different times after spreading the arachidic acid Langmuir monolayer on the octadecylamine secondary bilayer capped silver sol (pH = 9) as the subphase - 15 min after spreading (curve A); 60 min after spreading (curve B) and 120 min after spreading arachidic acid. (curve C). The dashed line is the π-A isotherm of the fatty acid Langmuir monolayer on pure water at pH = 9.
B) Cartoon showing the electrostatic immobilization of the amine derivatized sol with the arachidic acid Langmuir monolayer for which the π-A isotherms are shown in A. The cutaway shows a magnified view of the expected structure of the interdigitated bilayers which leads to amine derivatization of the silver sol.

As in the previous case, expansion of the Langmuir monolayer is observed with time clearly showing electrostatic interaction between the ionized carboxylic acid groups of the Langmuir monolayer and the amine groups of the silver colloidal particles. The corresponding cartoon (Fig.4.15b) shows how the electrostatic immobilization of the

clusters at the air-water interface occurs to the arachidic acid Langmuir monolayer with the cutaway indicating how the interdigitated bilayer leads to amine derivatization of the colloidal particle surface. Controlled π-A isotherm measurements with octadecylamine and octadecanol Langmuir monolayers for this case also yielded a negative result showing that amine derivatization had indeed taken place and that the complexation is a result of an attractive electrostatic process.

### 4.6-2 UV-visible spectroscopy

The formation of good quality films of nanoparticles is important from an application point of view. After measurement of the π-A isotherms was complete, the monolayer was compressed to a surface pressure of 25 mN/m and multilayer films of different thickness were transferred onto hydrophobized quartz substrates and gold coated quartz crystals by the LB technique for study by optical absorption spectroscopy and QCM respectively. Fig.4.16a shows the optical absorption spectra recorded as a function of number of monolayers transferred from the carboxylic acid derivatized silver colloidal subphase onto hydrophobized substrates.

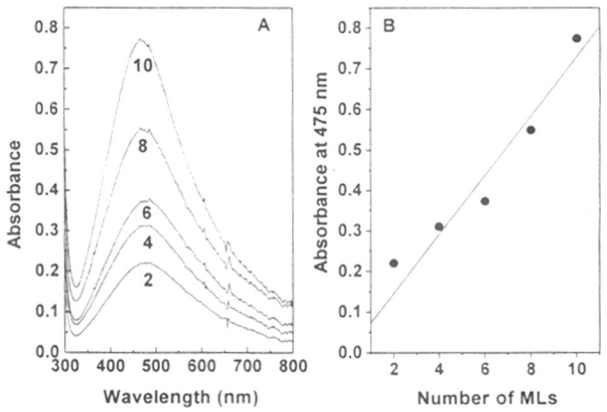


Figure 4.16 :A) Optical absorption spectra recorded from octadecylamine LB films as a function of number of monolayers transferred onto hydrophobized quartz substrates from the lauric acid secondary monolayer capped silver sol. The number of monolayers in the films is indicated next to the respective spectra.

B) The surface plasmon resonance intensity at 475 nm plotted as a function of number of monolayers in LB films grown from the lauric acid secondary monolayer capped silver sol (optical absorption spectra shown in A). The solid line is a least squares fit to the experimental data.

It can be seen that there is an increase in the intensity of the surface plasmon resonance, which occurs at ca. 475 nm, with number of monolayers transferred

(numbers given next to the respective spectra). Fig.4.16b shows the plot of the intensity of the absorbance at 475 nm as a function of number of monolayers transferred. A linear increase in the absorbance is seen indicating that good layer-by-layer transfer of the silver colloidal particles had occurred. Similar optical absorption spectra recorded for arachidic acid-amine derivatized silver colloidal particle films is shown in Fig.4.17a. In this case as well, a progressive increase in the resonance intensity with number of monolayers transferred occurs at ca. 475 nm. The resonance intensity at 475 nm for the spectra shown in Fig.4.17a is plotted as a function of number of monolayers transferred in Fig.4.17b. Thus, good quality multilayer colloidal cluster films can be transferred onto solid substrates by the LB method without significant deviation in the colloidal particle density in the monolayers during successive depositions.

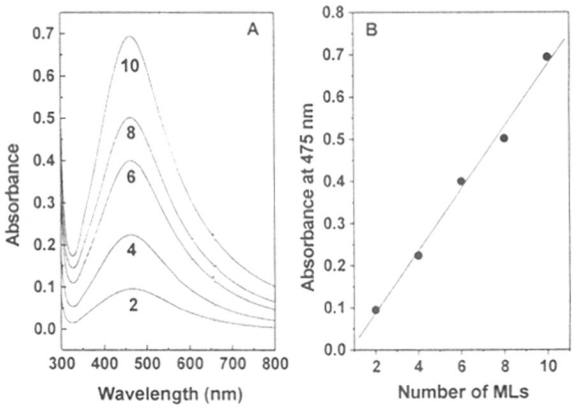


Figure 4.17 :A) Optical absorption spectra recorded from arachidic acid LB films as a function of number of monolayers transferred onto hydrophobized quartz substrates from the octadecylamine secondary monolayer capped silver sol. The number of monolayers in the film is given next to the respective spectra.

B) The surface plasmon resonance intensity at 475 nm plotted as a function of number of monolayers in LB films grown from the octadecylamine secondary monolayer capped silver sol (optical absorption spectra shown in A). The solid line is a least squares fit to the experimental data.

### 4.6-3 Quartz Crystal Microgravimetry

While optical absorption spectroscopy does provide information on the quality of the colloidal films, quantification of the cluster density requires a more direct method such as microgravimetry/nanogravimetry. The mass uptake during successive monolayer transfers has been studied using QCM for the two colloidal solutions studied above and is shown in Fig.4.18 (solid circles, films transferred from the carboxylic acid derivatized silver sol and filled squares, films transferred from the amine derivatized sol).

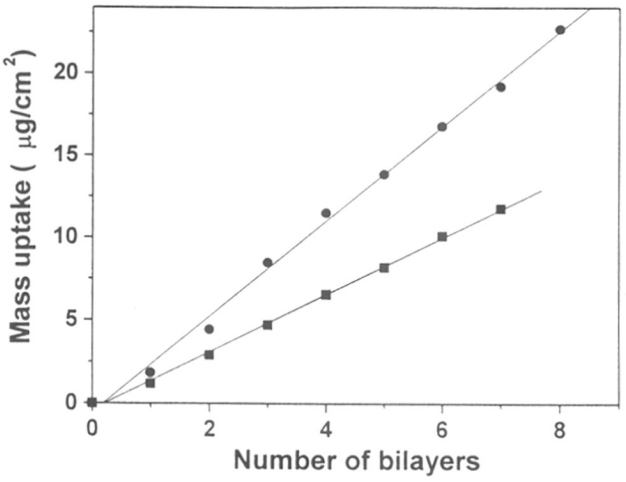


Figure 4.18 : QCM mass uptake as a function of number of monolayers transferred from the lauric acid secondary monolayer capped silver sol (solid circles) and from the octadecylamine secondary monolayer capped silver sol (solid squares). The solid lines are least squares fits to the QCM mass uptake data.

A least squares fit to the data yielded a mass uptake/bilayer (corresponding to one immersion cycle of the quartz crystal in the colloidal subphase) of 2885 ng/cm$^2$ and 1730 ng/cm$^2$ for the films transferred from the carboxylic acid and amine derivatized colloidal subphases respectively. This mass uptake translates into a surface coverage of the silver colloidal particles in the bilayers of 27 and 15 % for the carboxylic acid and amine derivatized cluster films respectively. The surface coverage for the amine derivatized film is close to the surface coverage obtained by Natan *et al* in their study of self-assembly of gold colloidal particles on surface modified polymers [7]. While electrostatic repulsive interactions are known to limit the surface coverage of self-assembled colloidal particles to rather small values, in the case of colloidal particles trapped in Langmuir monolayers, the not inconsiderable attractive van der Waals interactions between the hydrocarbon chains could lead to stabilization of the surface coverage at larger values as observed for the colloidal films transferred from the carboxylic acid derivatized silver sol. Such large colloidal particle coverage has been observed for LB films of bifunctional capped silver particles discussed in section 4.3 of this chapter. The fact that good quality colloidal particle films can be grown by the LB technique indicates that the bilayer assemblies on the colloidal particle surface are quite robust.

## 4.7 Conclusions

- It has been demonstrated that very good quality Langmuir-Blodgett films of surface modified colloidal particles, of silver, gold and cadmium sulfide can be deposited using electrostatic interactions.

- The cluster incorporation into the Langmuir monolayer was found to be pH dependent.

- UV-visible spectroscopy, Quartz crystal Microgravimetry and Ellipsometry measurements of the formed multilayer film indicated that the film growth was lamellar.

- Surface derivatization was brought about using 4-carboxythiphenol, as well as by forming interdigitated bilayers of fatty lipids.

- Hyposthesis of electrostatic interactions responsible for cluster complexation was tested by charging the monolayer and the clusters either way, and the cluster was found to complex in the both the cases.

## 4.8 References:

1. Henglein, A. *Top.Curr.Chem.* **1988**, *143*, 113.

2. Stroscio, J.A.; Eigler, D.M. *Science* **1991**, *254*, 1319.

3. Li, W.; Virtanen, J.A.; Penner, R.M. *Langmuir* **1995**, *11*, 4361.

4. Kim, Y.; Lieber, C. M.; *Science*, **1992**, *257*, 375.

5. Colvin, V.L.; Goldstein, A.N.; Alivisatos, A.P. *J.Am.Chem.Soc.* **1992**, *114*, 5221.

6. Chumanov, G.; Sokolov, K.; Gregory, B.W.; Cotton, T.M. *J.Phys.Chem.* **1995**, *99*, 9466.

7. Grabar, K.C.; Allison, K.J.; Baker, B.E.; Bright, R.M.; Brown, K.R.; Freeman, R.G.; Fox, A.P.; Keating, C.D.; Musick, M.D.; Natan, M.J. *Langmuir* **1996**, *12*, 2353.

8. Yang, J.; Meldrum, F.C.; Fendler, J.H. *J.Phys.Chem.* **1995**, *99*, 5500.

9. Yi, K.C.; Horvolgyi, Z.; Fendler, J.H.; *J. Phys. Chem.* **1994**, *98*, 3872.

10. Rajam, S.; Heywood, B.R.; Walker, J. B.A.; Mann, s.; Davey, R.J.; Birchall, J.D.; *J. Chem. Soc., Faraday Trans.*, **1991**, *87*, 727.

11. Heywood, B.R.; Rajam, S.; Mann, S.; *J. Chem. Soc., Faraday Trans.*, **1991**, *87*, 735.

12. Pan, Z.; Liu, J.; Peng, X.; Li, T.; Wu, Z.; Zhu, M. *Langmuir* **1996**, *12*, 851.

13. Urquhart, R.S.; Furlong, D.N.; Gegenbach, T.; Geddes, N.J.; Grieser, F. *Langmuir* **1995**, *11*, 1127.

14. Furlong, D.N.; Urquhart, R.; Grieser, F.; Tanaka, K.; Okahata, Y., *J.Chem.Soc.Faraday Trans.*, **1993,** *89* , 2031.

15. Mansur, H.S.; Grieser, F.; Urquhart, R. S.; Furlong, D.N.; *J. Chem. Soc., Faraday Trans.* **1995**, *91*, 3399.

16. Leloup, J.; Ruadel-Teixier, A.; Barraud, A. *Thin Solid Films* **1992**, *210/211*, 407.

17. Zylberajch, C.; Ruadel-Teixier, A.; Barraud, A. *Thin Solid Films* **1989**, *179*, 9.

18. Kotov, N.A.; Meldrum, F.C. ; Wu, C.; Fendler, J.H. *J.Phys.Chem.* **1994**, *98*, 2735.

19. Meldrum, F.C.; Kotov, N.A.; Fendler, J.H. *Langmuir* **1994**, *10*, 2035.

20. Nakaya, T.; Li, Y.; Shibata, K. *J.Mater.Chem.* **1996**, *6*, 691.

21. Zhao, X.K.; Xu, X.; Fendler, J.H. *J.Phys.Chem.* **1990**, *94*, 2573.

22. Tian, Y.; Wu, C.; Fendler, J.H. *J.Phys.Chem.* **1994**, *98*, 4913.

23. Peng, X.; Zhang, Y.; Yang, Y.; Zou, B.; Xiao, L.; Li, T. *J.Phys.Chem.* **1992**, *96*, 3412.

24. Yang, J.; Peng, X.; Zhang, Y.; Wang, H.; Li, T. *J.Phys.Chem.* **1993**, *97*, 4484.

25. Ringsdorf, H.; Schlarb, B.; Venzmer, J.; *Angew. Chem. Int. Ed. Engl.*, 1988, 27, 113.

26. Ghelis, C.; Yon, J.; *Protein* Folding, **1982**, 157-160, Academic Press, New York.

27. Bardosova, M.; Tredgold, R.H.; Ali-adib, Z.; *Langmuir*, **1995**, *11*, 1273.

28. Sastry, M.; Patil, V.; Mayya, K.S.; *J. Phys. Chem. B*, **1997**, *101*, 1167

29. Blodgett, K.B. *J.Am.Chem.Soc.* **1935**, *57*, 1007.

30. Sauerbrey, G. *Z.Phys. (Munich)* **1959**, *155*, 206.

31. Henglein, A. *J.Phys.Chem.* **1993**, *97*, 5457.,

32. Johnson, P.B.; Christy, R.W., *Phys.Rev.B.*, **1972**, *6*, 4370.

33. C.G. Granqvist and O. Hunderi, *Z. fur Physik B*, 1978, **30**, 47.

34. R.M.A. Azzam and N.M. Bashara, *Ellipsometry and Polarized Light,* North Holland, New York, 1977. The ellipsomety calculations for determination of the film thickness were done using an application written by M.S. in Mathcad (a commercial mathematical package of Mathsoft Inc.). The application, ELLIP1.MCD, is available from the Mathsoft public domain on the internet.

35. Grayer Wolf, S.; Landau, E.M.; Lahav, M.; Leiserowitz, M.; Deutsch, M.; Kjaer, K.; Als-Nielsen, J. *Thin Solid Films* **1988**, *159*, 29

36. Contact angles were measured with a Rame-Hart 100 goniometer on a sessile drop.

37. Ganguly, P.; Paranjape, D.V.; Sastry, M. *J.Am.Chem.Soc.* **1993**, *115*, 793.

38. Ganguly, P.; Paranjape, D.V.; Sastry, M. *Langmuir* **1993**, *9*, 577.

39. Yang, J.; Peng, X.; Zhang, Y.; Wang, H.; Li, T. *J.Phys.Chem.* **1993**, *97*, 4484.

40. Urquhart, R.S.; Hoffmann, C.L.; Furlong, D.N.; Geddes, N.J.; Rabolt, J.F.; Grieser, F. *J.Phys.Chem.* **1995**, *99*, 15987.

41. Hostetler, M.J.; Stokes, J.J.; Murray, R.W. *Langmuir* **1996**, *12*, 3604.

42. Rabolt, J.F.; Burns, F.C.; Schlotter, N.E.; Swalen, J.D. *J.Chem.Phys.* **1983**, *78*, 946.

43. P. Mulvaney, *Langmuir*, 1996, **12**, 788.

44. C.D. Bain and G.M. Whitesides, *Langmuir*, 1989, **5**, 1370.

45. G.L. Gaines Jr., *Nature*, 1982, **298**, 544.

46. Blatchford, C.G.; Campbell, J.r.; Creighton, J.A.; *Sur. Sci.*, **1982**, *120*, 435

47. Sastry, M; Ganguly, P.; Badrinarayanan, S.; Mandale, A.B.; Sainkar, S.R.; Paranjape, D.V.; Patil, K.R.; Chaudhary, S.K.; *J.Chem.Phys.*, **1991**, *95* , 8631.

48. Brust, M.; Walker, M.; Bethell, D.; Schiffrin D.J.; Whyman, R. *J.Chem.Soc.,Chem.Commun.*, **1994**, 801.

49. Wang Y.; Herron, N. *J.Phys.Chem.*, **1991**, *95*, 525.

50. V.L. Colvin, M.C. Schlamp and A.P. Alivisatos, *Nature*, 370 (1994) 354.

51. N.N. Ledentsov, J. Bohrer, D. Bimberg, S.V. Zaitsev, V.M. Ustinov, A. Yu Egorov, A.E. Zhukov, M.V. Maximov, P.S. Kopev, Zh.I. Alferov, A.O. Kosogov, U. Gosele and S.S. Ruvimov, in Proceedings of the Spring Meeting of the Materials Research Society, San Francisco, **1996**, CA, 8-12 April,.

52. A.P. Alivisatos, *Science*, 271 (1996) 933.

53. C. Zylberajch, A. Ruadel-Teixier and A. Barraud, *Synthetic Metals*, 27 (1988) B609.

54. R.S. Urquhart, D.N. Furlong, H. Mansur, F. Grieser, K. Tanaka and Y. Okahata, *Langmuir*, 10 (1994) 899.

55 L.E. Brus, *J.Chem.Phys.*, 80 (1984) 4403.

56. L.E. Brus, *J.Phys.Chem.*, 90 (1986) 2555.

57. A. Henglein, *Chem.Rev.*, 89 (1989) 1861.

58. J. Gottesman and W.F.C. Ferguson, *J.Opt.Soc.Amer.*, 44 (1954) 368.

59. R.S. Urquhart, D.N. Furlong, H. Mansur, F. Grieser, K. Tanaka and Y. Okahata, *Langmuir*, 10 (1994) 899.

# CHAPTER V

# Role of Spacer Molecule in the Electrostatic Immobilization of colloidal particles at the air-water interface

Electrostatic immobilization of colloidal particles has been further controlled using neutral and charged spacer molecule at the Langmuir Monolayer.

Work discussed in this chapter has been published: Mayya, K.S.; Sastry, M.; *Langmuir*, **1998**, *14*, 74.

## 5.1 Introduction

In chapter IV, from section 4.3 to 4.6, focus was on the use of charged fatty amine Langmuir monolayers for electrostatic immobilization of carboxylic acid derivatized colloidal metal particles at the air-water interface. It was shown that the cluster density at the air-water interface (and consequently in the built-up Langmuir Blodgett [LB] films) could be regulated through simple variation of the colloidal subphase pH. Another important variable for regulating the cluster density is by using either charged or neutral spacer molecule in the Langmuir Monolayer.

In this chapter, results of a study on the effect of electrically neutral spacer molecules (octadecanol) in regulating the charge in Langmuir monolayers of octadecylamine and consequent changes in the complexation of carboxylic acid derivatized silver colloidal particles with the amine monolayer is presented. The kinetics of cluster complexation at the air-water interface has been followed by measurement of the $\pi$-A isotherms for the Langmuir monolayer as well as indirectly through quartz crystal microgravimetry (QCM), UV-vis spectroscopy and ellipsometry measurements of the built-up LB films. It is observed that the cluster density at the air-water interface increases as the amine : octadecanol molar ratio in the Langmuir monolayer increases and is consistent with an electrostatically controlled process. An electrically neutral Langmuir monolayer surface containing equimolar quantities of octadecylamine (positively charged) and stearic acid ($CH_3(CH_2)_{16}COOH$, negatively charged) molecules showed negligible complexation, with the silver colloidal particles supporting further the electrostatic interaction concept. The complexation of the clusters with the Langmuir monolayer is slow and equilibrium cluster densities are obtained only after ca. 15 hours of spreading of the Langmuir monolayer. This is an interesting result given that the $\pi$-A isotherms stabilized within 2-3 hours of spreading the Langmuir monolayer on the colloid surface. This indicates that $\pi$-A isotherm measurements alone cannot yield unequivocal information on complexation processes occurring at the air-water interface. Details of the investigation are presented below.

The surface modified silver hydrosol is prepared as described in chapter III. The pH of the sol was adjusted to 9 using dilute $H_2SO_4$ since at this pH, both the amine and carboxylic acid groups are fully charged thereby leading to maximum electrostatic interaction between them. All measurements described in this chapter are for films

transferred from a pH 9 silver colloidal subphase. The colloidal particle size was determined from transmission electron microscopy (TEM) to be 73 ± 12 Å.

## 5.2 Pressure-Area Isotherms

The complexation of the derivatized silver colloidal particles with Langmuir monolayers containing octadecanol and octadecylamine molecules in the molar ratios 1 : 1, 3 : 1 and 9 : 1 respectively was followed by measurement of the surface pressure variation with area per molecule in the monolayer (π-A isotherms). A known quantity of the octadecylamine-octadecanol mixture in chloroform was dispersed on the silver sol (pH = 9, 25° C) and the π-A isotherms measured as a function of time using a Nima model 611 Langmuir trough equipped with a Wilhelmy plate for pressure sensing. π-A isotherms with time were also recorded for a Langmuir monolayer consisting of equimolar quantities of octadecylamine and stearic acid molecules spread on the surface of the silver sol. As mentioned earlier, the pH of the subphase hydrosol was adjusted to 9 since the amine molecules in the Langmuir monolayer and the carboxylic acid groups of 4-CTP are fully charged at this value. π-A isotherms are known to yield information on the interaction of Langmuir monolayers with counterions in the subphase[1] and has also been used to follow the complexation of colloidal particles at the air-water interface as described in chapter IV.

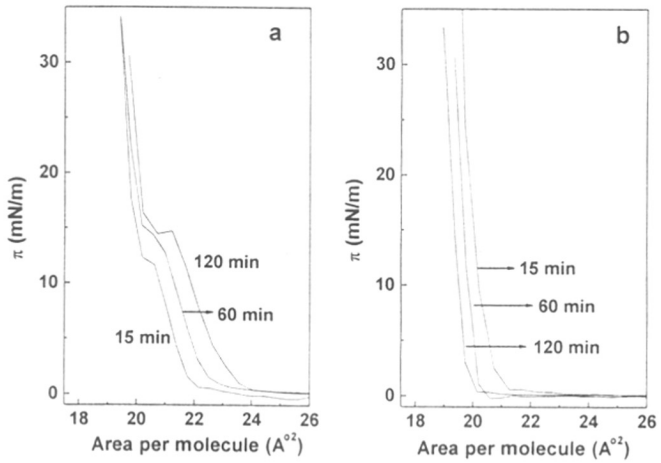


**Figure 5.1** : a) π-A isotherms as a function of time for an octadecanol : octadecylamine 1 : 1 Langmuir monolayer on the silver hydrosol (pH = 9). The time after spreading the monolayer is indicated next to the curves.
b) π-A isotherms as a function of time for a stearic acid : octadecylamine 1 : 1 Langmuir monolayer on the silver hydrosol (pH = 9). The time after spreading the monolayer is indicated next to the curves.

Proceeding in this spirit, π-A isotherms were measured at different time intervals after spreading the 1 :1, 3 : 1 and 9 : 1 octadecanol : octadecylamine Langmuir monolayers on the silver hydrosol and are shown in Figures 5.1a, 5.2a and 5.2b respectively.

The octadecanol molecule remains electrically neutral and acts as a spacer molecule in the octadecylamine Langmuir monolayer. Increasing the octadecanol molar ratio in the Langmuir monolayer reduces the surface charge density at the air-water interface arising

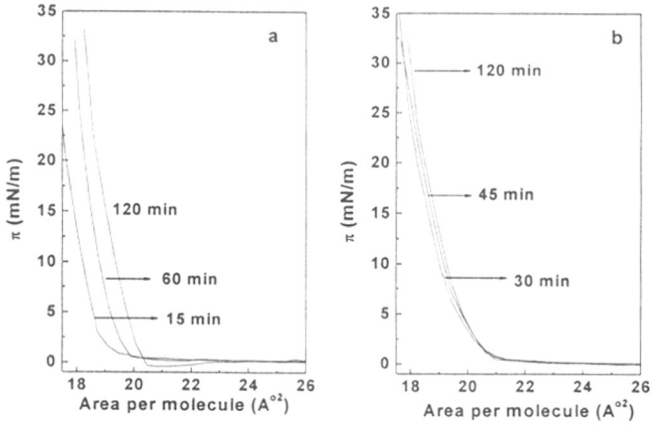


**Figure 5.2 :** a) π-A isotherms as a function of time for an octadecanol : octadecylamine 3 : 1 Langmuir monolayer on the silver cluster hydrosol (pH = 9). The time after spreading the monolayer is indicated next to the curves.
b) π-A isotherms as a function of time for an octadecanol : octadecylamine 9 : 1 Langmuir monolayer on the silver cluster hydrosol (pH = 9). The time after spreading the monolayer is indicated next to the curves.

from the positively charged amine molecules. π-A isotherms as a function of time were also measured for a 1 : 1 octadecylamine : stearic acid Langmuir monolayer on the silver hydrosol and is shown in Fig.5.1b. At pH = 9, the surface charge for this monolayer is expected to be close to zero due to balancing of the positive and negative charges from the amine and stearic acid molecules respectively. A comparison of Figures 5.1a, 5.2a and 5.2b show that there is an expansion of the monolayer with time and also that the expansion increases as the percentage of amine molecules in the monolayer increases. The form of the isotherms is also different for these monolayers, especially for the 1 : 1 case (Figure 5.1a). A possible explanation for the kinks seen in the π-A isotherms of Fig.5.1a could be phase separation of the octadecylamine and octadecanol components in the Langmuir monolayer. However, this is not likely for the following reasons. Firstly, the hydrocarbon chain length of the two molecules is nearly

identical making phase separation enthalpically not very favorable. Mixing of the two components would not only be entropically favorable but would also lead to minimization of the repulsive electrostatic interactions between the protonated amine groups due to increased separation arising from the presence of the spacer octadecanol molecules. In this context, the work of Kurnaz and Schwartz who have performed atomic force microscopy (AFM) studies on phase separation in LB films of arachidic acid/cadmium arachidate is of great importance [4-5]. They remark that the question of phase separation in acid/soap monolayers at the air-water interface is still open and that the phase separation observed in the AFM micrographs is likely to occur during transfer of the monolayers to solid supports. [5] While the system studied in this paper is quite different with complexation of large, highly charged colloidal particles being considered, the above highlights some of the problems associated with understanding phase separation in mixed monolayers purely from $\pi$-A isotherm measurements. The isotherms have been used mainly to follow trends in cluster complexation at the air-water interface as indicated by variation in the liftoff areas in the isotherms. A very small expansion of the monolayer was observed for the 9 : 1 case (Figure 5.2b). The monolayer expansion was observed to stabilize within ca. 2 hours of spreading the Langmuir monolayer. For the 1 : 1 octadecylamine : stearic acid case, a small decrease in the area per molecule was observed which also stabilized after 2 hours of spreading the monolayer (Figure 5.1b). While the reduction in the monolayer area is not understood, it is clear that significant complexation of the silver particles had not occurred for the mixed amine-stearic acid Langmuir monolayer. The above observations from the $\pi$-A isotherms (Figures 5.1 and 5.2) are consistent with a complexation of the clusters with the amine monolayer driven by attractive electrostatic interactions. These results thus provide further support to the work presented in the previous chapter, where an electrostatic interaction mechanism was used to explain the variation in cluster density at the air-water interface through regulation of the Langmuir monolayer surface charge via the colloidal subphase pH.

## 5.3 Quartz Crystal Microgravimetry

The time dependence of complexation of the silver colloidal particles with the different Langmuir monolayers was also studied using QCM. Figure 5.3 shows the mass uptake calculated for bilayer films deposited on the quartz crystals from the 1 : 1 (curve

A, squares), 3 : 1 (curve B, circles) and 9 : 1 (curve C, triangles) Langmuir monolayer covered surfaces at different times after spreading the monolayer.

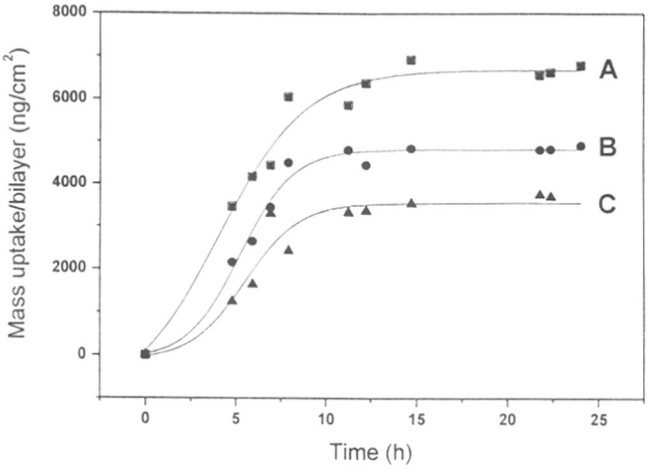


**Figure 5.3 :** Variation with time in the mass uptake per bilayer from QCM measurements for the 1 : 1 (curve A, squares), 3 : 1 (curve B, circles) and 9 : 1 (curve C, triangles) octadecanol : octadecylamine Langmuir monolayers on the silver cluster hydrosol (see text for details).

The solid curves have been drawn to aid the eye and have no physical significance. The following observations can be made from the QCM study. The equilibrium cluster density in the bilayers (and hence at the air-water interface) increases as the amine percentage in the monolayer increases and is consistent with an electrostatically driven immobilization process. The equilibrium mass loadings for the 1 : 1, 3 : 1 and 9 : 1 films is determined to be 6600, 4900 and 3700 ng/cm$^2$ respectively. Assuming an average cluster size of 70 Å, this translates to a cluster volume fraction of 30, 24 and 19.5 % for the above films respectively. The cluster volume fraction data is important for ellipsometric characterization of the films as will be demonstrated subsequently. QCM measurements of the mass per bilayer for the octadecylamine-stearic acid 1 : 1 monolayer as a function of time indicated transfer of only the amine-acid bilayer with no evidence for complexation of the silver colloidal particles.

The time for equilibration of the silver particle density at the air-water interface is estimated from the QCM data of Figure 5.3 to be ca. 15 hours for the 3 : 1, 9 : 1 and 1 : 1 Langmuir monolayers. This result is significant when one recollects that the expansion in the π-A isotherms stabilized within 2 hours of spreading of the Langmuir monolayers and indicates that π-A isotherms are rather insensitive to complexation of colloidal

particles, particularly when the monolayer is in an expanded state [chapter IV, section 4.3-1, page 61]. However, given that the time scale over which film preparation was done for the work described in Chapter IV, it is considerably smaller than the complexation times unequivocally determined in this work, the conclusions of the previous chapter are not altered significantly. It may be remarked that this aspect has escaped the notice of other groups as well [2-3].

## 5.4 UV-visible Spectroscopy

Silver colloidal particles are ideal for characterization using UV-vis spectroscopy due to the strong surface plasmon resonance exhibited by this metal.[6-7] In a parallel UV-vis spectroscopy experiment, 4 ML LB films from the different Langmuir monolayer covered colloidal subphases were grown on hydrophobized quartz substrates at different times after spreading of the Langmuir monolayers. For brevity, only the optical absorption spectra recorded for LB films transferred at different times from the 1 : 1 Langmuir monolayer (Fig.5.4a) is shown.

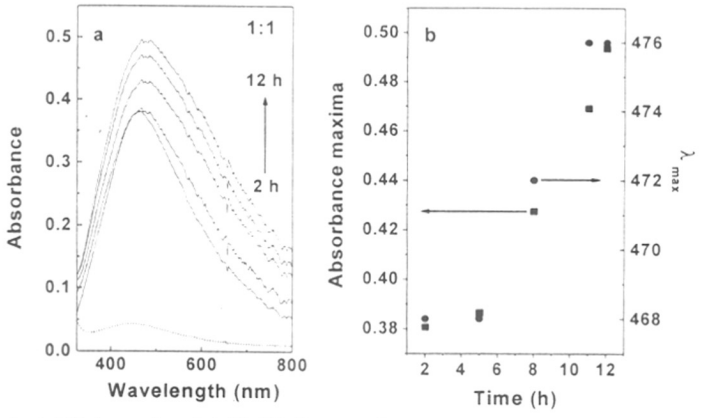


**Figure 5.4 :** a) UV-vis spectra of 4 ML LB films transferred onto hydrophobized quartz substrates from the octadecanol : octadecylamine 1 : 1 Langmuir monolayer on the silver cluster hydrosol as a function of time after spreading the monolayer. b) Time variation of the absorbance maximum (left axis, squares) and position of the plasmon resonance, $\lambda_{max}$ (right axis, circles) for the UV-vis spectra shown in Figure 5.4(a).

For comparison, the UV-vis spectrum recorded from a 4 ML LB film deposited from the octadecylamine-stearic acid 1 : 1 Langmuir monolayer after cluster density equilibration (i.e., deposition carried out 15 hours after spreading the Langmuir monolayer) is shown as a dotted line in Figure 5.4a. Fig.5.4b shows the time variation in the values of the absorbance maximum (left axis, filled squares) and position of the surface plasmon resonance, $\lambda_{max}$ (right axis, filled circles) for the corresponding UV-vis spectra shown in

Fig.5.4a. Figs.5.5a and b respectively, represents the values of the absorbance maxima and plasmon

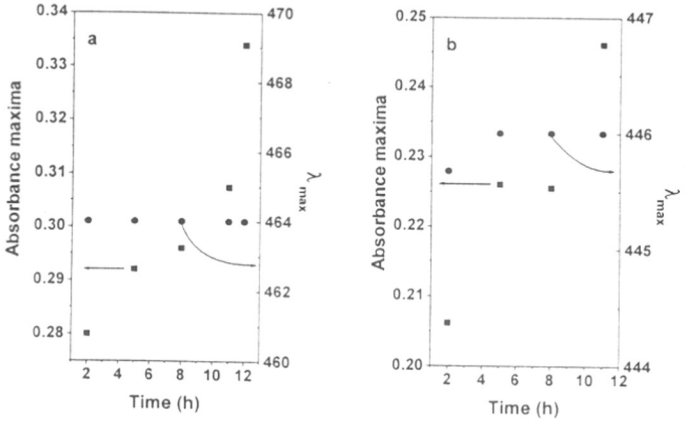


**Figure 5.5 :** a) Time variation of the absorbance maximum (left axis, squares) and position of the plasmon resonance, $\lambda_{max}$ (right axis, circles) for the UV-vis spectra recorded from 4 ML LB films transferred onto hydrophobized quartz substrates from the 3 : 1 Langmuir monolayer.
b) Time variation of the absorbance maximum (left axis, squares) and position of the plasmon resonance, $\lambda_{max}$ (right axis, circles) for the UV-vis spectra recorded from 4 ML LB films transferred onto hydrophobized quartz substrates from the 9 : 1 Langmuir monolayer.

resonance wavelength measured with time for the LB films transferred from the 3 : 1 and 9 : 1 Langmuir monolayers. It is observed from Figures 5.4 and 5.5 that the absorbance maximum intensity increases as a function of time and stabilizes close to 12 hours after spreading of the respective Langmuir monolayers. This implies that the cluster density at the air-water interface stabilizes in this time period, in agreement with the QCM results. Also in agreement with the QCM results which showed an increase in the equilibrium cluster density with increase in the charged amine concentration in the Langmuir monolayer are the values of the absorbance maxima (after equilibration of the cluster density at the air-water interface) for the different Langmuir monolayers. This value is highest for the 1 : 1 monolayer (0.5), least for the 9 : 1 monolayer (0.25) with the 3 : 1 monolayer showing an intermediate value of 0.33. A negligibly small absorbance was recorded for the amine-stearic acid Langmuir monolayer indicating poor complexation of the clusters for an effectively charge neutral surface. The UV-vis measurements on the LB films as discussed above thus clearly support the conclusions of the QCM measurements wherein a slow complexation of the negatively charged clusters with the positively charged amine Langmuir monolayers was observed which required ca. 12 hours for reaching equilibrium cluster densities.

A closer inspection of Figures 5.4 and 5.5 reveals an interesting point. While the absorbance maximum increases with time as observed and commented upon above, the position of the surface plasmon resonance, $\lambda_{max}$, is also a function of time. For the 1 : 1 Langmuir monolayer (Figure 5.4b), $\lambda_{max}$ increases with time from 468 nm to 476 nm whereas it is fairly constant at 464 nm (Figure 5.5a) and 446 nm (Figure 5.5b) for the 3 : 1 and 9 : 1 Langmuir monolayers respectively. The position of the surface plasmon resonance is a strong function of the effective refractive index of the film[6-7]. As the effective refractive index of the film increases, as would occur when the cluster density in the film increases, the surface plasmon shifts to larger wavelengths (to the "red"). The equilibrium values of $\lambda_{max}$ for the 1 : 1, 3 : 1 and 9 : 1 Langmuir monolayers show a progressive decrease from 476 nm to 446 nm which from the effective medium approximation[8-9] indicates a reduction in the equilibrium cluster density in the films as the percentage of charged amine molecules in the monolayer is reduced. This is clearly illustrated in Figure 5.6a where the UV-vis spectra of 4 ML LB films transferred after

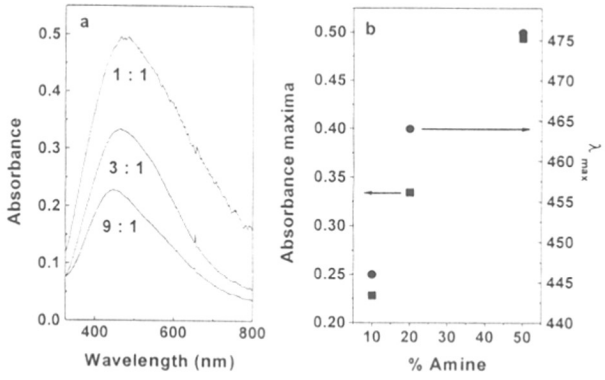


**Figure 5.6 :** a) UV-vis spectra of 4 ML LB films transferred onto hydrophobized quartz substrates from the 1 : 1, 3 : 1 and 9 : 1 octadecanol : octadecylamine Langmuir monolayers on the silver cluster hydrosol after equilibration of the cluster density at the air-water interface. The octadecanol : octadecylamine molar ratios are indicated next to the curves. b) Variation of the absorbance maximum (left axis, squares) and position of the plasmon resonance, $\lambda_{max}$ (right axis, circles) with percentage of octadecylamine in the monolayer for the UV-vis spectra shown in Figure 5.6(a).

equilibration of the cluster density at the Langmuir monolayer surface have been plotted for the different amine concentrations. The variation in the absorbance maximum (Figure 5.6b - left axis, filled squares) and $\lambda_{max}$ (Figure 5.6b- right axis, filled circles) are also shown for ease of visualizing the points discussed above. The fact that $\lambda_{max}$ does not change much with time for the 3 : 1 and 9 : 1 Langmuir monolayers indicates that the variation in the effective refractive index with cluster density for these films is not

large enough to yield experimentally measurable shifts in the surface plasmon resonance.

## 5.5 Ellipsometry

After determination of the equilibration times for the clusters from QCM and UV-vis spectroscopy studies at the different Langmuir monolayer surfaces, attempt has been made to determine ellipsometrically the thickness per bilayer for each of the three cases. After waiting for ca.15 hours after spreading the 1 : 1, 3 : 1 and 9 : 1 Langmuir monolayers on the silver sol, the ellipsometric angles were measured as a function of number of bilayers transferred from the different Langmuir monolayer surfaces onto hydrophobized Si (111) substrates and the thickness was calculated as described in chapter II [Page 30-33, section 2.5-1].

For the volume fractions of the clusters mentioned above, effective complex refractive indices of 1.687 - 0.549 i, 1.668 - 0.441 i and 1.64 - 0.35 i for the 1 : 1, 3 : 1 and 9 : 1 films respectively is obtained. The film thickness for different LB films as a function of number of bilayers transferred was then determined from the measured ellipsometric angles and the calculated complex refractive indices by solving the exact equation of ellipsometry.[8] Figure 5.7 shows the results of the ellipsometry study where the film thickness has been plotted for 5 immersion cycles (10 MLs film thickness) of the Si substrate.

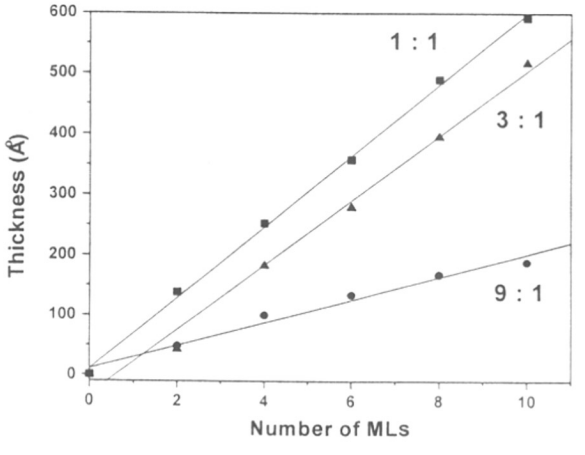


**Figure 5.7 :** Variation of film thickness determined ellipsometrically as a function of number of monolayers transferred onto hydrophobized Si substrates from the 1 : 1, 3 : 1 and 9 : 1 octadecanol : octadecylamine Langmuir monolayers on the silver cluster hydrosol after equilibration of the cluster density at the air-water interface. The octadecanol : octadecylamine molar ratios are indicated next to the curves. The solid lines are based on least squares fits to the data.

The thickness per bilayer was then determined from a least squares analysis of the data, the fit being indicated by solid lines in the figure. As can be seen from Figure 5.7, the increase in thickness as a function of number of bilayers transferred is linear indicating that the bilayers are transferred without much disruption in the integrity of the monolayer at the air-water interface. This is an important result since clusters of dimensions comparable to the bilayer dimensions of the amine/octadecanol molecules are sought to be transferred by the LB technique. The fit to the ellipsometry data for the 1 : 1, 3 : 1 and 9 : 1 monolayers yield thickness per bilayer values of 118, 107 and 39 Å respectively. In the first two cases, where the volume fraction of silver clusters is fairly high, the bilayer thickness value is consistent with transfer of 70 Å clusters with a fairly undistorted bilayer of the octadecylamine/octadecanol molecules (bilayer thickness for these molecules ~ 50 Å). [9] The small value of 39 Å for the 9 : 1 film indicates disorder in the film and reorganization of the clusters, possibly due to the small volume fraction of the clusters in this film. Since the techniques used in this investigation do not provide information on the depth profile of the clusters in the films, it is difficult to comment on the exact organization of the clusters in the films.

## 5.6 Conclusions

To conclude, it has been shown through the use of neutral spacer molecules in Langmuir monolayers of octadecylamine that an electrostatic interaction picture adequately describes the complexation of carboxylic acid derivatized silver colloidal particles at the monolayer surface. The complexation is slow, requiring ca. 15 hours for reaching equilibrium cluster densities at the air-water interface. Ellipsometry measurements indicate transfer of the cluster-octadecylamine/octadecanol monolayers without disruption in the cluster density in the monolayers. Films grown from a low cluster density Langmuir monolayer indicated a fair amount of disorder in the film and hence deviation from a "lamellar" growth mode.

## 5.7 References

1. Linden, M.; Rosenholm, J.B. *Langmuir.* **1995**, *11*, 4499.

2. Tian, Y.; Wu, C.; Fendler, J.H. *J.Phys.Chem.* **1994**, *98*, 4913.

3. Peng, X.; Zhang, Y.; Yang, J.; Zou, B.; Xiao, L.; Li, T. *J.Phys.Chem.* **1992**, *96*, 3412.

4. Kurnaz, M.L.; Schwartz, D.K. *Langmuir* **1996**, *12*, 4971 .

5. Kurnaz, M.L.; Schwartz, D.K. *J.Phys.Chem.* **1996**, *100*, 11113.

6. Henglein, A. *J.Phys.Chem.* **1993**, 97, 5457.

7. Mulvaney, P. *Langmuir* **1996**, *12*, 788

8. Azzam, R.M.A. and Bashara, N.M. *Ellipsometry and Polarized Light,* North Holland, New York, **1977**. The ellipsomety calculations for determination of the film thickness were done using an application written by M.S. in Mathcad (a commercial mathematical package of Mathsoft Inc.). The application, ELLIP1.MCD, is available from the Mathsoft public domain on the internet.

9. Ganguly, P.; Paranjape, D.V.; Sastry, M. *J.Am.Chem.Soc.* **1993**, *115*, 793.

# CHAPTER VI

## Partitioning of carboxylic acid derivatized clusters at the air-water interface based on their size

Immobilization of surface-modified colloidal particles at the air-water interface is advanced further through a study of the *simultaneous complexation* of carboxylic acid derivatized gold and silver colloidal particles.

The contents of the chapters are published in: K. S. Mayya, Murali Sastry, *J. Phys. Chem.B*, **1997**, *101*, 9790.

## 6.1 Introduction

In the previous chapters, it was shown that suitably charged colloidal particles can be immobilized at the air-water interface with oppositely charged Langmuir monolayers via simple electrostatic interaction. Furthermore, the electrostatic interaction and as a consequence, the cluster density in the Langmuir monolayers as well as the built-up multilayer LB films can be controlled by simple modulation of the subphase pH [ Chapter IV, Sections 4.3 to 4.6]. Studies on the variation in cluster density as well as the kinetics of cluster immobilization at the air-water interface by diluting the surface charge via incorporation of neutral spacer molecules in the Langmuir monolayers put the electrostatic interaction model on firm foundation [Chapter V]. In this chapter, the investigation into the electrostatic immobilization of surface-modified colloidal particles at the air-water interface is advanced further through a study of the *simultaneous complexation* of carboxylic acid derivatized gold and silver colloidal particles (130 ± 30 and 70 ± 12 Å diameter respectively) differing vastly in size with octadecylamine Langmuir monolayers. It is observed that even though expansion of the Langmuir monolayer, as evidenced by π-A isotherm measurements, is complete within 3 hours of spreading the monolayer, QCM and UV-vis spectroscopy studies indicate that the kinetics of cluster immobilization at the air-water interface is much slower, taking upto 12 hours for the cluster density to stabilize. Stabilization of the density of the larger gold clusters at the air-water interface occurs much more rapidly than for smaller silver clusters. LB films grown from a subphase consisting of a mixture of the two different colloidal particles show a higher than expected gold cluster density in the films. These observations are discussed in terms of an electrostatic model, which also takes into account the effects of cluster size dependent distortion to the fatty amine Langmuir monolayer.

## 6.2 Experimental details

The colloidal solutions of gold and silver and their capping with the bifunctional molecule, 4-carboxythiophenol (4-CTP) was accomplished as described in chapter III [section 3.2, page 44 ] . Thiolate linkage of 4-CTP with the gold and silver particle surface leads to carboxylic acid derivatization of the colloidal particles. Transmission electron microscopy (TEM) of the gold and silver sols yielded 130 ± 30 and 70 ± 12 Å diameter respectively. Hydrosols containing both silver and gold clusters were prepared

by mixing the individual sols in different volume ratios to obtain varying silver : gold cluster concentrations in solution. In this study, solutions of silver : gold ratios of 2 :1, 1 : 1 and 1 : 2 were prepared for use as the subphase. Unless otherwise mentioned, a ratio of x : y should be taken to imply a mixture of x parts (by volume) of the silver sol with y parts of the gold sol. The mixed hydrosol pH was adjusted to 9 using HCl since the cluster incorporation in the amine films was found to be maximum close to this pH.[Chapter IV, Section 4.3] The volume ratio of the individual sols used throughout this study is not to be confused with the actual cluster concentration ratios in the mixture. In fact, for the cluster sizes reported earlier and assuming complete reduction of the salt solution, a 1 : 1 solution would contain ca. 4 times as many silver clusters per unit volume as gold clusters. UV-vis spectra of the mixed sols indicated that the clusters were stable over weeks with no evidence for flocculation or cross-linking of the clusters.

Pressure-area ($\pi$-A) isotherms of octadecylamine Langmuir monolayers on the different colloidal subphases were recorded at a temperature of 25° C on a Nima 611 Langmuir trough equipped with a Wilhelmy plate for surface pressure sensing. The $\pi$-A isotherms were recorded as a function of time at a compression rate of 25 $cm^2$/min. Multilayer films of the octadecylamine monolayer complexed to the colloidal particles were grown by the Langmuir Blodgett technique on lead arachidate coated quartz substrates [1] as well as gold coated AT-cut quartz crystals for quartz crystal microgravimetry (QCM) and UV-vis spectroscopy measurements respectively. The film transfer was done at different times after spreading the octadecylamine monolayer on the colloidal subphase. *Ex-situ* QCM measurements were carried out on the 6 MHz quartz crystals using an Edwards FTM5 frequency counter which had a frequency stability and resolution of ± 1 Hz (~ 12 ng/$cm^2$ mass resolution). The change in the crystal resonance frequency on transfer of the films was converted to a mass loading using the Sauerbrey formula.[2] UV-vis measurements of the LB films transferred to hydrophobized quartz substrates were performed on a Hewlett Packard 8542 diode array spectrophotometer operated at a resolution of 2 nm. X-ray fluorescence (XRF) measurements were carried out on a Rigaku 3070 instrument.

## 6.3 π-A isotherms

Measurement of π-A isotherms can provide important information on the process of complexation occurring at the air-water interface in the presence of Langmuir monolayers [3, 4]. Figure 6.1 shows the π-A isotherms recorded as a function of time for the octadecylamine monolayer on a 1 : 1 colloidal subphase (solid lines; A - 30 minutes and B - 180 minutes after monolayer spreading) along with the isotherm for amine on pure water at pH = 9 for comparison (dashed line).

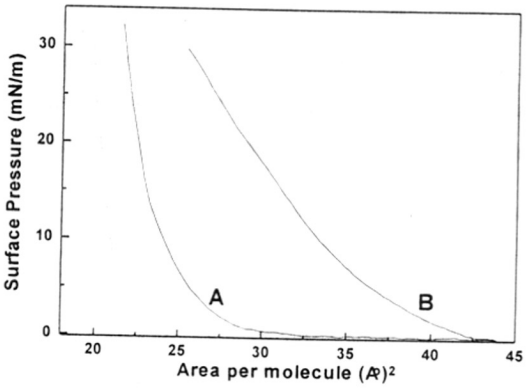


**Figure 6.1 :** π-A isotherms of an octadecylamine Langmuir monolayer spread on the 1 : 1 colloidal subphase at pH = 9 measured at different times after spreading the monolayer; curve a - after 30 minutes of monolayer spreading; curve b - after 180 minutes of monolayer spreading on the 1 : 1 subphase. Dashed line - isotherm for octadecylamine on pure water at pH = 9.

This isotherm is representative of the isotherms measured on the 2 : 1 and 1 : 2 colloidal subphases and is quite similar to the time dependence of the isotherms observed for the pure gold and silver subphase described in chapter4 [refer Fig. 4.1 and Fig. 4.5]. The important point of similarity is that an expansion of the monolayer occurs upto ca. 3 hours of spreading the amine monolayer after which negligible changes were observed.

## 6.4 Quartz Crystal Microgravimetry and UV-vis Spectroscopy

The kinetics of cluster immobilization at the air-water interface was also studied by QCM and UV-vis spectroscopy in the following manner. Bilayers of the octadecylamine monolayer complexed to the colloidal particles were transferred to the gold coated quartz crystals at a surface pressure of 25 mN/m at different times after spreading the amine monolayer on pure silver, 1 : 1 and pure gold subphases. For the UV-vis measurements, 4 monolayers (MLs) of the colloidal particle complex were transferred to hydrophobized quartz substrates in a similar manner. Figure 6.2 shows the QCM mass uptake per bilayer measured for the films transferred from the different subphases (a - 1 : 1 ; b - pure silver and c - pure gold subphase). The solid curves have been drawn to aid the eye and have no physical significance. It is seen that while the mass uptake per bilayer increases steadily with time upto ca. 12 hours for films transferred from the pure silver and 1 : 1 subphases, the mass per bilayer is fairly constant for bilayers transferred from the pure gold colloidal subphase.

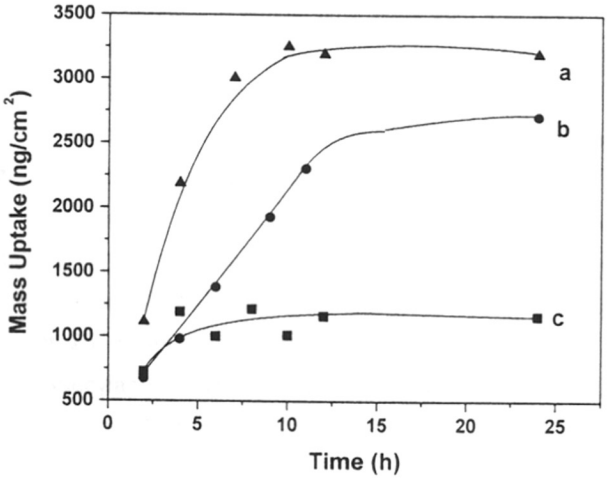


**Figure 6.2 :** QCM mass uptake per bilayer versus time after spreading octadecylamine monolayers on the different colloidal subphases. Curve a - 1 : 1 subphase; curve b - pure silver subphase and curve c - pure gold subphase.

This clearly shows that even though the π-A isotherms stabilize after 3 hours of spreading of the monolayer, the cluster density at the air-water interface increases

steadily with time and stabilizes only after 12 hours for the subphases containing silver particles. This is an important observation and indicates that π-A isotherms are insensitive to changes occurring at the air-water interface, especially when the monolayer is in an expanded state and also that the kinetics of cluster incorporation at the air-water interface is extremely slow. This however was not anticipated in the studies discussed in chapter IV, where the monolayer was compressed to 25 mN/m, allowed to remain under isobaric conditions until the change in the area/molecule was negligible and thereafter the monolayers transferred for additional measurements. However, since the observed time scale for equilibration of the cluster density at the air-water interface is much larger than the time required for preparation of multilayer LB films, the conclusions of the earlier investigations are not expected to be significantly different. The equilibrium mass uptake per bilayer for films deposited from the pure silver, 1 : 1 and gold subphases are 3200, 2700 and 1160 ng/cm$^2$ respectively (Figure 6.2).

While QCM measurements can detect overall mass changes in the film during the cluster diffusion process, it cannot differentiate between the presence of gold and silver clusters simultaneously in the film. UV-vis spectroscopy is an excellent tool for the study of partitioning of the clusters in amine films since gold and silver colloidal particles exhibit strong (and well separated) surface plasmon resonances [5-6]. This aspect has been highlighted in Chapter II [Page 23, Section 2.2]. The UV-vis spectra of 4 ML octadecylamine films complexed with the colloidal particles deposited at different times on hydrophobized quartz substrates is shown in Figures 6.3a-6.5a for monolayers transferred from pure silver, 1 : 1 and pure gold subphases respectively. The times indicated next to the curves refer to the time interval (in hours) after spreading the octadecylamine monolayer and as mentioned earlier, the transfers were carried out at a surface pressure of 25 mN/m. The surface plasmon resonance of silver and gold clusters in the octadecylamine LB films occur at ca.475 and 600 nm respectively (indicated by arrows, Figure 6.4a).

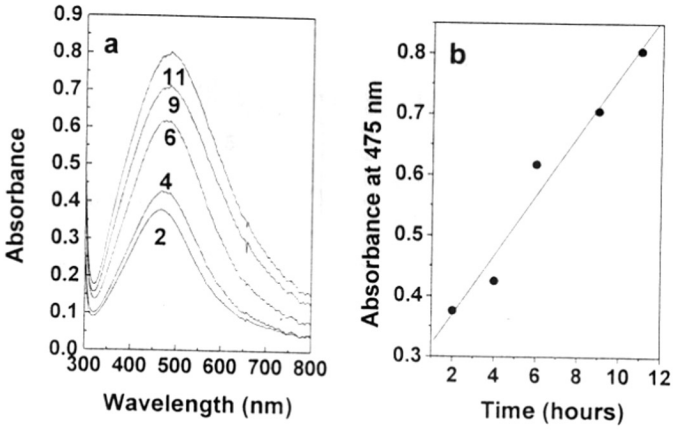


**Figure 6.3 :** a) UV-vis spectra of 4 ML octadecylamine films transferred from the pure silver subphase after different times of spreading the fatty amine monolayer. The times are indicated next to the curves.
b) Intensity of the plasmon resonance at 475 nm plotted as a function of time for the spectra shown in Figure 6.3a.

It is seen from the figures that except for the films transferred from the gold colloid subphase whose absorption spectrum stabilizes close to 5 hours after spreading the octadecylamine monolayer, the intensity of the absorption maximum increases steadily with time for the pure silver and 1 : 1 subphases. This is indicated clearly in Figures 6.3b-6.5b where the intensity of the absorption maximum has been plotted as a function of time for the corresponding UV-vis spectra.

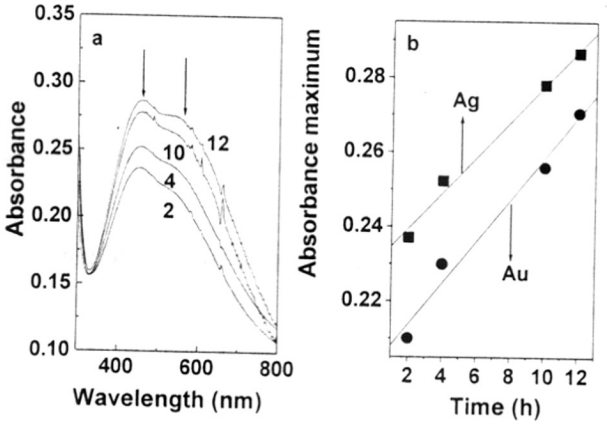


**Figure 6.4 :** a) UV-vis spectra of 4 ML octadecylamine films transferred from the 1 : 1 composite subphase after different times of spreading the fatty amine monolayer. The times are indicated next to the curves. The arrows indicate the position of the silver and gold plasmon resonances.
b) Intensity of the gold (600 nm) and silver (475 nm) plasmon resonance plotted as a function of time for the spectra shown in Figure 4a.

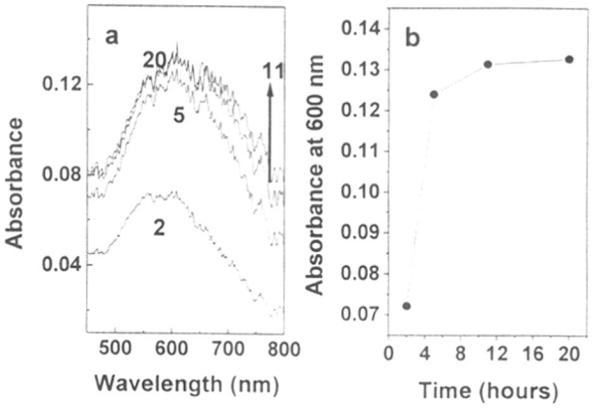


**Figure 6.5 :** a) UV-vis spectra of 4 ML octadecylamine films transferred from the pure gold subphase after different times of spreading the fatty amine monolayer. The times are indicated next to the curves.
b) Intensity of the plasmon resonance at 600 nm plotted as a function of time for the spectra shown in Figure 5a.

The resonance intensity increases until ca. 12 hours after spreading the fatty amine monolayer and is in agreement with the QCM results shown in Figure 6.2. While the UV-vis spectra of films transferred from the pure gold subphase showed changes until 5 hours of monolayer spreading, the QCM data (Figure 6.2, filled squares) indicated very small change in the cluster density in the bilayers after 2 hours of monolayer spreading. The reason for this discrepancy is not understood at present since identical film preparation conditions were used in both cases. From Fig.6.4a and b, it is seen that the resonance corresponding to gold (ca. 600 nm) increases slightly relative to the silver resonance at 475 nm with increasing time. This is interesting given that the cluster density in the pure gold films stabilize within 5 hours of spreading of the fatty amine monolayer.

As demonstrated above, the cluster density at the air-water interface stabilizes within ca. 12 hours of spreading the fatty amine monolayer on the different subphases. UV-vis spectra of 4 ML LB films of octadecylamine transferred onto hydrophobized quartz substrates after 15 hours of monolayer spreading were recorded and are shown in Figure 6.6 for the 2 :1 (filled circles), 1 : 1 (filled squares) and 1 : 2 subphases (filled triangles).

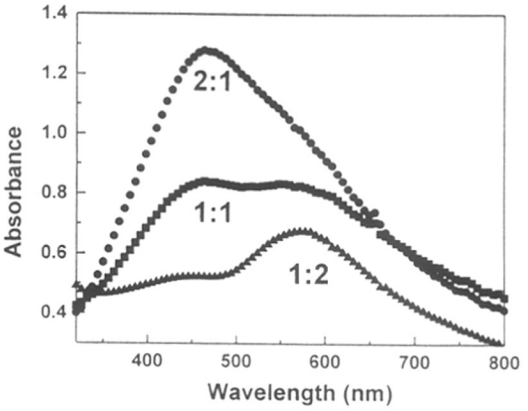


**Figure 6.6 :** UV-vis spectra of 4 ML octadecylamine LB films transferred after 15 hours of spreading the fatty amine monolayer on the different subphases. The subphase concentration ratios are indicated next to the curves.

As expected, the intensity of the gold plasmon resonance relative to the silver resonance (indicated by arrows in the figure) increases as the concentration of the gold clusters in the subphase increases. However, determination of the gold : silver cluster density ratio in the films would be illuminating. It is difficult to make an estimate of the molar concentration of Au and Ag in the mixed cluster films from the UV-vis spectra shown in Figure 6.6 due to damping and shifts of the surface plasmon resonance of the clusters on capping with the 4-CTP molecule, which currently cannot be quantified.[5] Multilayer films of different thicknesses transferred from the different subphases onto hydrophobized quartz substrates were studied by optical interferometry. A linear increase in thickness was observed with number of monolayers transferred indicating good layer-by-layer growth of the built-up films and is in agreement with the data presented in chapter IV on LB films of gold and silver colloidal particles. Attempts to image the LB films transferred onto electron microscope grids were not successful due to electron beam heating of the films which led to melting and a fair degree of aggregation of the colloidal particles.

An estimate of the gold : silver cluster density ratio for the 4 ML 1 : 1 film shown in Figure 6 may be made from X-ray Flourescence(XRF) [11] measurements of the film together with the QCM data presented in Figure 2 (curve a). The gold : silver molar ratio determined from XRF measurements for the 1 : 1 film was 4.5. For the cluster

sizes of this study, this molar ratio implies 0.7 clusters of gold for every silver cluster [7] in the 1 : 1 film. The main point to note from the above calculation is that while the gold : silver cluster density in the 1 : 1 subphase is 0.25, the corresponding cluster density in the LB film is 0.7 indicating that there is an enhancement of the gold cluster density in the film by a factor of 2.8. The mass balance constraint determined from QCM measurements can be written as :

$$n(Ag)\, m(Ag) + 0.7\, n(Ag)\, m(Au) = 3200 \text{ ng} \quad \ldots\ldots\{1\}$$

where n(Ag) is the number of silver clusters/cm$^2$ and m(Ag) and m(Au) are the mass per silver ($2 \times 10^{-9}$ ng) and gold clusters ($24 \times 10^{-9}$ ng) respectively. From Eq.{1}, the volume fraction of gold in the bilayers for the 1 : 1 film is determined to be 18.3 % while the corresponding value for silver clusters is 6.2 %. Comparison of these volume fractions with the volume fraction values of gold (13 %) and silver clusters (26 %) in the films transferred from the pure gold and silver subphases (Figure 6.2, curves c and b respectively) indicates that during simultaneous immobilization of the clusters at the air-water interface, the cluster density of gold is enhanced relative to the pure gold film and concomitantly, the silver cluster density is reduced. It appears, therefore, that the competitive process of electrostatic immobilization promotes the incorporation of large gold clusters in preference to the smaller silver clusters.

## 6.5 Summary

The main observations of the studies presented above may be summarized as follows :

1) $\pi$-A isotherm measurements show negligible expansion of the octadecylamine monolayer after 2 h of spreading of the monolayer whereas considerable change in the cluster density at the air-water interface is observed using QCM and UV-vis spectroscopy.

2) The cluster density of larger gold clusters at the air-water interface stabilizes faster than for the smaller silver clusters.

3) The cluster density ratios of gold and silver in the mixed cluster films is quite different from the cluster density ratios in the colloidal subphase. The gold : silver cluster density ratio in the 1 : 1 film is 0.7 whereas the concentration ratio in the 1 : 1 subphase is 0.25.

Observation 1 indicates that $\pi$-A isotherms are rather insensitive to changes in the cluster density occurring at the air-water interface when the monolayer is in an expanded state. Conclusion 2 appears contradictory at first since the diffusivity of the smaller silver clusters in the aqueous medium would be expected to be higher than for the bigger gold clusters. However, it must be kept in mind that the charge on the cluster for gold is nearly 3.5 times that for silver assuming complete ionization of the exposed carboxylic acid groups from 4-CTP. From a purely electrostatics point of view, the attractive interaction between the negatively charged colloidal particles and the positively charged amine monolayer would be much larger for the gold clusters and could account for the smaller diffusivity expected based on the cluster size.

Another factor contributing to the smaller stabilization times for gold colloidal particles at the air-water interface could be the following. During immobilization of the clusters at the fatty amine Langmuir monolayer, the amine molecules are expected to coordinate to the carboxylic acid terminal groups on the clusters through a coulombic attractive interaction. This leads to a disruption of ordering in regions of the amine monolayer in immediate contact with the clusters. Such a disruption in the packing of bilayers has been observed in LB films with clusters chemically inserted [8] as well as in stearate LB films with $Fe_2O_3$ nanoparticles attached at the air-water interface.[9] The area per terminal methyl group of the amine molecules on silver and gold clusters can be calculated to be 92 and 56 $Å^2$ respectively.[10] The larger surface curvature of the silver clusters leads to larger volumes available to the terminal groups of the amine molecules and consequently, weaker Van der Waals interaction between the chains. In other words, the immobilization of large colloidal particles would distort the packing of the hydrocarbon chains in the amine monolayers less than smaller clusters and would be energetically more favorable. The above two factors would satisfactorily explain the smaller cluster equilibration times observed for the gold clusters and would also explain observation 3 wherein the density of gold clusters in the films is larger than that in the composite subphase. This indicates that the energetics of the cluster immobilization

process is the same in both cases and further strengthens the results obtained in this investigation on the reverse fractionation at the air-water interface.

## 6.6 References

1. It was observed that hydrophobic substrates gave better monolayer transfer ratios and therefore, quartz substrates were rendered hydrophobic by transfer of 1 ML of lead arachidate. The gold coated quartz crystals for QCM were hydrophobic and used without further treatment.

2. Sauerbrey, G. *Z.Phys. (Munich)* **1959**, *155*, 206.

3. Ganguly, P.; Paranjape, D.V.; Sastry, M., *Langmuir*, **1993**, *9*, 577,

4. Blankenburg, R.; Meller, P.; Ringsdorf, H.; Salesse, C., *Biochemistry*, **1989**, *28*, 8214

5. Henglein, A. *J.Phys.Chem.* **1993**, 97, 5457.

6. Mulvaney, P. *Langmuir* **1996**, *12*, 788.

7. Assuming a volume of 16 $Å^3$ per silver atom in the cluster, the number of atoms in a 70 Å diameter cluster is $= [(4\ \pi/3)\ (35)^3] / 16 \approx 11225$. From a similar calculation, the number of gold atoms in a 130 Å size cluster is ca. 71897. Therefore, the gold : silver molar ratio in a film containing equal numbers of silver and gold clusters is 71897 / 11225 ≈ 6.5. Since the Au : Ag molar ratio from XRF measurements for the 1 : 1 film is 4.5, this implies a Au : Ag cluster density ratio of 4.5 / 6.5 ≈ 0.7.

8. Urquhart, R.S.; Furlong, D.N.; Gegenbach, T.; Geddes, N.J.; Grieser, F. *Langmuir,* **1995**, *11*, 1127.

9. Yang, J.; Peng, X.; Zhang, Y.; Wang, H.; Li, T. *J.Phys.Chem.* **1993**, *97*, 4484.

10. For a 70 Å diameter Ag cluster (R = 35 Å), the number of 4-CTP molecules on the surface (25 $Å^2$ area/4-CTP molecule) = $(4\ \pi\ R^2)/\ 25\ = 616$.

Assuming coordination of 1 amine molecule of length 25 Å to each 4-CTP molecule (of 7 Å dimension) leads to a modified cluster radius of 35 + 7 + 25 = 67 Å.

Area per terminal methyl group of the amine molecules on Ag clusters is therefore approximately : $(4\ \pi\ 67^2)/\ 616 = 92\ Å^2$. By a similar calculation, this value can be shown to be ca. 56 $Å^2$ for gold clusters of 65 Å radius.

11. **X-ray Fluorescence:** When a sample under study is irradiated with polychromatic x-rays, characteristic x-rays of elements in the samples are emitted. The origin of characteristic x-ray spectra can be briefly described as follows: When sufficient energy is introduced into the atom, an electron may be knocked out of one of the inner shells. The atom is then in an excited state. The place of missing electron is filled by an electron from a neighboring outer shell whose place in turn is filled by an electron from a still outer shell. The atom thus returns to the ground state in steps. In every step, i.e., in every electron jump, and electron from a higher energy level goes into a lower energy level emitting excess energy in the form of an x-ray quantum. The energy of the emitted radiation is characteriztic for the atomic number of the emitting element as well as for particular electronic transitions, taking place within the electron shell of the atom. By measuring respectively, the energy or the wavelength of the emitted radiation the particular element can be identified unambiguously.

# CHAPTER VII

## Conclusions

T

The thesis concludes with this chapter by summarizing the major results. The chapter (and thesis) ends with a discussion on possible future work in this area.

## 7.1 Summary of the work:

It has been demonstrated that good quality Langmuir-Blodgett films of carboxylic acid derivatized silver, gold, cadmium sulfide particles can be deposited. Through the work presented in the chapters of this thesis, it has been demonstrated that the method of *electrostatic complexation of surface modified colloidal particles at the air-water interface* can be used as a general strategy to deposit any kind of colloidal particle with suitable choice of surfactant molecule for surface modification of colloidal particles. It has also been demonstrated that cluster complexation at the air-water interface is pH dependent, and this argument has been comprehensively proved using the pH dependent measurements of, pressure-area isotherms and Quartz crystal Microgravimentry. An important highlight of the thesis is that fatty lipids can be used to derivatize colloidal particles with functional group of choice using interdigitated bilayers thus excluding the need of bifunctional molecule. It has also been shown that a neutral spacer molecule can be used to control the cluster density in addition to subphase pH. Incorporation of clusters into the Langmuir Monolayer was not observed for equimolar ratios of oppositely charged groups at air-water interface, which is an additional proof for the claim made in this thesis that the process is driven by elelctrostatic interactions. Simultaneous complexation of carboxylic acid derivatized silver and gold particles which vary vastly in size, with the Langmuir Monolayer of octadecylamine was performed. Gold particles which were bigger in size as compared to silver, was preferentially found to complex to the Langmuir Monolayer, in a competetive process. Kinetics of cluster complexation indicates that the incorporation of clusters to the Langmuir Monolayer saturates after 13 hours, which is quite faster as compared to the existing methods for organization of colloidal particles.

## 7.2 Advantages of the present method :

Air-water interface has been used by number of other groups for organizing colloidal particles. The following are the advantages of this technique over other methods.

1. Choice of the particles to be grown: Unlike chemical insertion route, where technique is material specific, using the present technique, colloidal particles of various materials can be deposited, with proper choice of surfactant for surface modification

2. Size distribution and shape of the colloidal particles: Unlike other methods, in this method, colloidal particles of known shape and size distribution are synthesized using wet chemical methods, and then organized at the air-water interface. Hence this method provides very good control over the size distribution of particles in the film.

3. Control of cluster density: pH dependent cluster complexation is observed in the method described in this thesis, which can easily be used to control the cluster density.

4. Simultaneous complexation of different colloidal particles are possible using this method.

## 7.3 Scope for future work:

The strategy of electrostatic immobilization at the air-water interface can be made use off in drug delivery systems, gene therapy, chemical sensors, strain sensors etc.

A detailed study of kinetics of cluster incorporation at the air-water interface may lead to understand better the problem of overcompensation of ions.

In addition to the above, Well defined superlattice structures are possible in this scheme through alternate transfers in different hydrosol subphases with different Langmuir monolayers. This shows promise for obtaining alternating metal-semiconductor nanoparticle.

## LIST OF PUBLICATIONS:

1. *"Lamellar multilayer gold cluster films deposited by the Langmuir Blodgett technique"*
K.S. Mayya, V. Patil and Murali Sastry, *Langmuir*, **13** (1997) 2575.

2. *"Langmuir Blodgett films of carboxylic acid derivatized silver colloidal particles : role of subphase pH on the density of clusters"*
Murali Sastry, K.S. Mayya, V. Patil, D.V. Paranjape and S.G. Hegde, *J.Phys.Chem.B.* **101** (1997) 4954.

3. *"Silver clusters via ion exchange in self-assembled monolayers of an aromatic bifunctional molecule"*
V. Patil, K.S. Mayya and Murali Sastry, *J.Mater.Sci.Lett.*, **16** (1997) 899.

4. *"On the stability of carboxylic acid derivatized gold colloidal particles : the role of colloidal solution pH studied by optical absorption spectroscopy"*
K.S. Mayya, V. Patil and Murali Sastry, *Langmuir* **13** (1997) 3944.

5. *"pH dependent changes in the optical properties of carboxylic acid derivatized silver colloidal particles"*
Murali Sastry, K.S. Mayya and K. Bandyopadhyay, *Coll.Surf.A.* **127** (1997) 221.

6. *"Incorporation of colloidal metal particles in thermally evaporated fatty amine films via selective ionic interaction"*
Murali Sastry, V. Patil and K.S. Mayya, *Langmuir*, **13** (1997) 4490.

7. *"Evidence for novel interdigitated bilayer formation of fatty acids during three-dimensional self-assembly on silver colloidal particles"*
V. Patil, K.S. Mayya, S.D. Pradhan and Murali Sastry, *J.Am.Chem.Soc.* **119** (1997) 9281.

8. *"A study of the influence of colloidal subphase pH on the deposition of multilayer Langmuir Blodgett films of gold clusters"*
K.S. Mayya, V. Patil and Murali Sastry, *J.Chem.Soc.Faraday Trans.*, **93** (1997) 3377.

9. *"A study of the partitioning of colloidal particles based on their size during electrostatic immobilization at the air-water interface using fatty amine monolayers"*
K.S. Mayya and Murali Sastry, *J.Phys.Chem.B.* **101** (1997) 9790.

10. *"Self-assembled multilayer formation of an aromatic bifunctional molecule via selective ionic interaction"*
V. Patil, K.S. Mayya and Murali Sastry, *Thin Solid Films* **307** (1997) 280.

11. *"Spontaneously organized molecular assembly of an aromatic disulfide on silver/platinum alloy surfaces : an angle dependent X-ray photoemission investigation"*
K. Bandhyopadhyay, K. S. Mayya, K. Vijayamohanan and Murali Sastry, *J.Electron Spectrosc.* **87** (1997) 101.

12. *"Preparation and characterization of silver particulate films on softened polystyrene substrates"*
K. Mohan Rao, M. Pattabi, K.S. Mayya, S.R. Sainkar and Murali Sastry, *Thin Solid Films* **310** (1997) 97.

13. *"Electrostatic Complexation of Carboxylic Acid Derivatized Silver Colloidal Particles to Fatty Amine Langmuir Monolayers : Role of Neutral Spacer Molecules in the Monolayer"*
K.S. Mayya and Murali Sastry, *Langmuir* **14** (1998) 74.

14. *"On the deposition of Langmuir Blodgett films of Q-state CdS nanoparticles through electrostatic immobilization at the air-water interface"*
K.S. Mayya, V. Patil, P. Madhu Kumar and Murali Sastry, *Thin Solid Films*, **312** (1998) 308.

15. *"Organization of monolayer films of polymer-capped platinum colloidal particles at the air-water interface"*
Murali Sastry, V. Patil, K. S. Mayya, D.V. Paranjape, P. Singh and S.R Sainkar, *Thin Solid Films* **324** (1998) 239.

16. *"Bilayer surfactant assemblies on nanoscale curved surfaces : a new strategy for surface modification of colloidal particles"*
Murali Sastry, K.S. Mayya and V. Patil, *Langmuir* **14** (1998) 5921.

17. *"Organization of nanoparticles at the air-water interface and formation of multilayer nanoparticle films"*
Murali Sastry and K.S. Mayya, proceedings of the 4th Meeting of the Royal Society-Unilever Forum on Structure and Dynamics of Materials in the Mesoscopic Domain, Imperial College Publication (1998).

18. *"Inter-colloidal particle monolayer transfer in mixed metal colloids"*
K.S. Mayya and Murali Sastry, *Langmuir* **14** (1998) 6344.

19. *"A new technique for the spontaneous deposition of colloidal nanoparticle superlattices"*
K.S. Mayya and Murali Sastry, *Langmuir* **15** (1999)1902.